LAPPEENRANTA UNIVERSITY OF TECHNOLOGY
LUT School of Engineering Science
Degree Programme in Chemical Engineering

Miia Vähäaho

DUST EXPLOSION MODELLING METHODS

Master's Thesis 2018

Examiners: Prof. Tuomas Koiranen
M.Sc. Anna Savunen (Pöyry Finland Oy)

Advisor: M.Sc. Simo Tenitz (Pöyry Finland Oy)

TIIVISTELMÄ

Lappeenrannan teknillinen yliopisto
School of Engineering Science
Kemiantekniikan koulutusohjelma

Miia Vähäaho
Pölyräjähdysten mallinnusmenetelmät

Diplomityö

2018

102 sivua, 29 kuvaa, 27 taulukkoa ja 6 liitettä

Tarkastajat: Prof. Tuomas Koiranen
DI Anna Savunen

Hakusanat: pölyräjähdys, seurausmallinnus
Keywords: dust explosion, consequence modelling

Tämän tutkimuksen tavoitteena on löytää sopiva mallinnusmenetelmä sovellettavaksi pölyräjähdysten painevaikutusten tutkimiseen eri teollisuudenalojen prosesseihin. Räjähdysvaarallisia tiloja, niissä olevia laitteita sekä työskentelyä säätelee ATEX-lainsäädäntö. Vaikka pölyräjähdyksiä pyritään välttämään tilaluokitusten, teknisten ja organisatoristen ratkaisujen ja toimenpiteiden avulla, on niiden riski silti monissa laitoksissa olemassa. Pölyräjähdysten mallintamiseen ei ole yksiselitteisiä mallinnusmenetelmiä vielä käytössä, toisin kuin kaasuräjähdyksille, joiden seuraukset ja mallintamismahdollisuudet tunnetaan jo paremmin.

Tutkimus tarkastelee pölyräjähdysten mekanismia sekä niiden seurauksia saatavilla olevaan kirjallisuuteen perustuen. Huomioon on otettava räjähtävien pölyjen eri ominaisuudet, jotka vaikuttavat räjähdyksen syntymiseen sekä ylipaineen aiheuttamiin vaikutuksiin. Mahdollisia mallinnusmenetelmiä myös etsitään kirjallisuudesta ja niiden soveltumista pölyräjähdysten mallintamiseen teollisuuden prosesseihin tutkitaan. Tavoitteina mallinnusmenetelmälle ovat sen sovellettavuus erityyppisille pölyille sekä menetelmän luotettavuus. Tarkempaan tarkasteluun valitaan nämä tavoitteet parhaiten täyttävät menetelmät, joiden soveltuvuutta tutkitaan mahdollisia teollisuuden pölyräjähdysvaaran skenaarioita hyödyntäen. Löytynyttä menetelmää tullaan hyödyntämään eri teollisuuden alojen pölyräjähdysten seurausmallinnuksessa.

Räjähdyspaineiden määrittämiseen löytynyttä reaktiotasapainoon perustuvaa mallia testataan useilla orgaanisilla yhdisteillä. Saadut tulokset mallilla korreloivat hyvin kirjallisuuden arvoihin. Painevaikutusten määrittämiseen erityisesti pölyräjähdyksille ei malleja ole juuri tutkittu, joten kaasuräjähdyksille kehitettyjä malleja testataan. Nämä mallit eivät tuota toivottuja tuloksia pölyräjähdyksille, joten jatkotutkimusta niiden osalta vielä kaivataan.

ABSTRACT

Lappeenranta University of Technology
School of Engineering Science
Degree Programme of Chemical Engineering

Miia Vähäaho
Dust explosion modelling methods

Master's Thesis

2018

102 pages, 29 pictures, 27 tables and 6 appendices

Examiners: Prof. Tuomas Koiranen
M.Sc. Anna Savunen

Keywords: dust explosion, consequence modelling
Hakusanat: pölyräjähdys, seurausmallinnus

This study aims to find a modelling method for the studying of the pressure effects of dust explosions in processes of variable industries. The explosion hazard areas, the equipment in them and working in these areas is regulated by ATEX legislation. The possibility of a dust explosion exists in many industrial processes despite of the area classifications, technical and organizational solutions and measures. The modelling methods for dust explosions are not as well-known and used as modelling methods for gas explosions.

The mechanism of dust explosions and their consequences are studied relying on available literature. The characteristics of different dusts are to be regarded since they affect the formation of explosions as well as their pressure effects. The possible modelling methods and their applicability for industrial processes are also researched from literature. The optimal method is applicable for various dust sources and reliable. The most promising modelling methods fulfilling these goals are taken into a closer view and tested using possible industrial dust explosion scenarios. The obtained method will be used for the consequence modelling of dust explosions in different industries.

A model based on reaction balances is tested for the evaluation of explosion overpressure with various organic materials. The obtained results with the model correlate well with the values found in literature. Models for overpressure effect estimation for dust explosions are have not been researched in detail. Thus, models for gas explosion pressure effect estimations are tested for the use in the case of dust explosions. These models do not result in desired results and further research of the problem is still required.

ACKNOWLEDGEMENTS

This research was done in cooperation with Pöyry Finland Oy to investigate this new topic. I would like to thank Pöyry Finland Oy for providing me with this interesting and challenging topic. And my supervisors, Anna and Simo, for the support and valuable opinions throughout this project. A huge thank you to my advising professor, who guided me and gave me constructive comments all through the way. I would also like to thank all the parties participating and helping in this research.

Working with my thesis was really a great journey. It was full of excitement, desperate moments, trying to survive and stay afloat as well as laughing with my fellow workers, sharing ideas and joyful moments and discovering this fascinating world of dust explosions as well as learning about myself. I owe a lot to my dear Dippakommuuni for all the great moments and laughter shared, and especially to Juho and Pekka for making the journey with me.

Writing these words is ending one part of my life, my student life. It was full of some of the greatest moments of my life and the greatest people I have met. Of course, a lot of frustration and wanting to give up was also involved in those years. But overall, it really seems like a very happy and joyful time and I shall carry it and all the dear friends that I made along the way with me for the rest of my life.

Through all these years and this final project, I've received warm support from my dear family to whom I'm thankful for everything, good and bad genes included. And to my closest support, my dear Tatu, thank you. You've supported me and cheered me up, believed in me when I didn't, and finally also raced me to the finishing line, together.

"I have not failed. I've just found 10,000 ways that won't work." - *Thomas Edison*

Vantaa, 6th of August 2018

Miia Vähäaho

TABLE OF CONTENTS

LIST OF SYMBOLS AND ABBREVIATIONS

Symbols

Roman letters

a_0	Acoustic velocity at ambient conditions,
A	Arrhenius constant, s^{-1}
c	Concentration, g/m^3
C_p	Specific heat, J mol^{-1} K^{-1}
C_v	Specific heat,
d	Particle diameter, m
D	Vessel diameter, m
dp/dt	Rate of pressure rise, bar s^{-1}
$(dp/dt)_{max}$	Rate of pressure rise, bar s^{-1}
E_A	Activation energy, J
E_t	Total energy release from explosion center, J
f	Burn fraction, -
F	Force, N
h	Dust layer thickness, m
h_c	Heat transfer coefficient,
H	Dust cloud height from a layer, m
ΔH_r	Reaction heat per mole of combustible, J mol^{-1}
$\bar{i}$	Dimensionless explosion impulse, -
k	Reaction rate constant,
K_{St}	Volume normalized rate of pressure rise, bar m s^{-1}
L_F	Flame length, m
M	Metal, -
n	Amount of substance, mol
$n_{C,0}$	Initial amount of carbon, mol
$n_{O2,0}$	Initial amount of oxygen, mol
p	Pressure, bar

p_0	Initial pressure, bar
p_{ex}	Explosion pressure, bar
$p_{ext,max}$	Maximum external pressure, bar
$p_{ext,r}$	External pressure, bar
p_{max}	Maximum explosion pressure, bar
$p_{red,max}$	Maximum reduced pressure, bar
$\overline{P}$	Dimensionless overpressure, -
r	Reaction rate,
r	Distance from explosion source, m
r_p	Pyrolysis reaction rate,
R	Gas constant, J/Kmol
$\overline{R}$	Dimensionless distance from explosion center, -
S_u	Laminar burning velocity, m/s
t_c	Characteristic time of internal heat transfer, s
t_{comb}	Characteristic time of combustion reaction, s
t_e	Characteristic time of external heat transfer, s
t_{pyro}	Characteristic time of pyrolysis reaction, s
ΔT_i	Temperature difference between particle and surrounding gases, K
T	Temperature, K
T_0	Initial temperature, K
T_{ad}	Adiabatic flame temperature, K
T_{CL}	Minimum explosion temperature of dust cloud, K
T_{ex}	Explosion temperature, K
u’	Velocity fluctuation, m/s
V	Volume, m^3
X	Conversion rate of the combustible, -

Greek letters

α	Direction of explosion pressure from vent, °
γ	Specific heat ratio, -

δ_F	Flame thickness, m
ε	Emissivity
λ	Thermal conductivity of solid material,
ρ_{bulk}	Bulk density of a dust layer,
σ	Stefan-Boltzmann constant,
τ_c	Burning time, s

Abbreviations

ATEX	Atmosphères Explosible
Bi	Biot number
BM	Bradley and Mitchelson model
BST	Baker-Strehlow-Tang model
CFD	Computational fluid dynamics
Da	Damköhler number
DEDE	Dust explosion domino effect
DESC	Dust explosion simulation code
EPD	Explosion Protection Document
FLACS	Flame acceleration simulator
L/D	Length-to-diameter ratio
LOC	Lower oxygen concentration
MEC	Minimum explosion concentration
MEM	Multi-energy model
MIE	Minimum ignition energy
MIT	Minimum ignition temperature
NCV	Nagy, Conn and Verakis model
Pc	Dimensioless number
Th	Thiele number
VCE	Vapor cloud explosion

1 INTRODUCTION

Process safety is important part of any industrial process. Process safety is to be taken into account when designing a new process plant and when changes are made to the process. Also, evaluations of process safety should be conducted regularly during the entire life cycle of the process. The aim of process safety is to avoid possible losses of life, health, environment and material. (Tukes, 2016) There are many ways to improve process safety both when the process is in the design phase and when the process is already in use. Layout design, facility and equipment placing are part of process engineering whereas employee training and improvement of mode of operations can improve process safety in an already existing and functioning process (Tukes, 2016).

The safety in process environment is regulated with regional legislations. In Finland, process safety is regulated by European legislation, which is implemented in Finnish national legislation. The European Seveso III directive (2012/18/EU) brought the requirements for consequence analysis on major accidents in facilities in the EU area. The supervision of enforcement of these legislative requirements is carried out by the Finnish Safety and Chemicals Agency (Tukes). All industries are required to follow the legislation, standards and instructions issued by Tukes. Legislation concerning areas and equipment used in areas where the possibility of explosion hazard exists, ATEX (Atmosphères Explosible) came into effect in 2003 (Tukes, 2015[a]). ATEX legislation requires that the process owner or operator evaluates and identifies possible explosion hazards in the process and updates equipment and practices accordingly. The process owner or operator also has the responsibility to prepare Explosion Protection Document (EPD) and update it when needed. ATEX area classification should be updated in case the properties of flammable chemicals or the process changes.

Explosions create a severe safety hazard in many industries. Industries commonly containing the risk of explosions are for example oil and natural gas industries, chemical, petrochemical and metallurgical process industries, mechanical processing and special processes (Eckhoff, 2005). The possibility of explosions in processes is in general minimized as far as possible. In spite of preventative methods, explosions occasionally occur causing severe consequences. The consequences caused by accidents can be predicted and evaluated by consequence modelling

giving also the possibility to prepare equipment and structures to withstand the effects. The most common explosion sources in industrial processes are gases and dusts. Gas explosions are regarded as great process safety hazards and the methods and means to avoid them are well known and established. Dust explosions in turn are far less acknowledged as serious and common process safety hazards.

1.1 Background

Dust explosions generate severe hazards in many industries and their consequences yield to great losses. The danger of lingering and layering dust in processes is not acknowledged greatly because the mechanism and effects of dust explosions are not widely known. A dust layer in a wood saw plant might seem harmless and common but it can be the cause of a wide explosion taking down even multiple buildings. Dust explosions are more common risk than many would realize. There are documented dust explosion cases from wood and paper industry, food industry (flour and sugar), textile industry (cotton, wool, linen), metal industry, power industry (coal and peat), plastic and rubber industry, chemical process industry and mining industry (Amyotte & Eckhoff, 2010), just to name a few.

With the ATEX legislation came the requirements for industries to analyze and examine their processes for the possible explosion hazards. Consequence modelling is needed for the reason to understand the effects and consequences of possible accident scenarios. The results of consequence analyses are used in layout engineering and land use planning. Previously, explosions experiments have been conducted to gain information about the parameters and characteristics of combustible dusts and their explosion (Eckhoff, 2003). The hope for the future is to be able to resolve these problems computationally without the need for comprehensive and expensive experiments.

Gas explosions are a well-studied and researched subject and the modelling methods for gas explosion modelling are well-known and quite established. There are several computational softwares intended mainly for gas modelling. A previous master's thesis has been completed comparing gas explosion models and their utilization in consequence analysis of major accidents by Simo Tenitz (2013) in co-operation with Pöyry Finland Oy. The purpose of this research is

to continue in the same field of explosion hazard research focusing entirely on dust explosions and the modelling methods suitable for them.

As the knowledge of dust explosions is not so well established, also the modelling methods for dust explosions are less-known. There are some researches focusing on finding modelling methods for dust explosions, but many are still under further development (Skjold et al., 2006; Russo & Di Benedetto, 2013). The history of dust explosion modelling is mainly in Computational Fluid Dynamics (CFD) (Russo & Di Benedetto, 2013). A new, adjustable and easily employed modelling method could give valuable information about dust explosions and their consequences thus helping industries to prepare accordingly for the possibility of dust explosions.

1.2 Objectives and scope

This research aims to find a suitable and applicable modelling method for dust explosions and their consequences in processes of different industries. The modelling methods created for gas explosion modelling can't be used for dust explosion modelling without making some assumptions or modifications to the model due to the solid nature of the dust particles. The attempt in this research is to find a new modelling method for dust explosion applications and not to modify a functioning model intended for gas explosions. This way the research process is focusing on finding solutions and not fixing problems.

The research has two main themes, what are dust explosions and how can they be modelled. From these themes, three research questions can be separated to aid the main goal of the research. The first research question focuses mainly on the understanding of dust explosions as a phenomenon and the consequences of them. The remaining two research questions focus on the modelling methods of dust explosions, which is the main object of this research. The research questions are presented in **Table I**. By answering these research questions, the main goal of the research can be achieved.

The ATEX legislation determines the equipment used in explosion hazard areas by dividing them into two groups, I and II. Group I includes equipment and processes used in mines and above the ground parts of mines where the explosion hazard is caused by methane gas.

Equipment used everywhere else is included in Group II. (Tukes, 2015[a]) This study focuses mainly on processes classified as Group II by ATEX. The research is scoped to all industries within the group and dust characteristics of dust from multiple industries are studied. It is assumed in this research that the explosion reaction in the processes occurs between dust and air.

Table I The research questions of the study and their objectives.

Research question	Objective
RQ1: *How do dust explosions occur in most industrial processes?*	• To understand the risk of dust explosions • To understand the mechanism of dust explosions • To identify the factors in dust explosions • To identify the consequences of dust explosions
RQ2: *How can dust explosions be modelled?*	• To find earlier modelling methods for dust explosions • To identify the advantages and defects of earlier models
RQ3: *What is required of a suitable modelling method?*	• To identify the needed input for the model • To identify the required output of the model • To create a suitable modelling method for testing

1.3 Execution of the study

The research process follows the research questions by starting with finding answers for the first question about dust explosions as a phenomenon and then the second question about earlier studies regarding modelling methods. Understanding of the mechanism, parameters and consequences of dust explosions as well as previous modelling methods intended for dust explosion modelling are researched from literature consisting of legislations, directives, standards, books and scientific articles. From this knowledge, the objectives and scope of the desired model can be obtained and set. Information and data from earlier dust explosion accidents are requested and searched from authorities to obtain more accurate information about the subject.

The actual research material for the testing of possible modelling methods is obtained from current client cases in Finland from several relevant industries. The purpose of this is to gain valuable information about the functionality and flexibility of the possible models to be used for applications in different industries. The chosen sources of cases, and thus sources of different dusts, are from industries where the hazard of dust explosions has been present and where the need for the understanding of their consequences is vitally important. Also, the intention is to test the modelling methods with varying dusts to get a good representation of the applicability of the model for different industries.

The research process extends from February 2018 until July 2018. The process is divided in tasks for the available months. The dust explosion mechanism and earlier modelling methods are searched from literature during February and March. In March, the tested models and client cases are chosen, and the testing is assumed to last until June. The results and final presentation of the suggested modelling method are prepared in June and July resulting in a final report in July.

1.4 Structure of the report

This report consists of two parts, literature review of the subject and experimental study on the methods found in the literature review. In the literature review, the basic phenomenon of dust explosion is explored as well as the important parameters having a significant effect on the mechanism. The consequences of dust explosions are searched and studied. Finally, the reported modelling methods for dust explosions are searched and their potential is evaluated.

In the experimental study of the report the potential modelling methods are presented. The research material from client cases is introduced and the implementation of the models for each case is documented. The chosen methods are verified using data derived from reported dust explosion accidents and from validated dust explosion database. The models are evaluated considering the used data and other application possibilities, their strengths and weaknesses reported. The applicability and accuracy of the used models is evaluated and compared with verification data and the optimal modelling method is suggested among the possibilities. The chosen method may also be obtained by combining different models to achieve desirable results.

In the end, suggestions for follow-up research are presented. As a matter of interest, the dust explosion scenarios may be modelled with the modelling methods intended for gas explosions to compare their functionality and accuracy for the case in the very end of the research process.

2 DUST EXPLOSION

Dust explosion can be determined in different ways (Eckhoff, 2003). In this research, *dust explosion* is understood as a rapid combustion of dust-air mixture in industrial processes. Like any other explosion, dust explosions need three main components to form, fuel, oxygen and ignition source (Stahl, 2004). The three components together form a *fire triangle*, illustrated in **Figure 1**.

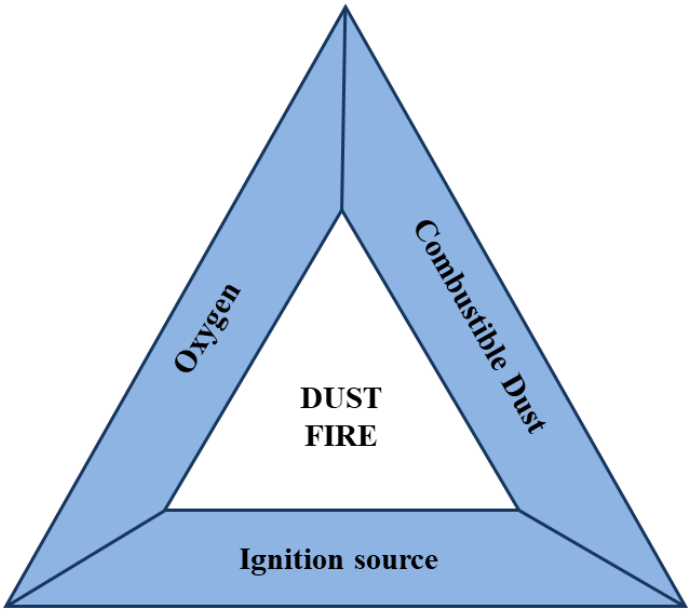

Figure 1 The fire triangle illustrating the three components needed for a fire to occur (Stahl, 2004).

With the three components, a dust fire can be formed. For a dust explosion to develop, two additional components are needed. (Rahman & Takriff, 2011) These are mixing of the dust with the oxygen source to form a *dust cloud* and confinement of the dust cloud into an enclosed or limited area (CCOHS, 2008). Adding the two components into the fire triangle, an *explosion pentagon* in obtained (Amyotte, 2014), illustrated in **Figure 2**. Dobashi (2017) determines the difference of fire and explosion so that fire is a reaction where flame spreads through non-premixed medium and explosion a reaction where flame propagates through a premixed medium containing fuel and air.

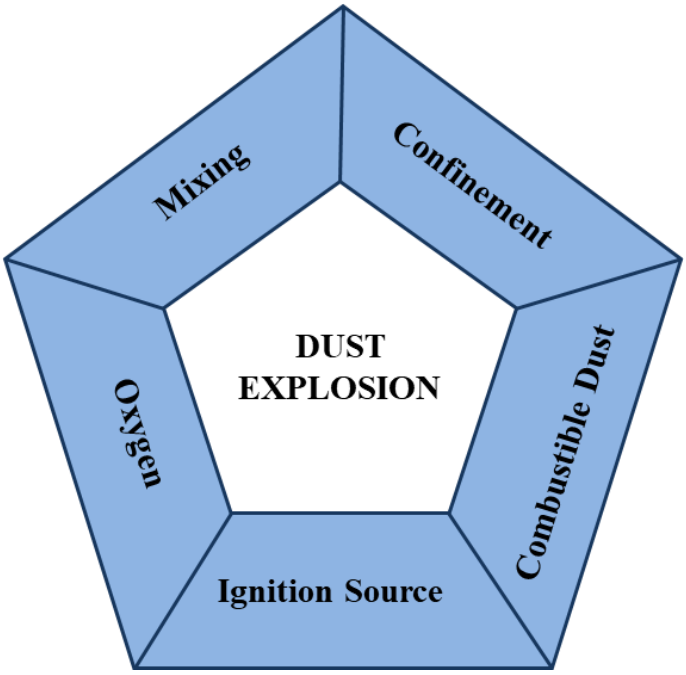

Figure 2 The explosion pentagon describing the five components required for the formation of a dust explosion (Amyotte, 2014).

Dust is defined as a small particle of solid material. *Combustible dust* is a dust material that creates a risk of combustion when in contact with oxygen. The size definition of combustible dust varies depending on the source or authority. The European standards EN 1127-1:2011 and EN 60079-10-2:2015 define combustible dust as a fine solid particle with a diameter of lower than 500 µm while the US national Fire Protection Association defines dust as a finely divided solid with 420 µm diameter or less in standard NFPA 68 (2013). Skjold (2014) mentions in his thesis for the degree of philosophiae doctor (PhD) that the characteristic particle size for combustible dusts is in the range of 1-100 µm. Not all materials, even with small particle sizes, can create combustible dusts. These non-combustible materials are stable oxide materials (Eckhoff, 2003). In general, all non-stable oxides have the ability to create combustible dust mixtures with oxygen. Most natural and synthetic organic materials, such as grain, wood, plastics and pesticides, as well as coal and peat form combustible dusts when divided into fine particles. Also, inorganic materials, most often metals, can be sources of combustible dust hazards. (Eckhoff, 2003)

Combustible dust creates an explosive *dust-air mixture* when mixed with air. The oxygen source can also be other gas than air and these mixtures consisting of dust and gas other than air are referred to as *hybrid mixtures*. The combustion of dust requires oxygen, so the combustible dust needs to be in contact with the oxygen source for the explosion to form. It has been noted that the creation of a dust cloud by mixing combustible dust and air always requires turbulence (Skjold et el., 2006). The chemical composition, especially the amount of oxygen, of the gas phase is important to know as well as the chemical composition of the dust (Skjold, 2014).

2.1 Ignitability of dust-air mixtures

A dust-air mixture has certain limitations in regards of its ignitability. Skjold (2014) lists the important parameters related to dust-air mixtures as the concentration of the dust and oxygen in the mixture, initial temperature and pressure of the mixture and the flow conditions. The minimum explosion concentration (MEC) is the lowest possible concentration of a combustible dust cloud that ignites and can support the flame propagation thus generating a dust explosion. It can be defined as the lowest possible concentration of dust where the explosion occurs or as the highest concentrations of dust where the explosion does not occur (Chawla et al., 1996). Usually, the definition is the former. Pressure and temperature affect the concentration area by widening it when increased (SFS-EN 1127-1, 2011). The limiting oxygen concentration (LOC) is the lowest oxygen concentration in the gas phase that supports the combustion. Stoichiometric concentration is the theoretical concentration of dust that is required to consume all the oxygen in the air of the gas phase. The maximum pressure of dust explosion is generally achieved above the stoichiometric concentration of the dust, sometimes from two to three times greater than the stoichiometric concentration (Ogle, 2016, p. 14, 478) or even much higher (Kim et al., 2016). It has been found though, that only approximately 10 % of the dust participates in the combustion reaction and 90 % of the dust remains unreacted resulting in a risk of fire after the explosion (Kim et al., 2016).

Figure 3 is a demonstration of the different limits of dust clouds. The explosible and nonexplosible regions are separated in the graph.

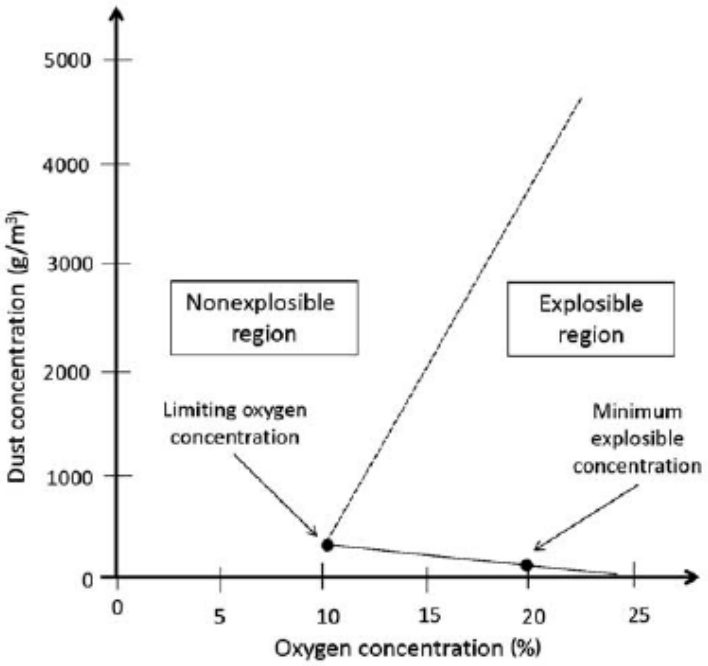

Figure 3 A generalizing diagram of combustible dust explosability limits (Ogle, 2016, pp. 480).

Dust clouds with dust concentration below the MEC are seen as non-combustible in general but this generalization is rarely valid on its own. The dust cloud is not a homogenous mixture and the dust concentration in the cloud varies in different areas (SFS-EN 1127-1:2011; SFS-EN 60079-10-2:2015). This makes the effect of the concentration limits less meaningful than with gases (SFS-EN 1127-1:2011) and it is why a dust cloud with a lower dust concentration than MEC can still possess a dust explosion hazard since the dust concentration in some part can reach over the MEC. The concentration of dust is usually expressed as mass concentration, the mass of dust in the air (kg/m^3) (Ogle, 2016, pp. 61). Eckhoff (2003) has found that the combustible range of dust concentration for many organic dusts falls in the range of 50-100 g/m^3 to 2-3 kg/m^3.

The initial *primary dust explosion* usually occurs in situations, where the dust-air mixture is already present, although layers of dust also possess the possibility to cause an explosion. Often the layers of dust in process plants are not seen as explosion hazard, especially when the layers are thin. **Figure 4** however demonstrates how even a dust layer of 1 mm can cause a combustible dust-air mixture if dispersed into air.

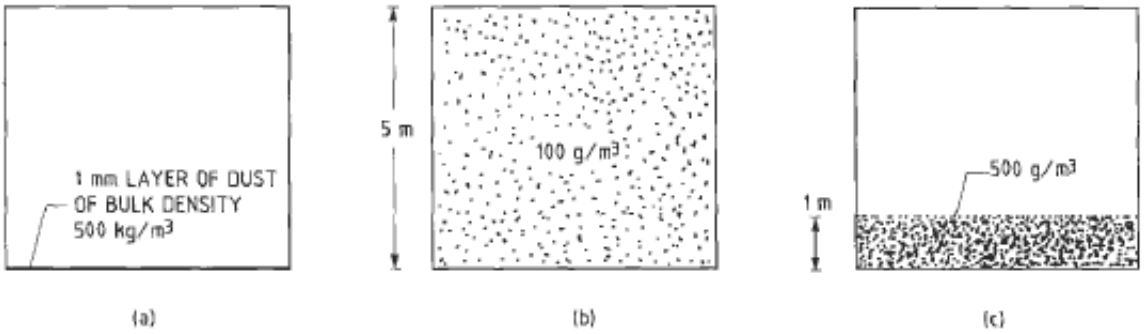

Figure 4 Illustration of the bulk density of a thin dust layer (Eckhoff, 2003).

The bulk density of the dust cloud from a layer of dust is calculated with **Eq. (1)**

$$c = \rho_{bulk} \frac{h}{H} \tag{1}$$

Where
- c dust concentration
- ρ_{bulk} bulk density of the dust layer
- h thickness of the dust layer
- H height of the dust cloud formed from the layer (Eckhoff, 2003, pp. 10)

A dust explosion needs a confined area, limited by walls or equipment or other obstacles, to occur. Usually, primary dust explosions occur inside process equipment such as silos, mills, dryers and grinders, (Eckhoff, 2003; Amyotte & Eckhoff, 2010) where the concentration range is high enough for the explosion criteria and is higher than the allowed concentration in industrial hygiene considerations (Amyotte et al., 2007; Eckhoff 2003). The confinement can be complete or partial but it is required for an overpressure to develop transforming a fast-burning flame into a dust explosion (Amyotte, 2014). The knowledge of the volume and geometry of the confined area is important in evaluating the effects of dust explosions. Dust explosion usually causes most hazards in highly confined process equipment, such as silos where the walls delimit the area for the flame propagation and cause the development of overpressure resulting in dust explosions (Skjold, 2014).

Dust explosions always need a source for the ignition of the combustion. Many industrial processes possess several potential ignition sources for dust explosions. The possible ignition sources in most industrial processes are defined in standard EN 1127-1:2011 and are listed in

Table II. For combustible dust materials, a *minimum ignition energy* (MIE) is determined to evaluate the energy required to ignite a dust cloud. Also, a *minimum ignition temperature* (MIT) is determined for many dusts and it needs to be taken into account when choosing process equipment for an explosion hazardous area.

The combustion first occurs at the particles nearest the ignition source. The temperature of the ignited particles increases and thus the combustion spreads as the ignited particles act as ignition source for the cloud surrounding them. This creates the combustion zone or flame of the explosion that propagates through the cloud. (Proust, 2004) In addition to dust cloud ignition, layers of dust can also ignite through smoldering. In the case of smoldering, a minimum thickness of the dust deposit is added to the fire triangle as a requirement (Ogle, 2016, pp. 9).

Table II The ignition sources of dust clouds in industrial processes (SFS-EN 1127-1:2011).

Ignition source	Dust explosion possibility
Hot surfaces	Combustible dust cloud comes into contact with hot surfaces Combustible dust layer created on hot surface
Flames and hot gases	Combustible dust comes into contact with open flames or hot gases from flames or other origins, processes such as welding or cutting work
Mechanically generated sparks	Combustible dust ignites from sparks created by friction, impact or abrasion processes, such as grinding
Electrical apparatus	Combustible dust ignites from electric sparks or hot surfaces created by opening and closing electric circuits, loose connections or stray currents
Stray electric currents, cathodic corrosion protection	Combustible dust ignites due to faults in the electrical installations of short-circuit or short-circuit to earth
Static electricity	Incentive discharges of static electricity
Lightning	Combustible dust cloud ignites always when stuck by lightning
Radio frequency (RF) electromagnetic waves from 10^4 Hz to $3x10^{11}$ Hz	With powerful enough radiation field and sufficiently large receiving aerial, combustible dust cloud can ignite from conductive parts
Electromagnetic waves from $3x10^{11}$ Hz to $3x10^{15}$ Hz	The radiation can ignite combustible dust clouds when focused and absorbed into the cloud or solid surfaces
Ionizing radiation	Combustible dust cloud ignites due to energy absorption
Ultrasonic	Combustible dust cloud ignites due to heat created by emitted energy from ultrasonic sound waves
Adiabatic compression and shock waves	Combustible dust ignites due to high temperatures created by compression or shock waves
Exothermic reactions, including self-ignition of dusts	Combustible dust cloud or dust layer ignites due to heat created in an exothermic reaction exceeding heat loss to the surroundings

Removing one of these five components of the explosion pentagon can prevent the possibility of a dust explosion (Abuswer et al., 2013). A common way of preventing dust explosions is to

try to remove the occurrence of dust in process plants through good cleaning and working methods. Evaluating the areas for possible ignition sources and removing them is another preventative method. Still, other mitigation methods for the possibility of dust explosions are widely used in industrial processes and the designing is done through process safety planning. The goal in process safety planning is firstly to make the process inherently safe and after that, engineered and procedural safety is taken into consideration. The inherent safety aims to remove the possibility of dust explosion hazard by choosing of materials and equipment carefully to remove the possibility of ignition. The inherent safety means can be divided to four main methods, minimization, substitution, moderation and simplification. (Amyotte et al., 2007; Amyotte & Eckhoff, 2010) The minimization refers to minimizing the occurrence of dust deposits and enabling the formation of dust clouds of concentration below the MEC. Substitution can be exploited by substituting the materials used in the process if possible or substituting the equipment, work procedures, hardware or process routes. The process can be moderated by increasing the particle size of the dust material, changing the dust composition by using inerting materials together with the dust material or by changing the position of the process units in relation to other units. The process can also be simplified by designing the process equipment to withstand errors and other unexpected events to mitigate the possibility of accidents. The engineered safety can be passive or active and is usually on the form of machinery safety mechanism that triggers by explosion pressure, such as in the case of pressure relief valves, or by the changes in the process parameters, such as pressure or temperature. The most commonly used mitigation method in process industries is venting, although it only reduces the overpressure of the explosion (Skjold, 2014). The procedural safety methods include work permits for hazardous areas and instruction for safe working methods and ethics. The latter two methods start with the assumption that the possibility of a dust explosion is present in the process. (Amyotte & Eckhoff, 2010)

For the dust explosion parameters, the MIT and particle size are important in the case of single particle combustion and dust cloud concentration as well as the reaction mechanism in the case of dust cloud combustion. (Amyotte et al., 2003)

2.2 History of dust explosions

Dust explosions are a continuous safety hazard in many industrial factories. There have been reported cases of dust explosions from the 18th century, all through the 20th century and the latest cases occurring in the last decade. The first reported dust explosion accident dates back to December 14, 1785 in a flour warehouse of a bakery in Turin, Italy and it was reported by Count Morozzo (1795), cited in Eckhoff (2003). A boy was collecting the flour of the bakery in a flour warehouse containing two parallel rooms, and as he collected a large amount of flour from the lower chamber flour from the upper chamber fall into the lower chamber causing a thick cloud of flour dust to appear in the chamber. This dust cloud was ignited immediately by a lamp hanging on the wall resulting in a dust explosion. The accident caused no fatalities but destroyed the windows and window frames of the shop. This dust explosion accident wasn't gravely dangerous but it represents the generality of dust explosion occurrence and the importance to understand the effects of them.

The U.S. Chemical Safety Board (2006) launched an investigation on dust explosion accidents after three accidents occurred in the United States during 2003, causing total of 14 fatalities. The investigation expanded to study accidents that had occurred in the United States between the years of 1980 and 2005 and resulted in a report in 2006. In the report, the total number of dust explosion accidents in the general industry in the United States was 281 resulting in total of 119 fatalities and 718 injuries. These numbers highlight the constant and current danger of dust explosions in different industries.

A known dust explosion accident from the past decade occurred in a sugar refinery of Imperial Sugar Company in Port Wentworth, Georgia, United States on February 5, 2008. The accident has been investigated by the U.S. Chemical Safety Board (2009). The dust explosion started in a conveyor belt carrying granulated sugar below three sugar silos that had been enclosed with stainless steel panels just the year before the accident. The sugar was introduced to the belt from shuts that from time to time had clumps in them causing the granulated sugar to spill in the tunnel. The concentration of the sugar increased above the explosive concentration in air and finally the dust was ignited by a nearby ignition source and exploded. The refinery was kept under a poor housekeeping and dust layers had accumulated around the building in different

process steps. The primary explosion rapturing the entire tunnel underneath the silos caused a secondary explosion in the building. The accident resulted in total of 14 deaths and 38 other injuries.

One of the most catastrophic dust explosion accidents of the recent decades occurred in China on February 24, 2010 causing the fatality of 146 people and injuring 114 (Li et al., 2016). Yuan et al. (2015) has collected information of over 2000 dust explosion accidents worldwide between the years of 1785 and 2012. The accidents are reported from a variety of industries, the main industries being food, wood, metal and coal respectively. The early 1900th resulted in a peak of dust explosion accidents mainly in Europe and United States. A second peak in the accidents is noticed from 1960 to 1980 when dust explosion accidents increased in number in China and Japan. One of the worst coal mine accidents occurred in Liaoning province, China in April 26, 1942 when a gas and coal dust exploded in Benxihu Colliery coal mine causing the death of 1594 people and injuring 246 (Mining Technology, 2014; Yuan et al., 2015).

Dust explosion accidents are also recorded in Tukes VARO register (2013) from different industries in Finland. Between the years of 2006 and 2015, there are total of 17 incidents reported from multiple different industries, such as saw, power plant, wood processing and chemical processing industries. In 2017, a dust explosion occurred in a plywood mill in Jyväskylä, Finland, breaking the windows of the lowest building level from nearly 100 m distance and causing a fire on the building roof. Two workers were injured in the accident. (MTV Uutiset, 2017; Savon Sanomat, 2017) Dust explosion accidents are also recorded from a bio-oil plant in Joensuu, Finland (Yle Uutiset, 2015) and from a feed factory in Turku, Finland (Yle Uutiset, 2017), just to name a few.

2.3 Particle size

The particle size of the dust has significant effects on the other parameters of the dust explosion. When a solid material is divided into smaller particles, the specific surface area of the material increases. This causes the rate of combustion to increase and the combustion is faster. Smaller particles have the ability to stay in suspension with air (Cashdollar, 2000; Callè et al., 2005) while larger particles are more difficult to maintain in the suspension due to sedimentation (Callé

et al., 2005). For dust particles, this results in rapid combustions causing explosions. Larger dust particles require more time to increase particle temperature from the initial temperature to the ignition temperature (Kosinski & Hoffmann, 2005). The smaller particle size is also found to result in higher combustion temperatures (Ogle, 2016, pp. 84). With smaller particle sizes, the ignition of a particle becomes easier. This means that less energy is required to ignite the particle and less oxygen is required in the gas phase. (Eckhoff, 2003) In turn, the maximum pressure released in the explosion increases with decreasing particle size (Ogle, 2016). This leads to the assumption that increasing the particle size of a combustible dust decreases the dust explosion hazard and the effects of it. (Amyotte et al., 2007) The effects of decreasing particle size are illustrated in **Figure 5**.

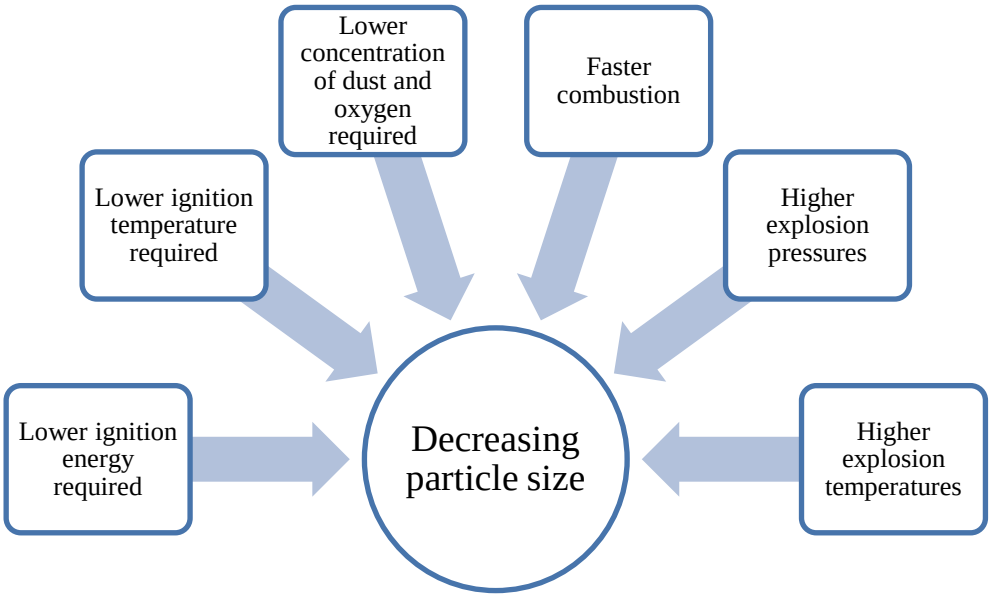

Figure 5 The effects of decreasing particle size.

The effect of decreasing particle size continues until a *critical particle size*. It has been found that after the critical particle size, the explosion rate is not controlled by the devolatilization no longer (Eckhoff, 2009) and the decrease in the particle size will not affect the combustion. This limiting particle size varies for different materials (Eckhoff, 2005) and Di Benedetto et al. (2010) suggested that the critical particle size is somewhere near the size of 30 µm in general. After the critical particle size, the combustion reaction is controlled mainly by homogenous combustion (Russo & Di Benedetto, 2013). The critical particle size is often smaller for metals than for most

organic materials and coal. Organic materials produce a homogenous combustible gas phase by pyrolysis while metals burn as separate entities. (Eckhoff, 2009) It has also been observed that the MEC is affected by the particle size at sizes greater than the critical value (Dufaud et al., 2010). For particle sizes lower than 100 µm, the particle settling due to gravity is often neglected but for larger particles, the gravity settling affects the dust concentration distribution (Ogle, 2016, pp. 432).

For very small particle sizes agglomeration has been reported when the dust is mixed with air (Eckhoff, 2003). Agglomeration causes the small particle to attach together thus increasing the particle size. (Eckhoff, 2009) A dust material rarely has particles of the same size and thus the particle size distribution of a given dust material is important to know (Amyotte & Eckhoff, 2010).

Combustible dust has other parameters as well affecting the rate of combustion. The porosity of dust material increases the specific surface area of the particle having the same effects on the explosion parameters as related to the particle size decrease. The particle shape also affects the specific surface area of the particle. A material might have a variance in particle shapes as well as in its sizes. Often, the dust particles are assumed to be spherical but in reality some materials have flocculent, flake of fiber particles (Amyotte & Eckhoff, 2010). Marmo & Cavallero (2008) noted that in case of fibers, the dominant size of a particle affecting the combustion is the particle diameter and not the length, although the length of the particle also has an influence. They also noticed that when the fibers started to melt before ignition, their shape started to resemble that of a spherical thus increasing the particle diameter. Some researchers have noted that flocculent particles have better ability to maintain dispersion in air due to their shape and thus increasing the probability of their ignition (Amyotte et al., 2012).

2.4 Different dust materials

Combustible dusts are often found in industries, such as food processing industry in the form of grain or sugar dust, wood industry, textile industry, metal handling industry. Dust can be a waste, side product or the desired final product of a process. Ogle (2016) has listed five important properties of dusts that can affect the behavior of a combustible dust. These are the chemical

composition, physical structure and thermal, electrical and optical properties. The chemical composition of the dust material has effect on the explosion mechanism and is to be considered when investigating the explosion mechanism of dust explosions (Skjold, 2014). Some materials have lower MIT and MIE values making them more easily ignitable. Also, for some materials the dust particles are not homogenous in chemical composition throughout the particle and the surface of the particle might differ from the inside of the particle. The thermal properties give information about the melting and boiling points, heat capacity, enthalpy of combustion and thermal conductivity of the material. The electrical properties indicate if the material has electrical conductivity and the optical properties inform about the light scattering behavior and refractive index of the material. (Ogle, 2016).

Ogle (2016, pp. 244) divided organic solid materials to three different groups depending on their combustion mechanism. These materials are non-charring, charring, and non-volatile solids. For the non-charring solid materials, the combustion process goes to completion and the materials consist of completely volatile solids. The charring materials consist of partially volatile solids and the combustion reaction leaves residues. The non-volatile solids are materials that don't go through the combustion reaction at all.

Considering the consequences of dust explosions, the maximum explosions pressures of materials are different and depend also on the dust cloud concentration. In lower dust concentrations, the variation of dust concentrations in the dust cloud has stronger effect on the explosion overpressure than in higher dust concentrations (Chen et al., 2017). The same concentration of dust can generate different explosion pressures depending on the material in question (Eckhoff, 2003). Coal dust has very high maximum explosion pressures even at lower concentrations compared to other dusts thus making it a very dangerous dust; some consider even the most dangerous dust among many dusts. The consequences caused by coal dust explosions are more severe than those caused by flour dusts. (Salamonowicz et al., 2015)

2.5 Explosion risk assessment of an industrial plant

Explosion risk assessments are required for all industrial plants that handle or use flammable chemicals or dusts. The risks are assessed in two phases:

- Phase I – Explosion hazard identification and assessment
- Phase II – Ignition hazard identification and assessment

The first stage of risk evaluation is to identify the explosion hazard. This includes identifying the probability of a combustible dust-air mixture existence. The risk evaluation is prepared following guidelines presented in standard IEC 60300-3-9. The evaluation of the severity of the explosion hazard is done using different matrixes. All the equipment containing explosion risk need to be evaluated separately and included in the EPD. According to the results of the assessment from Phase I and Phase II the possible scenarios are chosen for modelling. This research focuses on the determination and assessment of pressure effects of possible explosions.

2.5.1 Explosion risk assessment – Phase I

The outcome of Phase I is the hazardous area classification. Hazardous areas are classified in ATEX directive 1999/92/EY (APPENDIX I) based on the probability for the occurrence of an explosive mixture. Different hazardous areas are classified for gas and dust explosion atmospheres. For gases, the hazardous areas are identified as zone 0, zone 1 and zone 2, and for dusts the zones are zone 20, zone 21 and zone 22. The dust zones are descripted in **Table III.**

Table III Dust explosion area classification into zones (ATEX 1999/92/EY) and the common appearance (SFS-EN 60079-10-2:2015).

Zone	Presence of dust	Description
20	The presence of combustible dust-air mixture is constant, chronic or often	Inside of ducts and equipment of producing and handling
21	The presence of combustible dust-air mixture is occasionally during normal operation	Areas in the vicinity of zone 20
22	The presence of combustible dust-air mixture is unlikely and short-timed during normal operation	Limited dust spreads in the area from primary dust source

2.5.2 Ignition risk assessment – Phase II

For the areas classified as hazardous, the ignition risk assessment is required according to the Government Decree 856/2012. The assessment includes the identification of possible ignition sources in the area. The possible ignition sources are to be removed from the area or, if not

possible, required safety actions are to be taken to otherwise prevent the ignition possibility or to minimize the possible consequences with protective measures. The possible ignition sources are presented in EN 1127-1:2011 standard, shown earlier in **Table II**.

3 COMBUSTION REACTION

The understanding of the combustion reaction of dust is needed for the possible model assembling. Also, the consequences of dust explosions are a result of the combustion reaction.

3.1 Reaction mechanism

Explosion is an exothermic reaction. In a combustion reaction, the combusting fuel reacts with available oxygen generating oxides and heat. A simplified combustion reaction is presented in **Eq. (2)** (Eckhoff, 2003).

$$fuel + oxygen \rightarrow oxides + heat \quad (2)$$

In real reactions, the oxygen source often contains other gas components as well and thus the reaction generates other reaction products in addition of oxides. In the case of organic combustible dusts containing carbon, hydrogen and oxygen, also known as hydrocarbons, the reaction produces carbon dioxide, water and the remaining gas from the oxygen source. When air is used as the oxygen source, the remaining gas is mainly nitrogen. The general reaction of organic combustion is presented in **Eq. (3)**, where the reactant is a general form of a hydrocarbon and the molar composition of air is assumed to be 79 % of nitrogen (N_2) and 21 % oxygen (O_2) resulting in a mole ratio of 3.76 moles of nitrogen (N_2) to every mole of oxygen (O_2). (Ogle, 2016)

$$C_xH_yO_z + \left(x + \frac{y}{4} - \frac{z}{2}\right)(O_2 + 3.76N_2) \rightarrow xCO_2 + \frac{y}{2}H_2O + 3.76\left(x + \frac{y}{4} - \frac{z}{2}\right)N_2 \quad (3)$$

In the case of inorganic combustible dusts, usually metals, the metal reacts with oxygen source producing metal oxides and a remaining gas phase remaining from the oxygen source. The general reaction of inorganic combustion of metals is presented in **Eq. (4)**, where *M* refers to metal and the gas phase assumption is similar to that in the **Eq. (3)**. (Ogle, 2016)

$$xM(solid) + y(O_2 + 3.76N_2) \rightarrow M_xO_{2y}(solid) + 3.76yN_2 \quad (4)$$

These generalizing reaction equations are valid when the reaction is assumed to be stoichiometric, meaning that all the oxygen and fuel is consumed in the reaction. In reality, this

is rarely the case and the reactions result in other side products and unreacted reactants. The dust-air mixture is fuel-lean if the amount of dust in the mixture is below the stoichiometric concentration and an excess of oxygen is present and fuel-rich if the dust concentration is above the stoichiometric concentration and there is a deficiency of oxygen in the mixture. The limiting reactant in the combustion reaction is the component with concentration below the stoichiometric concentration. (Ogle, 2016, pp. 61) With the increase of fuel in the reaction, the concentration and variety of the side products and unreacted reagents products increases. Also, the adiabatic flame temperature rises with increasing dust concentration and the highest temperature values are usually observed in fuel-rich mixtures. The temperature rise stops at some point as the dust concentration increases too much. (Ogle, 2016, pp. 68)

Dust explosion reaction is usually understood at two different levels, the particle size level and dust cloud level. A single dust particle goes through combustion reaction creating heat and temperature rise. A dust cloud creates an overpressure wave that propagates in the available area. When a particle goes through combustion, heat is released, as can be seen from **Eq. (2)**. The increase of the temperature results in increase in the volume of the gas phase in the dust-air mixture. The volume of the solid particles doesn't increase as significantly. The increase in the volume of the mixture causes the pressure to rise. (Partanen & Partanen, 2010; Proust, 2004) If the reaction area has no limits and the explosion can expand freely, the pressure of the explosion can be assumed to remain constant and the reaction is called *constant pressure explosion*. Flash fire is an example of constant pressure combustion (Ogle, 2016) where the volume of the combustion area is large enough for the overpressure to relieve to the surroundings. In the case of dust explosions, the explosion is limited to a confined area where the pressure rises due to the confined volume. This reaction is referred to as *constant volume explosion*. (Ogle, 2016)

3.1.1 Homogeneous and heterogeneous combustion

The combustion reaction of the particle has two main mechanisms, homogeneous combustion and heterogeneous combustion. Hydrocarbons and other particles with low vaporizing temperature usually go through homogeneous combustion while metals usually go through heterogeneous oxidation on the particle surface. The mass of the metal increases in the reaction since the oxygen forms a layer on the metal surface. The reaction steps of the homogenous

combustion are 1) heating of the particle surface (external heating step), 2) the heat transferring into the particle from the surface (internal heating step), 3) formation of flammable gases, volatiles, due to decomposition of the heated particle (pyrolysis/devolatilization step) and 4) the flammable volatiles exit the particle mixing with the surrounding air leading to homogeneous combustion. (Fumagalli et al., 2016; Fumagalli et al., 2018) A schematic of these combustion reactions is presented in **Figure 6**.

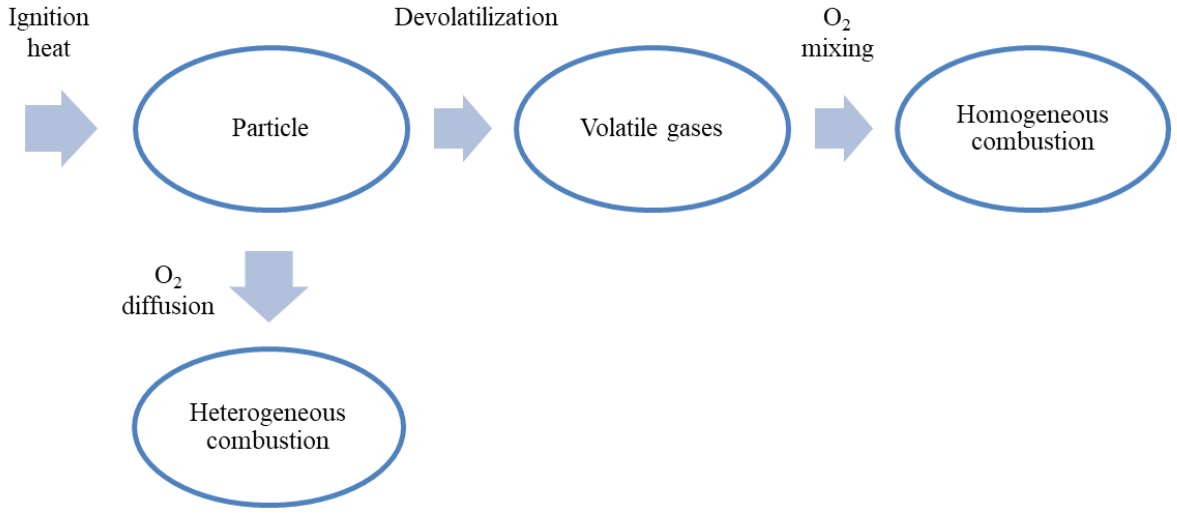

Figure 6 A schematic of heterogeneous combustion and homogeneous combustion (Fumagalli et al., 2016).

The chain of reactions that leads to homogeneous combustion starts with the combustible particle and heat. The ignition heat is introduced to the particle from the outside and eventually the heat is transferred to the inside of the particle. The heated particle then goes through pyrolysis reaction releasing volatiles. The pyrolysis reaction is endothermic reaction and the rate of pyrolysis increases with increasing temperature (Encyclopædia Britannica, 2018). The formed volatiles transfer outwards from the inside of the particle and exit the particle mixing with the surrounding gas phase. The homogeneous combustion occurs at the combustible volatiles-air mixture. Some authors assume the shrinking core model for the particle combustion (Di Benedetto et al., 2010; Dufaud et al., 2010). In the shrinking core model, the radius of the particle is assumed to decrease with time as the reaction proceeds while the density of the particle remains unchanged (Haseli et al., 2013). The volatiles content of the dust particle affects

the explosion parameters by increasing them with increasing volatiles content (Ogle, 2012, pp. 478). Usually, the volatiles formed in the pyrolysis of a hydrocarbon are water, H_2O, carbon monoxide, CO, carbon dioxide, CO_2, and tar. Aside from the volatile gases, char is also produced in the pyrolysis reaction. (Haseli et al., 2011) At high temperatures the char residue can be assumed to consist of only carbon, since the amount of hydrogen and oxygen can be neglected (Haseli et al., 2011).

Heterogeneous combustion occurs on the particle surface. The reaction can be divided into diffusion adsorption/desorption and surface reaction steps. The schematic of heterogeneous combustion was presented by Ogle (2016) and is presented in **Figure 7**.

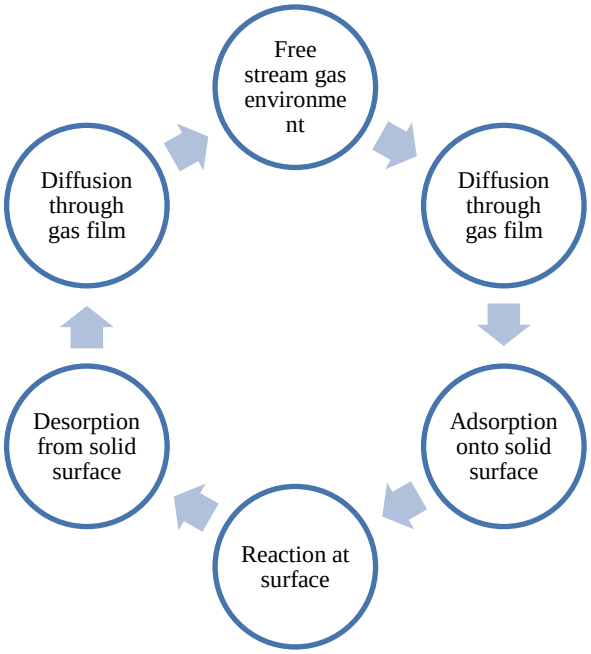

Figure 7 Schematic of heterogeneous combustion of a dust particle (Ogle, 2016, pp. 215).

Kosinski & Hoffmann (2005) presented a mechanism for organic dusts that is more complex. First, the volatiles from the dust particles are mixed in the gas phase and begin to burn. After that, the solid part of the particle ignites and goes through heterogeneous combustion.

Turbulence plays an important role in the combustion reaction. The dust cloud needs to have initial turbulence for the combustible dust-air mixture to form and for the dust particles to stay suspended. In general, a turbulent dust cloud burns faster than a laminar dust cloud but requires

higher ignition temperatures since the turbulence removes the heat from the ignition zone. The combustion of the dust cloud also creates turbulence in the burning dust cloud. In a turbulent burning cloud, a 3-dimensional structure of burnt, burning and unburnt mixture can be observed. (Eckhoff, 2009) The decreasing particle size has been reported to increase the turbulent burning velocity of a dust while the chemical composition didn't have a significant influence (Ogle, 2016, pp. 460).

3.1.2 Reaction rate determining step

For particles larger than the critical particle size, the reaction controlling the overall devolatilization process can be determined by the Biot number *Bi* by comparing the internal and external heat transfer, as shown in **Eq. (5)**.

$$Bi = \frac{t_c}{t_e} = \frac{d\left(h_c \Delta T_i + \varepsilon \sigma \Delta T_i^4\right)}{\lambda \Delta T_i} \tag{5}$$

Where
- t_c time of the internal heat transfer reaction step
- t_e time of the external heat transfer reaction step
- d the dust diameter
- h_c the heat transfer coefficient
- ε the emissivity
- σ the Stefan-Boltzmann constant
- λ the thermal conductivity of the solid
- ΔT_i the temperature difference between particle and surrounding gases

For reactions of Bi $\ll$ 1, the thermal conversion process is controlled by the external heat transfer and the internal heat transfer rate is much faster. For Bi $\gg$ 1 the internal heat transfer controls the reaction and the external heat transfer rate is much faster. (Di Benedetto et al., 2010). The heat transfer times are then compared to the chemical reaction times through the Damköhler number *Da* and the thermal Thiele number *Th*. The *Da* is used for the case of Bi $\ll$ 1 and *Th* for the case of Bi $\gg$ 1. The formulas for computing the *Da* and *Th* numbers are shown in **Eqs. (6)** and **(7)**.

$$Da = \frac{t_e}{t_{pyro}} = \frac{r_p \Delta T_i c_p d}{h_c \Delta T_i + \varepsilon \sigma \Delta T_i^4} \quad (6)$$

$$Th = \frac{t_c}{t_{pyro}} = \frac{r_p c_p d^2}{\lambda} \quad (7)$$

Where t_{pyro} time of the chemical reaction step

r_p pyrolysis reaction rate

c_p specific heat of solid

The reactions are divided into four regimes based on the calculated determination values *Bi*, *Da* and *Th*. The classification of the regimes is explained in **Table IV**.

Table IV The reaction regimes of the combustion reaction determined by the Biot, Damköhler and Thiele numbers (Di Benedetto et al., 2010).

Regime	Comparison	Conversion control
Regime I	Bi $\ll$ 1 & Da $\gg$ 1	Conversion occurs under external heat transfer control
Regime II	Bi $\ll$ 1 & Da $\ll$ 1	Conversion occurs under pyrolysis chemical reaction control
Regime III	Bi $\gg$ 1 & Th $\ll$ 1	Conversion occurs under pyrolysis chemical kinetic control
Regime IV	Bi $\gg$ 1 & Th $\gg$ 1	Conversion occurs under internal heat transfer control

When the reaction controlling the devolatilization process is determined and the regime is known, the pyrolysis reaction time is compared to the time of the combustion reaction by a dimensionless number *Pc* introduced by Di Benedetto et al. (2010), shown in **Eq. (8)**.

$$Pc = \frac{t_{pyro}}{t_{comb}} = \frac{\rho S_l}{r_p \delta_F} \quad (8)$$

Where t_{comb} time of the combustion reaction step

δ_F the flame thickness, usually determined to 1 mm

ρ density

S_l the laminar burning velocity

3.2 Flame propagation

In the dust explosion reaction, the formed flame propagates in the premixed dust-air medium consuming the unburned premixed medium. This phenomenon is called the *flame propagation*. The rate of the combustion reaction is mainly determined by the speed of propagation. As a difference to gas-air mixtures, the dust particles are not mixed with the air at molecular level. The dust flame has heterogeneous structure and a smooth flame front. The velocity of the dust particle and the oxygen are not always the same. (Dobashi, 2017)

In explosions in closed vessels, the flames are propagating from the ignition source from the center of the vessel towards the walls leaving the burnt mixture of gas and particles in the center. Simultaneously, the unreacted particles are transported to the vessel walls. (Ogle, 2016) The flame thickness and burning velocity differs at each time moment when the unreacted particles are pressed against the walls and the concentration in the unreacted mixture increases and the turbulence differs (Dahoe et al., 1996). The maximum temperature of the radial temperature profile is reached at the center (Ogle, 2016). **Figure 8** illustrates the flame propagation in a spherical vessel from the burnt mixture towards the unburnt mixture.

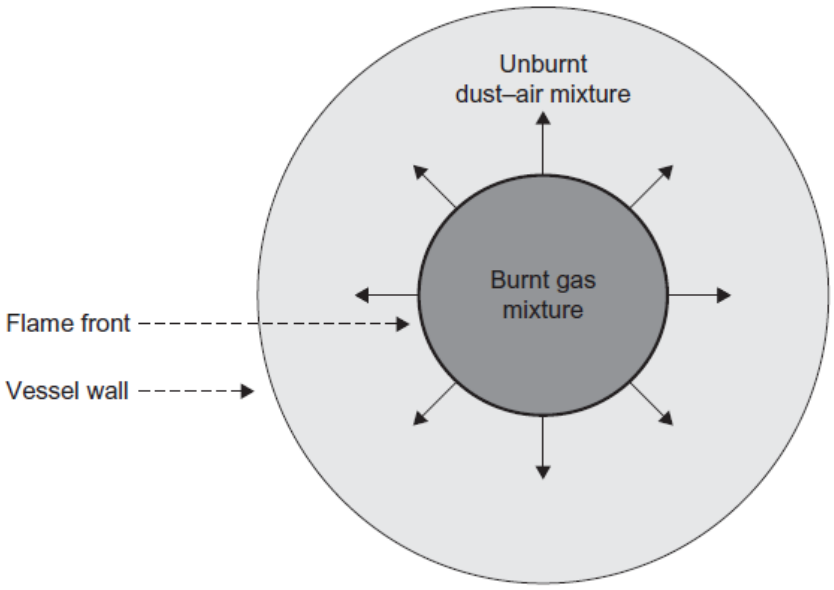

Figure 8 The schematic of spherical flame propagation in a closed vessel (Ogle, 2016, pp. 411).

4 CONSEQUENCES OF DUST EXPLOSIONS

Dust explosions cause overpressure, heat and gases. The generated over pressure forms a shock wave that is received by the walls of the vessel. If the structures surrounding the dust explosion are not designed to withstand the received overpressure the dust explosion results in rupture of the structures and vessel walls. (Ogle, 2016) Shock waves always travel faster than the speed of sound (Ogle, 2016, pp. 112). The severity of dust explosions is often estimated with the parameters deflagration index, also known as the volume-normalized maximum rate of pressure rise, K_{St} and maximum pressure p_{max} (Di Benedetto & Russo, 2007; Amyotte et al., 2012). The maximum explosion pressure is a thermodynamic parameter whereas K_{St} is a kinetic parameter more greatly influenced by particle size and gas admixtures (Amyotte et al., 2012).

4.1 Pressure

The explosion reaction generates overpressure due to expanding gas volume and rising temperature. The explosion pressure p_{ex} increases with time during the explosion reaction and reaches the maximum value p_{max} at the vessel walls. The maximum explosion pressure in a pressure-time curve is presented in **Figure 9**.

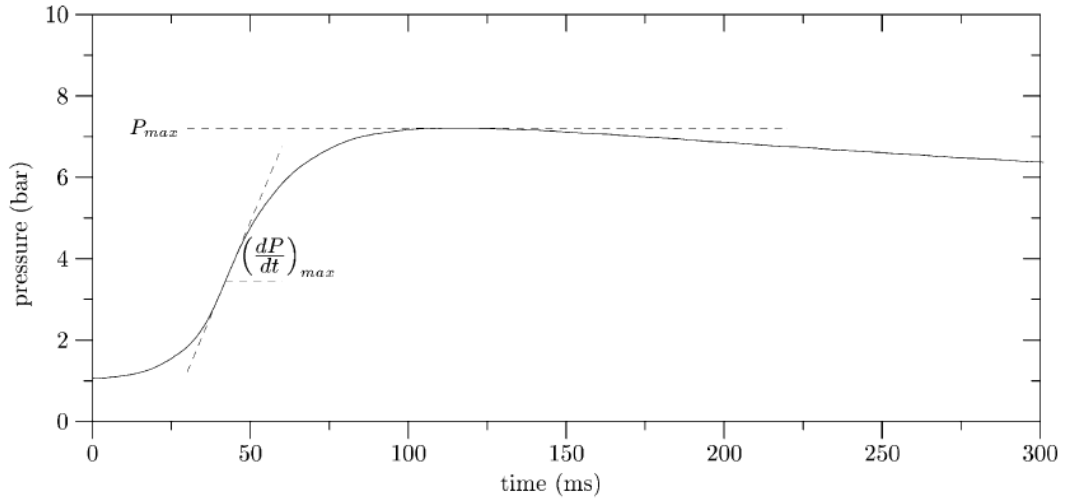

Figure 9 The maximum explosion pressure and maximum rate of pressure rise shown in an explosion pressure-time data (Dahoe et al., 2001).

The rate at which the explosion pressure rises varies also during the reaction and the maximum rate of pressure rise $(\mathrm{d}p/\mathrm{d}t)_{max}$ can be determined from pressure-time data as shown in **Figure 9**. The pressure-time curve tapers off towards the end due to heat losses at the vessel walls and thus the maximum rate of the pressure rise is observed before the maximum explosion pressure in explosion experiments.

The maximum rate of pressure rise is solved mathematically with **Eq. (9)**

$$\frac{\mathrm{d}p}{\mathrm{d}t} = \frac{3(p_{ex}-p_0)}{r_{vessel}} \left[1 - \left(\frac{p_0}{p}\right)^{\frac{1}{\gamma}} \frac{p_{ex}-p}{p_{ex}-p_0}\right]^{\frac{2}{3}} \left(\frac{p}{p_0}\right)^{\frac{1}{\gamma}} S_u \tag{9}$$

Where p_0 the initial pressure in the vessel

r_{vessel} the radius of the spherical vessel

γ the specific heat ratio $C_\mathrm{p}/C_\mathrm{v}$

S_u the laminar burning velocity

When studying the explosion of dust particles, the particles are usually assumed to have very small particle size. In these cases, the combustion is mainly controlled by homogeneous combustion. The product water is assumed to be in gas form due to the high temperatures reached in the combustion reactions. Since the products of the combustion process are mainly gases, the explosion pressure can be defined with the ideal gas equation, shown in **Eq. (10)** (Cashdollar, 2000).

$$pV = nRT \tag{10}$$

The explosion pressure can also be calculated using the adiabatic flame temperature, initial temperature and initial pressure of the mixture. The relationship between these parameters is presented in **Eq. (11)** (Ogle, 2016, pp. 85)

$$p_{\mathrm{ex}} = \gamma p_0 \left(\frac{T_{ad}}{T_0}\right) \tag{11}$$

Where T_{ad} the adiabatic flame temperature

T_0 the initial temperature of the mixture

The equation can also be used to estimate the explosion temperature with existing value of explosion pressure. The temperature value is expected to be less than the adiabatic flame temperature due to heat losses at the walls of the vessel. (Ogle, 2016, pp. 85)

The propagating radial flame is observed to occur in real dust explosion accident scenarios. Even though the mixing in real cases as well as the concentration uniformity is not as ideal as in the test settings, the pressure rise is still observed to be linear in relation to the fraction of burned fuel. This relationship of burn fraction to pressure is expressed in **Eq. (12)** and a similar relationship of burn fraction to temperature is expressed in **Eq. (13)**

$$f = \frac{P - P_0}{P_{ex} - P_0} \tag{12}$$

$$f = \frac{T - T_0}{T_{ex} - T_0} \tag{13}$$

Where f the burn fraction (Ogle, 2016, pp. 87)

4.2 Deflagration index K_{St}

The severity of a dust explosion can be estimated by the volume normalized rate of pressure rise, K_{St}, value. The K_{St} value has also been referred to as the cubic-root law of the rate of pressure rise. It can be calculated as shown in **Eq. (14)**.

$$K_{St} = \left(\frac{dp}{dt}\right)_{max} V^{\frac{1}{3}} = constant \tag{14}$$

Where $(dp/dt)_{max}$ the maximum rate of pressure rise
V the volume of the vessel

Usually, the K_{St} is calculated from dust explosion experiment data where the explosion pressure is presented as a function of time, as shown in **Figure 9**.

The dusts are divided into three explosion classes in SFS-EN 14034-2+A1 depending on the K_{St} value that has been determined for them experimentally. An additional class for non-explosible dusts is also added by some authors (Fumagalli et al., 2016). The dust explosion classes and the K_{St} values that they presented are shown in **Table V**.

Table V The dust explosion classes by the K_{St} value (SFS-EN 14034-2 + A1; Fumagalli et al., 2016).

Dust explosion class [-]	**K_{St} value [bar·m/s]**	**Explosibility [-]**
St 0	0	Non-explosible
St 1	0 - 200	Weak
St 2	200 - 300	Strong
St 3	> 300	Very strong

The K_{St} value reaches its maximum value when the flame thickness is infinitely thin, usually assumed to be 1 mm. The flame thickness is found to be thicker for dust flames than premixed gaseous flames (Ogle, 2016, pp. 422). The peak K_{St} values are also reached for particles of the critical value.

The consequences and parameters of dust explosions are tested in standardized dust explosion experiments according to standards EN 14034-1 + A1 and EN 14034-2 + A1. The standard vessel sizes of the explosion tests are 1 m^3 and 20 L. In the combustion experiments for dust explosions, the ignition is assumed to occur in the center of the vessel and the flame propagates radially. Depending on the ignition point, the forming overpressure can vary depending on the vessel size (Skjold et el., 2005).

Explosion experiments have been conducted for many years determining the K_{St} values and maximum explosion pressures for various dust materials with different properties. The experimental values are widely reported in literature and are also listed in a database GESTIS-DUST-EX. Some researchers have found that the two explosion parameters, K_{St} and p_{max}, are not dependent on the vessel volume and thus the values obtained from standardized experiments can be used in project safety assessment. It has been found though that the test results obtained from 20 liter vessel and the 1 m^3 vessel are not comparable for marginal dusts with K_{St} value estimated lower than 50 bar m/s. For these dusts, the dust cloud might be ignited in the smaller vessel but not in the larger due to energy release and turbulence. (Ogle, 2016, pp. 455)

4.3 Pressure wave

The explosion reaction creates an increasing pressure in the confined area and a pressure wave propagates from the explosion site extending to the surroundings and finally diminishing due to the increasing volume area. In case of dust explosions, the pressure wave is assumed to be a half ball, similarly to sound waves. The peak overpressure of the explosion reaction determines how the pressure wave diminishes into the surroundings. It has been found that the higher the explosion overpressure, the shorter the duration of the explosion pressure wave (Tenitz, 2013). The deflagration index also affects the behavior of the pressure wave. For faster explosion reactions, obtaining higher K_{St} values, the pressure wave propagation is also expected to be faster and fiercer. The pressure wave might effect on shorter distances though if the pressure drops fast.

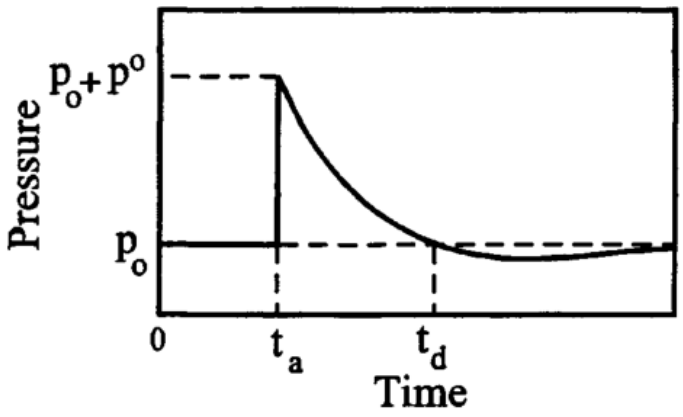

Figure 10 Pressure profile of explosion pressure. The pressure decreases after the peak overpressure and a drop below the ambient pressure is observed at refraction time t_d before the pressure normalized (CCPS, 2000).

When a process equipment explodes, the energy in the system transforms into the expanding shock wave and to kinetic energy to the flying fragments. Different estimates from 40 % to 80 % have been presented as to how much of the system energy is transformed into the shock wave. (CCPS, 2000) For dust explosions, the pressure waves are expected to dissipated faster than with gas explosions.

4.4 Secondary dust explosion

A serious and yet common consequence of a dust explosion is a *secondary dust explosion*. Secondary dust explosion can occur due to poor housekeeping when dust particles are allowed to accumulate to form dust layers. (Ogle, 2016, pp. 94) Secondary dust explosion is a result of the overpressure wave generated in the initial, primary explosion. When the overpressure wave propagates to a secondary location containing combustible dust, the dust is dispersed into air due to the pressure and a new combustible dust-air mixture is created. This new combustible dust-air mixture can ignite due to the released heat from the primary explosion (Abbasi & Abbasi, 2007). A schematic of secondary dust explosion and dust explosion domino effect (DEDE) if shown in **Figure 11**.

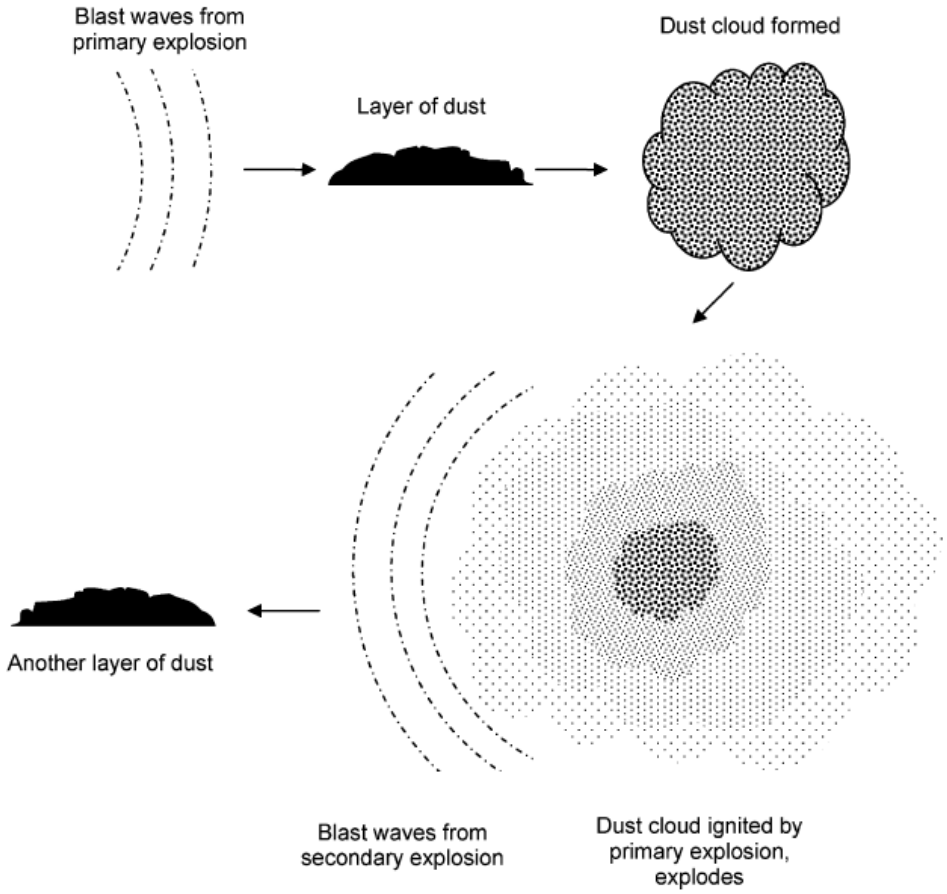

Figure 11 Formation of secondary dust explosion and DEDE hazard (Abbasi & Abbasi, 2007).

If the flame propagation of the primary explosion reaches the secondary dust cloud, the explosion expands creating an even bigger fireball (Ogle, 2016, pp. 94). This is an important notification when considering the possibility or the possible consequences of secondary dust explosions. The secondary combustible dust area might not fulfill the MEC criterion if the dust layer is not thick enough, but the unburnt dust propagated from the primary explosion can add to the amount of combustible dust in the secondary location and can thus create an explosion hazard.

When evaluating the possible explosion pressures of secondary dust explosions, the assumption that the entire dust layer participates in the explosion often results in overestimations of the consequences (Ogle, 2016, pp. 97). The consequences of secondary dust explosions are usually more severe than those of primary dust explosions (Eckhoff, 2003; Ogle, 2016, pp. 94). Secondary dust explosions can also progress to a chain reaction where multiple secondary explosions occur in a process plant resulting in a large-scale dust explosion accident (Kirkwood Community College, 1997). A secondary dust explosion can also occur as a consequence of a gas explosion as is often the case in coal mines where methane causes a gas explosion creating an overpressure that lifts dust layers and pockets creating a combustible dust-air mixture and finally a dust explosion (Amyotte & Eckhoff, 2010).

4.5 Effects on layout design

The explosion consequences are to be considered when designing a new process plant. The effects of the shock wave and the missiles wherever possible are to be known and the process plant to be designed accordingly. The effects of the shock wave are determined by the overpressures in Tukes guide (2015[b]) and the instructions for the placement of equipment and process plants are given accordingly. The description of explosion blast wave effects are shown in **Table VI**.

Table VI Effects of explosion blast waves (Tukes, 2015[b]).

Overpressure [kPa]	Effects on buildings and people	Possible types of structures or buildings
30	Rupture of bearing structures, possibility of expansion of the accident	Industrial equipment and structures
15	Partial ruptures of buildings, risk of permanent injury	Buildings and structures with special approved permission, e.g. pressure resistant industrial equipment
5	Small damages on building structures, possibility of injury	Buildings and areas with people in normal activity

The safety distance from an explosion is determined to be the distance where the overpressure doesn't increase the value of 5 kPa. These areas include places where people are normally present in buildings. The next distance of 15 kPa overpressure causes partial raptures of buildings and the possibility of permanent injury. Buildings and frameworks in this area are accepted with estimated pressure withstanding properties. The strongest shock wave effect area with 30 kPa overpressure causes raptures in buildings and in their bearing structures and gives possibility of expansion of the accident. The effects of shock wave are illustrated in **Figure 12**.

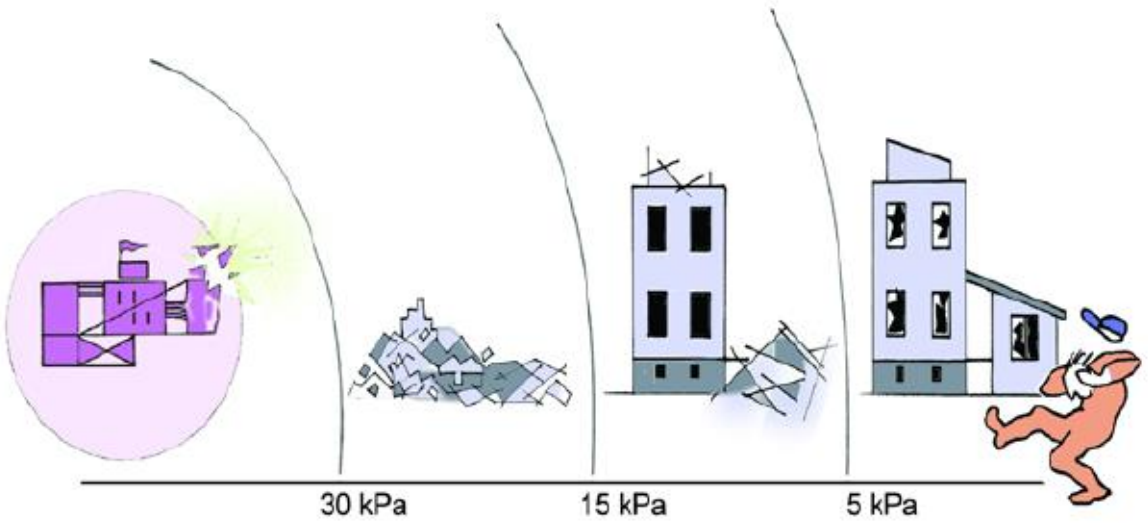

Figure 12 The effects of a shock wave in case of explosions (Tukes, 2015[b]).

The behavior of possible missile due to the explosion is harder to evaluate and it depends on the initial velocities of the worst missiles, the angles of the worst missiles and the air resistance.

The outer barriers of the safety area can be roughly estimated with reasonable accuracy by experiments made on initial velocities. These limitations need to be taken into consideration when designing the layout of a new process plant. Also, the safety of existing process plants can be evaluated by these limits and possible alterations can be made accordingly. (Tukes, 2015[b])

In the layout planning, it is important to design the building containing dust explosion hazard at a distance from other buildings to minimize the effects of possible explosions to other buildings. Also, process parts should be isolated from each other to minimize the possibility of dust explosion spreading. (Eckhoff, 2003, pp. 116) In process engineering and preparing for damages, the worst-case scenario is the safest way to design so that the means are effective enough. This is rarely possible in industry due to high expenses and the impossibility to design such a case so usually a realistic worst-case approach is more suitable. (Skjold, 2006)

4.6 Explosion venting

Process equipment containing explosion hazard can be designed with explosion venting systems. The aim of explosion venting is to reduce the explosion pressure to a level safe for the equipment. Also with explosion venting, the escaping pressure wave can be directed to a chosen direction. In these cases, the area where the explosion is vented to needs to be secured from risk to other equipment and personnel. (SFS-EN 14491:2012) The vent area needs to be designed so that the relieved pressure remaining in the vessel does not exceed the pressure that the vessel can withstand. If the reduced explosion pressure exceeds that pressure, serious damages and even rupturing of the vessel are likely to occur.

The most important parameters in pressure releasing vent design are the static activation overpressure p_{stat} and the venting efficiency of the venting device. The static activation overpressure is the value of overpressure at which the vent opens. The remaining maximum reduced overpressure $p_{red,max}$ in the vessel as well as the length-to-diameter radio *L/D* of the vessel are used when designing the vent area needed to reduce the explosion pressure. (SFS-EN 14491:2012)

Assuming that the equipment can withstand the vented explosion pressure, the escaping pressure wave from the valve has significant consequences. The venting system needs to be directed in

a safe direction avoiding damages to nearby equipment. Also, the releasing area needs to be safe from any personnel. (SFS-EN 14491:2012) The size of the room, where the equipment exist effects on the possible consequences. If the room is significantly larger than the explosion vessel in volume, the relieved explosion pressure can be assumed to attenuate into the room volume. In other cases it is important to separate the room from surrounding areas. (Barton, 2002)

5 MODELLING METHODS

The base of dust explosion modelling is to understand the chemical kinetics and thermodynamics involved in dust explosion reactions. Due to the solid nature of the dust particles, the modelling of dust explosions can be divided into particle combustion, dust cloud combustion and the effects on the surroundings. Many of the modelling methods devoted to dust explosion modelling focus on modelling of the single particle combustion, dust cloud modelling and on determining the explosion parameters p_{max} and K_{St} with accuracy. In this chapter the research of dust explosion modelling found in literature is presented from the past few decades.

5.1 CFD modelling methods

The CFD (computational fluid dynamics) modelling uses numerical solvers to calculate fluid mechanism in even complicated systems and geometries. The popularity of CFD in industrial applications rose in the late 20th century with the increasing research of mathematics related to it and the fast development of computers and software (Ogle, 2016, pp. 569). The increasing popularity has raised the interest of dust explosion researchers to expand the use of CFD in the simulation of dust explosions as well. Most of the work with CFD for dust explosions has occurred in the 21st century and is still an ongoing research area. Probably the most significant research project in this area is the development of a dust explosion simulation code (DESC).

The dust explosion simulation code DESC is a CFD code designed especially for dust explosion modelling. The development of the DESC code has begun in 2002 supported by the European Commission and it has total of 11 participants varying from different universities, institutes to laboratories and other participant. (Skjold, 2007) The first version of the DESC code was released in 2005 (Skjold et al., 2006) and has since been developed. The development of DESC originates from the CFD code FLACS (FLame ACceleration Simulator) intended for gas explosion modelling. The results in the simulations with DESC and FLACS depend on the grids used for the simulations (Skjold, 2014). In the first version of DESC, the modelling was limited to only primary explosions (Skjold et al., 2005) of organic dusts in dust-air mixtures (Skjold et al., 2006). The dust cloud was modelled as a thick gas with a very high molecular weight (Skjold et al., 2005). The Eulerian approach was used to model the particle-laden flow with the limiting case of the Stokes number approaching zero assuming a dynamic and thermal equilibrium

between the dust particles and the gas phase (Skjold et al., 2006). The objective for the future development of the first version of the DESC code was to include the particle settling models as well as the models for dust layer dispersion. This could enable the modelling of secondary explosions as well. (Skjold et al., 2005) The DESC code relies on empirical test results in the standardized 20 L vessel (Skjold, 2007). The parameters such as stoichiometric concentration, adiabatic flame temperature and constant volume pressure have limited use in the simulation of dust explosions since the combustion reaction rarely goes to completion (Skjold et al., 2005).

Other researchers have also exploited the use of CFD in simulating dust explosion phenomenon together with other methods. Di Benedetto & Russo (2007) developed a thermo-kinetic model that assumes the pyrolysis or the devolatilization step to be very fast and the dust explosion is mainly controlled by homogenous gas phase combustion. The model aims to calculate the most conservative values of the explosion parameters p_{ex} and K_{St} using parameter values determined for the critical particle sizes. The laminar burning velocity of the reaction is calculated with a CFD plug-in chemistry solver CHEMKIN that can be incorporated with other CFD software packages (Reaction Design, 2015). The explosion parameters are then calculated with the same basic equations as previously presented in Chapter 3.

5.2 Modelling methods for explosion severity

Many modelling methods have been studied based on the severity of dust explosions. The methods created in the early stages of dust explosion modelling are rather simple compared to methods derived with the development of CFD modelling. Many modelling methods are reported in the literature during 1980's and 1990's, when the models mainly consisted of the explosion parameters of maximum explosion pressure, maximum rate of pressure rise, dust deflagration index and laminar burning velocity (Nagy & Verakis, 1983, cited in Eckhoff, 2003, pp. 294-297). These models neglect the effect of particle size distribution and particle shape on the dust explosion mechanism which have been included in the more recent studies on dust explosion modelling, mainly in CFD modelling.

The combustion of small particles was found to be mainly controlled by homogeneous combustion by Di Benedetto & Russo (2007). By calculating the explosion parameters for particles with lower particle size than the critical size, the received values are conservative and

give the estimation of the worst possible hazard. When calculating the parameters for larger particle sizes, the obtained values are lower and give a prediction of a less hazardous case. When the combustion reaction is controlled by internal heat transfer, the value of the deflagration index is much lower and thus the explosion isn't as severe. (Di Benedetto et al., 2010) In general, the thermodynamic analysis of dust combustion reactions can give the maximum or minimum approximations of the possible consequences (Ogle, 2016, pp. 89).

In many models, the rate of pressure rise is assumed to gain its maximum value when the explosion pressure reaches its maximum value at the end of the explosion reaction. When investigating the plots retrieved from explosion experiments of pressure versus time, it can be seen that the curve slope decreases towards the end. This suggests that the maximum rate of pressure rise is obtained somewhere between the initial and the maximum pressure and not at the maximum pressure when the slope would be closer to zero. The model assumption can be justified with the assumption that no heat loss occurs at the vessel walls and the pressure increases with increasing rate until the maximum pressure value. (Ogle, 2016)

The reliable and accurate dust explosion model should include the turbulence of the flame propagation. (Skjold et al., 2006) Zhen & Leuckel (1997, cited in Fumagalli et al., 2018) presented a formula for the evaluation of turbulent burning velocity through the laminar burning velocity as shown in **Eq. (15)**.

$$S = S_j \left(1 + 3{,}5 \frac{u'^{0.5}}{S_j}\right) \tag{15}$$

Where S_j the laminar burning velocity

u' the velocity fluctuation (Dahoe et al., 2001)

Dahoe et al. (2001) estimated the velocity fluctuation to be 2.68 m/s. The laminar burning velocity of a gas mixture can be calculated utilizing the Le Chatelier's principle, shown in **Eq. (16)**. The laminar burning velocities for some components can be found in literature.

$$S_j = \frac{1}{\frac{x_1}{S_{L,1}} + \frac{x_2}{S_{L,2}} + \frac{x_3}{S_{L,3}} + \cdots} \tag{16}$$

Where x_i the molar amount of component i

$S_{L,i}$ the laminar burning velocity of component i

Other required parameters are the complete geometry, the initial flow field, chemical composition of the dust (and gas phase), location of the ignition source and the possibility of gaining more fuel from dust deposits. (Skjold et al., 2006)

Dust explosion modelling is challenging because of the varying properties and characteristics of the dust particles. Dust particles of the same material may vary in shape, size and chemical properties. In general, models with fewer inputs are easier to handle but give uncertain results. When more inputs are added to a model, the certainty and accuracy of the model increase. It should be noted though, that by adding too many inputs to a model can increase the uncertainty if all the input is not obtainable or determinable. The assumption of the dust particle shape always gives error in the models. The particle size distribution of the dust deposit may also vary during transportation or handling if the material is friable. (Ogle, 2016)

5.2.1 DZLS model

Dahoe et al. (1996) studied dust explosions in closed spherical vessels and created a modelling method referred to as DZLS model, named after the authors Dahoe, Zevenbergen, Lemkowitz and Scarlett. They suggested two models for dust explosion modelling, the thin-flame model and the three-zone model. The schematic of these models is presented in **Figure 13**.

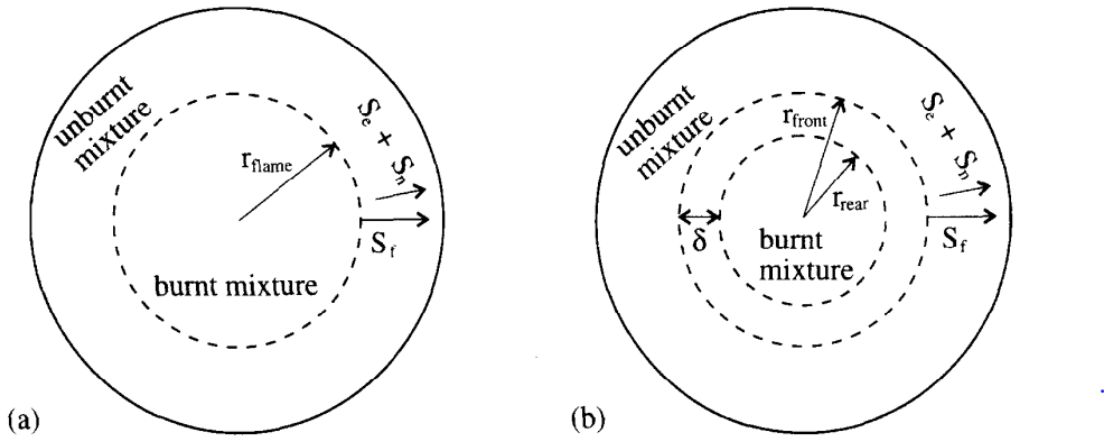

Figure 13 The schematic of (a) thin-flame model and (b) three-zone model of dust explosions where r_{flame} is the location of the flame front, S_e is the expansion velocity, S_n the conversion velocity, S_f the flame speed, δ the flame thickness, r_{front} the radius from the center to the front of the flame and r_{rear} the radius from the center to the rear end of the flame. (Dahoe et al., 1996).

Both models treat the dust-air mixture in the vessel as ideal gases. As a base for the models, Dahoe et al. presented a suitable equation to represent the flame thickness in explosions affected by the changes in the burning velocity and the burning time of the particles, as shown in **Eq. (17)**.

$$\delta = S_u \tau_c \tag{17}$$

Where δ the flame thickness

S_u the burning velocity of the burning zone

τ_c the burning time

In the thin-flame model, the flame thickness is assumed to be infinitely thin and the ignition is assumed to occur at the middle of the spherical vessel. A spherical region of completely burned, reacted mixture occupies the center area of the vessel area and the radius of the flame, r_{flame}, reaches the line of the reacted region. Between the reacted region and the vessel walls is the unburned, unreacted region of the mixture. For this scenario, the equation for the rate of pressure rise is obtained according to **Eq. (11)** presented in Chapter 3.1. The cube-root law of the K_{St} value is retrieved from the thin-flame model assuming the flame thickness to be infinitely thin.

In the three-zone model, the thickness of the flame is studied as it changes during the combustion reaction. The flame region is where the continuous transition from completely unburnt to burnt mixture takes place. The calculation process for the explosion pressure and the maximum rate of pressure rise follows several complex integral formulas. The explosion reaction is divided into three phases representing the different phases of the flame propagation. The first phase represents the start of the explosion reaction where the flame front moves towards the walls of the vessel and the tail of the flame region remains at the center of the vessel. In the second phase, both the flame front and the tail propagate towards the walls of the vessel. The third phase is achieved when the flame front reaches the walls of the vessel. The maximum rate of pressure rise for these phases is derived from **Eq. (18)**

$$\frac{\mathrm{d}p}{\mathrm{d}t} = -\frac{(p_{ex}-p_0)\left(\frac{p}{p_0}\right)^{\frac{1}{\gamma}}}{V_{vessel}\left[1+\frac{1}{\gamma}\frac{p_{ex}-p}{p}\right]}\frac{d}{dt}\iiint_{V_{fl}} f(r)\mathrm{d}V \tag{18}$$

Where *f(r)* scalar function of location *r* and time *t*

The integral part on the right-hand side of **Eq. (18)** varies for each phase and thus the rate of pressure rise is determined for each phase. The rate of pressure rise for the first phase is shown in **Eq. (19)**, for the second phase in **Eq. (20)** and for the third phase in **Eq. (21)**.

$$\frac{\mathrm{d}p}{\mathrm{d}t} = -\frac{(p_{ex}-p_0)\left(\frac{p}{p_0}\right)^{\frac{1}{\gamma}} 4\pi S_u\left[\frac{r_{front}^3}{3\delta}+r_{front}^2\right]}{V_{vessel}\left[1+\frac{1}{\gamma}\frac{p_{ex}-p}{p}\right]} \tag{19}$$

$$\frac{\mathrm{d}p}{\mathrm{d}t} = -\frac{(p_{ex}-p_0)\left(\frac{p}{p_0}\right)^{\frac{1}{\gamma}}}{V_{vessel}\left[1+\frac{1}{\gamma}\frac{p_{ex}-p}{p}\right]} \cdot 4\pi S_u\left[\frac{r_{front}^3}{3\delta}-\frac{4r_{rear}^3}{3\delta}+r_{front}^2+\left(\frac{r_{front}}{\delta}-1\right)r_{rear}^2\right] \tag{20}$$

$$\frac{\mathrm{d}p}{\mathrm{d}t} = -\frac{(p_{ex}-p_0)\left(\frac{p}{p_0}\right)^{\frac{1}{\gamma}}}{V_{vessel}\left[1+\frac{1}{\gamma}\frac{p_{ex}-p}{p}\right]} \cdot 4\pi S_u\left[\frac{4R_{vessel}^3}{3\delta}-\frac{r_{rear}^3}{3\delta}-\frac{r_{rear}R_{vessel}^2}{\delta}\right] \tag{21}$$

The final cube-root law can be calculated for each phase with the determined rates of pressure rise.

5.2.2 Reaction-balance-based model

Calle et al. (2005) presented a mathematical modelling scenario for the calculation of the explosion pressure through various calculation steps. The first part concerns the reaction balance of the reactants and calculates the reaction rate constant *k* through Arrhenius equation. The reaction temperature is solved from thermal balance equations and finally the explosion pressure is solved from the ideal gas equation assuming the products of the combustion reaction and the reactants of the explosion reaction to be gases. The equations for the model as well as a schematic for the use of the equations are presented below in **Eqs. (22)-(32)** and in **Figure 14.**

The reaction balance of a hydrocarbon can be given according to **Eq. (22)**

$$0 = r \cdot V + n_{\mathrm{C},0} \frac{\mathrm{d}(1-X)}{\mathrm{d}t} \tag{22}$$

Where
- r the reaction rate
- $n_{\mathrm{C},0}$ the initial amount of carbon in the hydrocarbon in moles
- X the conversion rate of the combustible

The reaction rate can be calculated from the concentrations of the reactants according to **Eq. (23)**

$$r = k \cdot \left[C_x H_y O_z\right] \cdot [O_2] = k \cdot n_{\mathrm{C},0} \cdot \frac{(1-X)}{V} \cdot \frac{\left(n_{\mathrm{O}_{2,0}} - x \cdot X \cdot n_{\mathrm{C},0}\right)}{V} \tag{23}$$

Where
- k the reaction rate constant
- V the volume of the vessel
- $n_{\mathrm{O2},0}$ the initial amount of oxygen in moles
- x the mole amount of carbons in the hydrocarbon

The reaction rate constant is calculated with the Arrhenius equation, shown in **Eq. (24)**

$$k = A \cdot \exp\left(-\frac{E_{\mathrm{A}}}{RT}\right) \tag{24}$$

Where
- A the pre-exponential factor
- E_{A} the activation energy of the reaction
- R the gas constant

The pre-exponential factor *A* has different values depending on the particle size of the combustible. By changing the value to represent a specific size, the model can be used to take into account the particle size of the dust.

$$X(t+\mathrm{d}t) = \frac{n_{O_2,0} \cdot F_X(t) - E(t)}{x \cdot n_{C,0} \cdot F_X(t) - E(t)} \tag{25}$$

Where

$$F_X(t) = \frac{1 - X(t)}{n_{O_2,0} - x \cdot n_{C,0} \cdot X(t)} \tag{26}$$

and

$$E(t) = \exp\left[\frac{\left(n_{O_2,0} - x \cdot n_{C,0}\right) \cdot k(t)}{V} \cdot \mathrm{d}t\right] \tag{27}$$

Where *x* the mole amount of carbon in the hydrocarbon

The total amount of reactants in the reaction at time *t* is given in **Eq. (28)**

$$n(t) = n_{\mathrm{O_2}} + n_{\mathrm{CO_2}} + n_{\mathrm{H_2O}} + n_{\mathrm{N_2}} = n_{\mathrm{O_2},0} + n_{\mathrm{N_2},0} + z \cdot X(t) \cdot n_{\mathrm{C},0} \tag{28}$$

Where *z* the mole amount of oxygen in the hydrocarbon

The model calculates the reaction temperature through thermal balance calculations following **Eqs. (29)** and (**30).**

$$[X(t+\mathrm{d}t) - X(t)] \cdot n_{\mathrm{C},0} \cdot \Delta H_{\mathrm{r}}(t) = \sum_{\mathrm{gas},i}\left[n_i \cdot C_{\mathrm{p},i}\left(T(t)\right)\right] \cdot [T(t+\mathrm{d}t) - T(t)] \tag{29}$$

$$\Delta H_{\mathrm{r}}(t) = \Delta H_{\mathrm{r},0} + \int_{T(t)}^{0} \sum_i v_i \cdot C_{\mathrm{p},i}(T) \cdot \mathrm{d}T + \int_{0}^{T(t)} \sum_i v_j \cdot C_{\mathrm{p},j}(T) \cdot \mathrm{d}T \tag{30}$$

Where
- ΔH_{r} the reaction heat per mole of combustible
- C_{p} the specific heat of gas
- v the stoichiometric coefficient
- i, j refer to the reactants

The specific heat of each gas is calculated with **Eq. (31)**

$$C_p = a + b \cdot T + c \cdot T^2 + d \cdot T^3 \tag{31}$$

Where *a*, *b* and *c* parameters that can be found in literature for each component

Table VII Gas parameters for the calculation of specific heat as a function on temperature (CRC, 1986).

Gas	a	b	c	d
O_2	27.035	$7.337 \cdot 10^{-3}$	$-2.350 \cdot 10^{-6}$	$3.120 \cdot 10^{-10}$
N_2	28.723	$0.338 \cdot 10^{-3}$	$2.110 \cdot 10^{-6}$	$-6.000 \cdot 10^{-10}$
CO_2	30.189	$27.224 \cdot 10^{-3}$	$-1.150 \cdot 10^{-5}$	$1.880 \cdot 10^{-9}$
H_2O	32.304	$2.485 \cdot 10^{-3}$	$2.790 \cdot 10^{-6}$	$-7.45 \cdot 10^{-10}$

Through solving *n* and *T* for the reaction, the final pressure at time *t* can be solved from the ideal gas equation according to **Eq. (32)**

$$p = \frac{nRT}{V} \tag{32}$$

The calculation can be computed for several steps using the values obtained from the previous step as initial data for the next one finally reaching the maximum explosion pressure. The calculation procedure for the first two steps is shown in **Figure 14**.

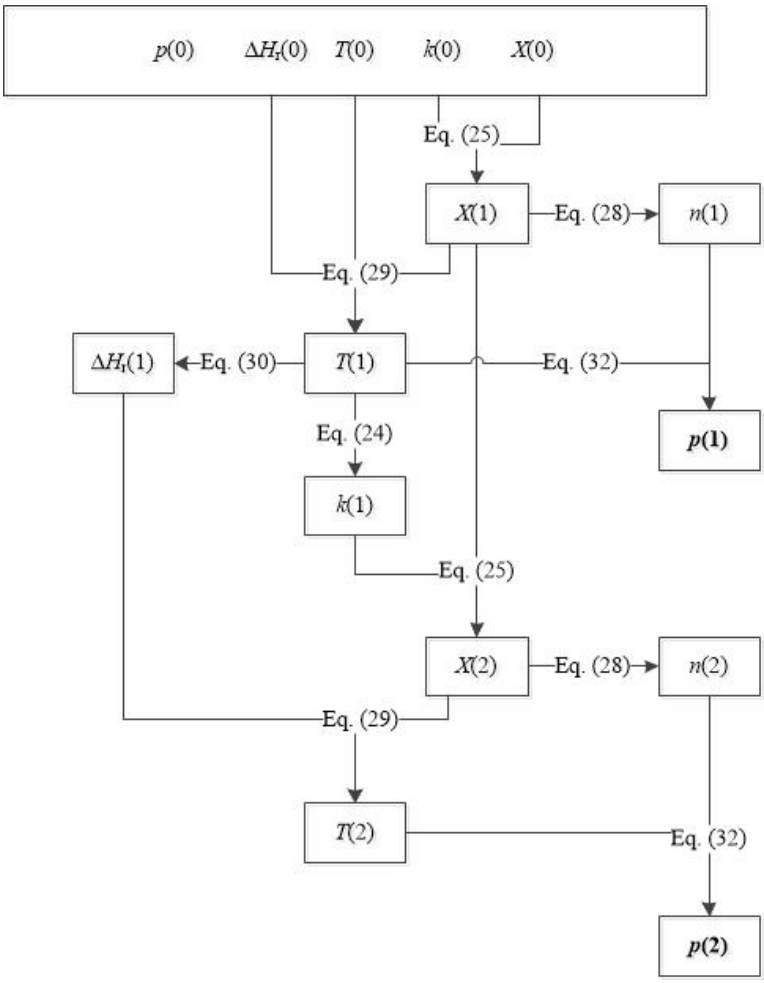

Figure 14 The calculation procedure for the calculation of explosion pressure (Callè et al., 2005).

The authors tested the model on three different particle sizes of cellulose and received good agreement of the model calculations when compared to experimental values. The comparison of the modelled and tested values is shown in **Figure 15**, where the markers show the experimental values and the lines the modelled values.

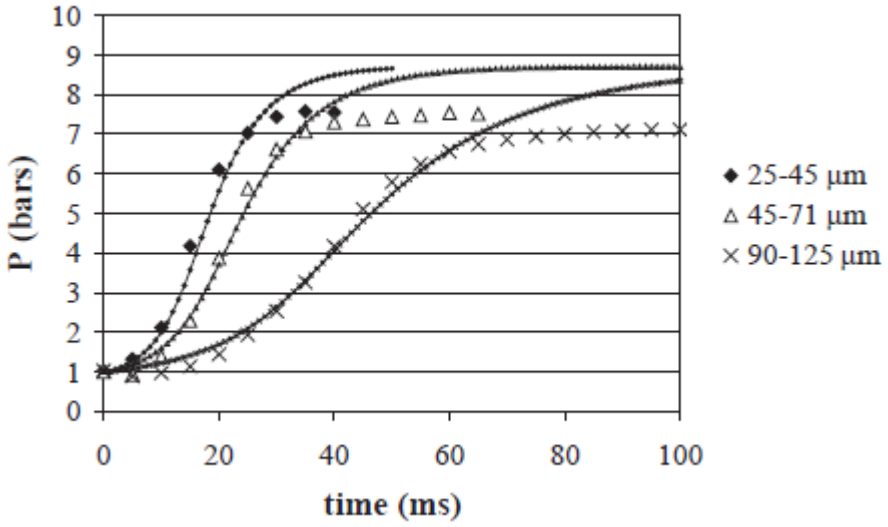

Figure 15 Comparison of modelled values (lines) and tested values (markers) of cellulose dust explosion data of three different particle sizes by Callè et al. (2005).

5.2.3 Integral models

Ogle (2016) presented two different integral models for dust explosions with which the explosion severity through the K_{St} value can be estimated. The first model was formulated by Bradley and Mitcheson (1976) and the model is referred to as BM model. The BM model assumes uniform concentration distribution of the dust in the vessel, ignition at the center of the vessel, rigid, adiabatic and impermeable walls, constant mixture heat capacity ratios, ideal gas equation, thin-flame situation and the laminar burning velocity is assumed to be constant. The K_{St} value is calculated with **Eq. (33)** following the BM model assumptions.

$$K_{St}(BM) = \left(\frac{\mathrm{d}p}{\mathrm{d}t}\right)_{\max} V^{1/3} = (36\pi)^{1/3}\,(p_{ex} - p_0)\left(\frac{p_{ex}}{p_0}\right)^{1/\gamma_u} S_u \tag{33}$$

The other model was introduced by Nagy, Conn and Verakis, referred to as NCV model, and it assumes the compression to be isothermal instead of adiabatic and thus derived **Eq. (34)** for the K_{St} value.

$$K_{St}(NCV) = \left(\frac{\mathrm{d}p}{\mathrm{d}t}\right)_{\max} V^{1/3} = (36\pi)^{1/3}\left(\frac{p_{ex}}{p_0}\right)(p_{ex} - p_0)S_u \tag{34}$$

In **Figure 16** the different pressure-time curves from the BM and NCV models are shown together with experimental data. As can be seen from the picture, the models assume the highest

rate of pressure rise when the explosion pressure reaches its maximum value while in the experiment the rate of pressure rise decreases towards the maximum explosion pressure due to heat loss through the vessel walls which is neglected in the models.

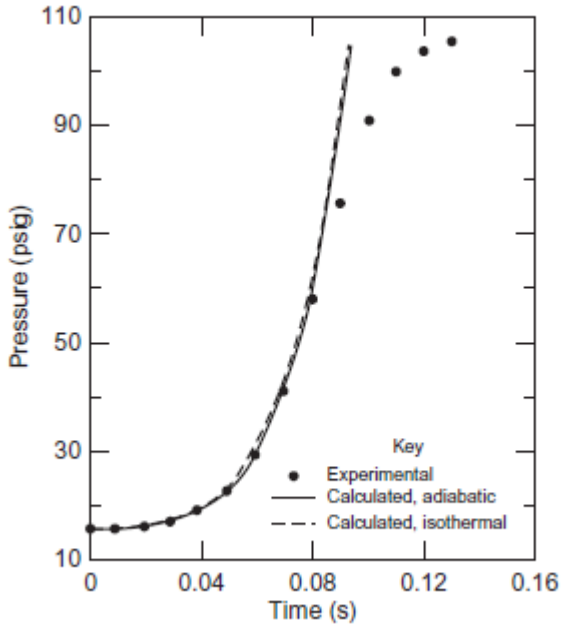

Figure 16 Comparison of adiabatic (BM) and isothermal (NCV) models against experimental data (Ogle, 2016, pp. 450).

5.3 Modelling methods for overpressure effects on the surroundings

The models designed for dust explosion modelling focus mainly on determining the explosion pressure and the deflagration index. When these parameters are known, the effects of the pressure shock wave on the surroundings are of interest. The change of pressure at different distances can be derived from the basic formula of pressure **Eq. (35)**

$$p = \frac{F}{A} \tag{35}$$

Where F the force

A the area where the force focuses on

The generating pressure wave can be understood as a half ball propagating from the ignition center. Assuming the explosion to contain the same amount of force on a larger area, a simple proportional equation can be obtained as shown in **Eq. (36)**.

$$p_1 A_1 = p_2 A_2 \tag{36}$$

The maximum pressure of the explosion is reached at the surface area of the initial dust cloud and in the pressure wave, the pressure is assumed to focus on the surface area of the ball wave. Therefore, the relationship of the radius of the surface area of the dust cloud and the expanding pressure wave at different pressure values is calculated using the surface area equation of a half ball according to **Eq. (37)**.

$$p_1 2\pi r_1^2 = p_2 2\pi r_2^2 \tag{37}$$

Where r the radius of the area

From this equation, the distance at which a certain pressure can be expected can be calculated according to **Eq. (38)**

$$r_2 = \sqrt{\frac{p_1}{p_2}} r_1 \tag{38}$$

For dust explosions occurring inside process equipment, the initial dust cloud volume is substituted to also assume the shape to be a half ball. The comparison can thus be calculated with the radius determined for a half ball with the same volume as the initial equipment. This is illustrated in **Figure 17 a)** and **b)**.

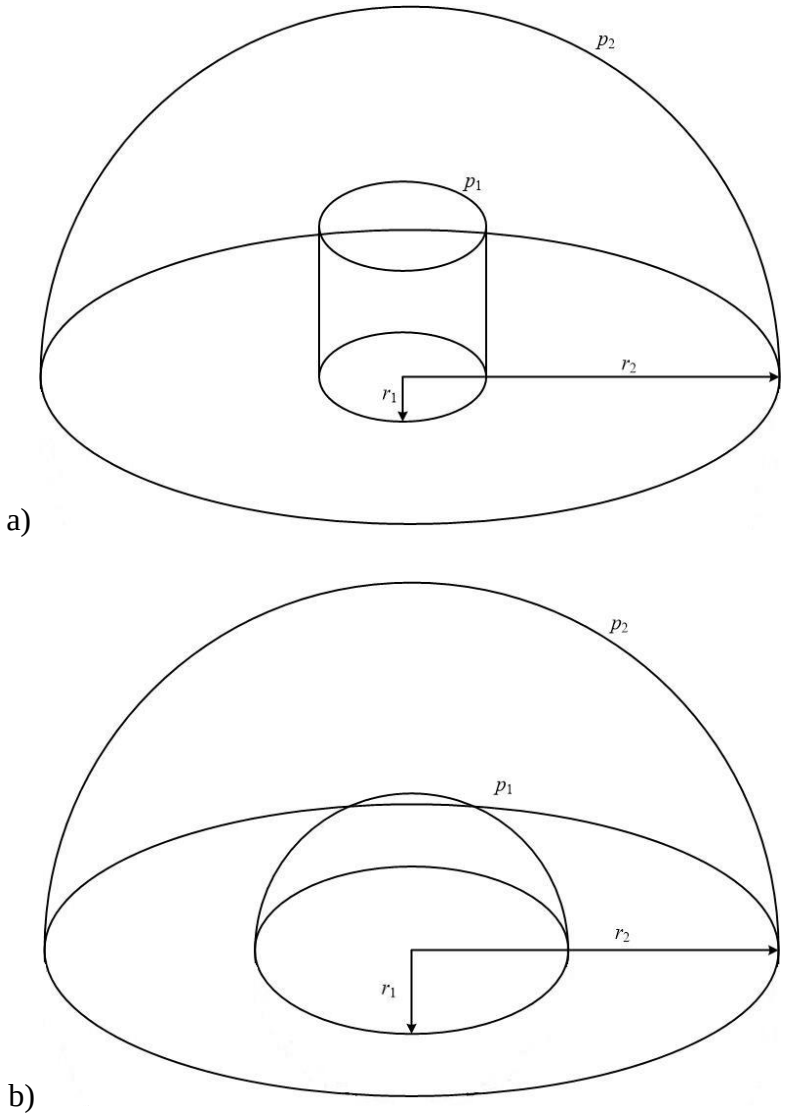

Figure 17 Schematic of a) cylindrical process equipment and the ball pressure wave expanding from it and b) the volume of the process equipment is transformed to equal the half ball shape of the pressure wave.

There are many methods used for the evaluation of the pressure as a function of distance from the explosion site.

5.3.1 TNT model

The TNT model, also referred to as TNT equivalence model, is a method that has been used to evaluate the blast effects of explosions for many centuries. The model parameters have been determined with experiments and the model is based on the calculation of the equivalent mass of TNT transformed to the explosion energy.

$$W = \frac{\eta \cdot m_{HC} \cdot E_c}{E_{TNT}} \tag{39}$$

Where W the equivalent mass on TNT

η an empirical explosion efficiency

m_{HC} the mass of hydrocarbon

E_c heat of combustion of the flammable gas

E_{TNT} the heat of combustion of TNT

E_{TNT} is usually 4437 – 4765 kJ/kg. The explosion efficiency is assumed to be lower for explosions where the total quantity of explosive is released whereas higher explosion efficiency is reached with dispersed clouds (CCPS, 2000). The distance R from the explosion center is calculated with the scaled distance Z as shown in **Eq. (40)**.

$$Z = \frac{R}{W^{\frac{1}{3}}} \tag{40}$$

The scaled overpressure p_s is calculated with the explosion overpressure and initial pressure as shown in **Eq. (41)**.

$$p_s = \frac{p_{ex}}{p_0} = \frac{p - p_0}{p_0} = \frac{p}{p_0} - 1 \tag{41}$$

The scaled overpressures against scaled distance are read from curve presented in **Figure 18**.

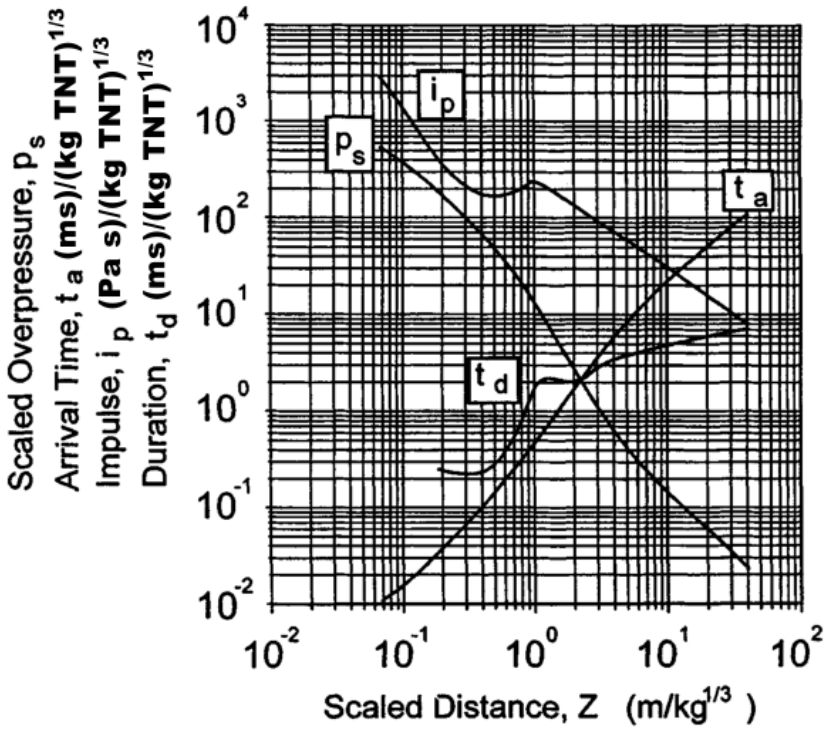

Figure 18 TNT equivalent model curves of side-on overpressure vs. scaled distance where p_s is the scaled distance, Z the scaled distance, t_a arrival time, t_d duration and i impulse. (CCPS, 2000).

The main source of error in the TNT model is the estimation of the explosion efficiency (CCPS, 2000) which has many different interpretations.

5.3.2 TNO multi-energy model

The TNO multi-energy model (TNO MEM) is a similar estimation method to the TNT model specifically developed for gas explosions. The original multi-energy model (MEM) was developed based on the TNT model. The new parameter values were updated to the model by the Netherlands Organisation for Applied Scientific Research (TNO) thus creating the TNO MEM model and a set of blast curves. The main assumption in the TNO MEM is that the congestion affects strongly the energy of the explosion rather than the fuel in the cloud which has less of an effect. The pressure wave is assumed to have the shape of hemisphere.

The peak side-on overpressure of the explosion is calculated using Sachs-scaled overpressure $\overline{P}$ according to **Eq. (42)**. The Sachs-scaled distance $\bar{R}$ from the ignition point is presented in **Eq. (43)** and the explosion impulse $\bar{i}$ in **Eq. (44)**.

$$\overline{P} = \frac{p - p_0}{p_0} \tag{42}$$

$$\bar{R} = \frac{R}{(E_t/p_0)^{\frac{1}{3}}} \tag{43}$$

$$\bar{i} = \frac{i a_0}{E_t^{1/3}\, p_0^{2/3}} \tag{44}$$

Where $\overline{P}$ the Sachs-scaled dimensionless overpressure

$\overline{R}$ the Sachs-scaled dimensionless distance from the explosion center

E_t the total energy release from the explosion source

$\bar{i}$ the dimensionless impulse

a_0 the acoustic velocity at ambient conditions

The total amount of energy released from the explosion source is calculated as in **Eq. (45)**

$$E_T = V_p \cdot E_V \tag{45}$$

Where V_p the volume of the burning cloud

E_V the combustion energy of the stoichiometric gas-air mixture

For most hydrocarbons E_V = 3.5 MJ (Harris, 1983, cit. CCPS, 2000). The scaled overpressures are presented against the scaled distances in **Figure 19**, where the different curves present different explosion strengths.

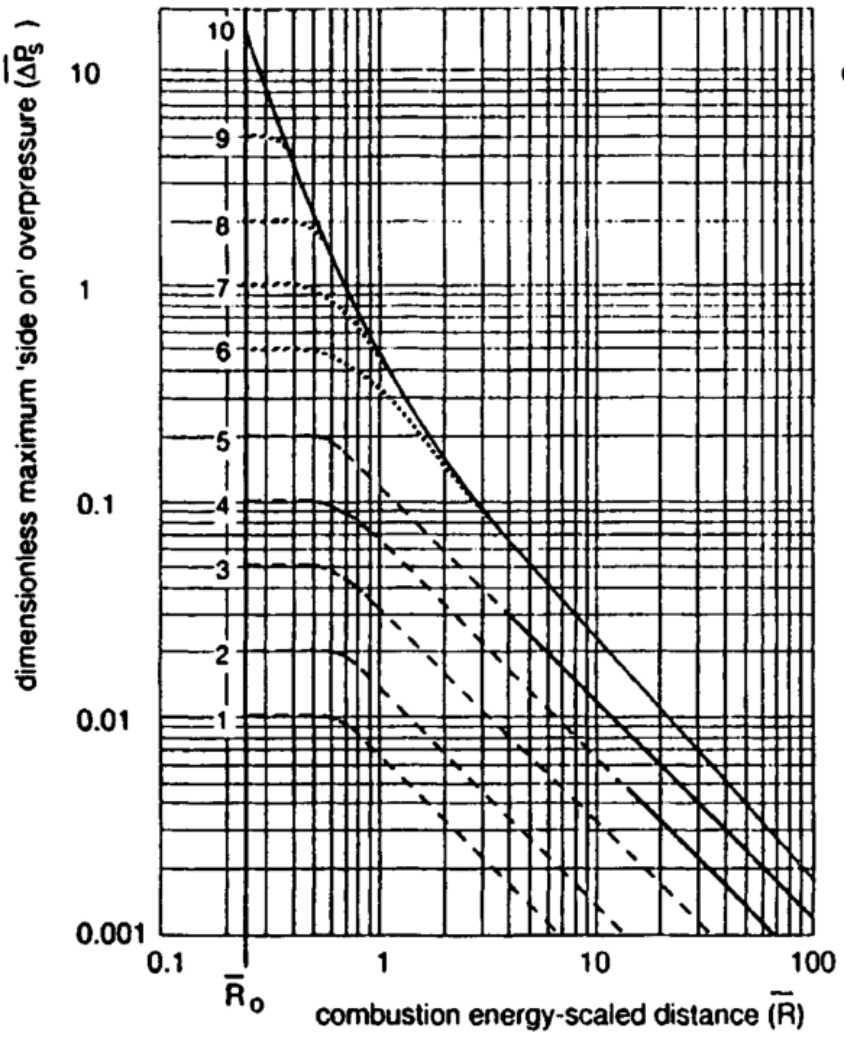

Figure 19 The scaled overpressure curves against the scaled distance from charge where $\overline{\boldsymbol{P}}$ is the scaled overpressure and $\overline{\boldsymbol{R}}$ the scaled distance (CCPS, 2000).

5.3.3 BST model

The Baker-Strehlow-Tang (BST) model was developed based on the TNO MEM model. Their assumption of the cloud shape is spherical. The BST model uses blast curves to determine pressures and distances from the explosion center determined with flame speed calculations unlike the TNO MEM model. The explosion pressure and the distance from the explosion center are expressed as dimensionless parameters. The parameters for the BST model can be calculated with **Eqs. (42)-(44)** and a set of blast curves, shown in **Figure 20**. (Sari, 2010; Tang & Baker, 1999) With BST model, for explosions occurring near ground level the total available energy E_T is multiplied by two to consider the reflection on the ground, as shown in **Eq. (46)**.

$$E_T = 2 \cdot V_p \cdot E_V \tag{46}$$

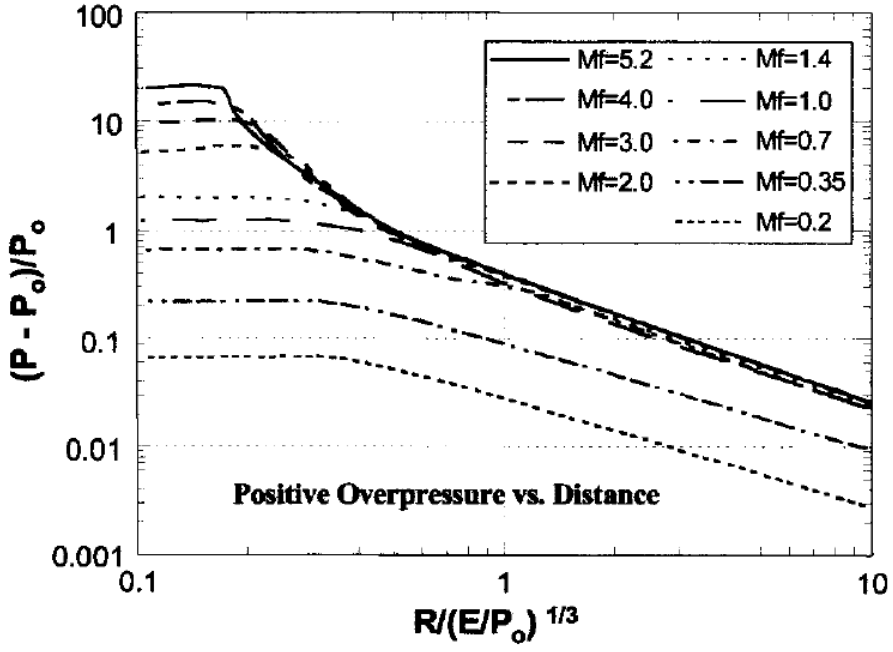

Figure 20 BST model blast curves for positive overpressures where P is the explosion pressure, P_0 the ambient pressure, R the distance from the explosion center, E the explosion energy and M_f the explosion strength (Tang & Baker, 1999).

The explosion strength is presented as an apparent flame Mach number M_f which is fixed relative to the observer. The relation of M_f to the Langrangian velocity Mach number M_w for near sonic flames is described in **Eq. (47)**

$$M_f = \left(\frac{\rho_u}{\rho_b}\right)^{1/3} M_w \tag{47}$$

For supersonic waves, the following relationship is valid, shown in **Eq. (48)**

$$M_f = M_w \tag{48}$$

5.3.4 Pressure release from vented vessels

The standard EN 14491 gives guide on sizing of dust explosion vents. The pressure effects of dust explosion outside the vented enclosure can be calculated with **Eq. (49)**

$$p_{ext,max} = 0.2 \cdot p_{red,max} \cdot A_V^{0.1} \cdot V^{0.18} \tag{49}$$

Where $p_{ext,max}$ the maximum external overpressure
$p_{red,max}$ the maximum reduced explosion overpressure
A_V the geometric vent area
V the volume of the vessel

The distance where the maximum external overpressure can be expected can be calculated with **Eq. (50)**

$$R_S = 0.25 \cdot L_F \tag{50}$$

Where L_F the flame length

The flame length is calculated with **Eq. (51)** for horizontal flames and with **Eq. (52)** for vertical flames.

$$L_F = 10 \cdot V^{1/3} \tag{51}$$

$$L_F = 8 \cdot V^{1/3} \tag{52}$$

The external overpressure decreases with distance according to **Eq. (53)**

$$p_{ext,r} = p_{ext,max} \cdot \left(\frac{R_S}{r}\right)^{1.5} \tag{53}$$

Where r the distance measured from the venting area and $r > R_S$

The external overpressure at any given distance can be calculated with **Eq. (54)**

$$p_{ext,r} = 1.24 \cdot p_{ext,max} \cdot \frac{\left(\frac{D}{r}\right)^{1.35}}{1+\left(\frac{\alpha}{56}\right)^2} \tag{54}$$

Where D the hydraulic diameter of the vent
α defines the direction towards the vent

When the direction is in front of the vent area, $\alpha = 0°$ and sideways $\alpha = 90°$. (SFS-EN 14491)

6 TESTING OF MODELLING METHODS

The testing of dust explosion modelling methods was divided into two parts, modelling methods for explosion severity and for overpressure effects. The modelling methods for explosion severity for various materials were tested and compared against data derived from the GESTIS-DUST-EX database. The modelling methods for overpressure effects were tested against available accident data. Consequence analysis was also computed for three process scenarios with the chosen modelling methods to test the usability of the models for possible client cases. Simulation results computed with a CFD STAR-CCM+ software were also received for the client cases as a comparison data. The testing focuses on organic dusts since they are the most common dusts handled in industry in Finland.

6.1 Choosing of modelling methods

The reaction balance based (RBB) model for the explosion severity calculation by Callè et al. (2005) (Chapter 5.2.2) was tested for the evaluation of the explosion overpressures for various organic dust materials. The needed input for the model is rather well available in the literature for various materials, apart from the Arrhenius equation parameters. The input for the Arrhenius equation provided by the authors was used for all calculations. Since the Arrhenius equation parameters were fitted against experimental data, the reliability of those parameters is uncertain. Thus, a simplified calculation method utilizing the same main principle of calculation was developed dismissing the Arrhenius equation.

The two expansion models for gas explosions, TNO multi-energy and Baker-Strehlow-Tang models, were tested for the use in overpressure effect estimations in the case of dust explosions. The TNT model was chosen for testing due to the solid form of TNT in the model. The models were expected to have limitations in this application, but the relative accuracy was of interest. The disproportional calculation for distance evaluation was also utilized in comparison with the other models. The models were calculated against accident data from two major dust explosion accidents that occurred in the United States. The chosen modelling methods for testing are collected into a process chart shown in **Appendix I**.

6.2 Execution of calculations

The calculations were conducted following the principles of the modelling methods presented earlier in Chapter 5. The specific parameter values and assumptions chosen for the specific cases in the calculations are presented in more detail.

6.2.1 Calculation of explosion severity

The calculations for explosion severity with the reaction-balance-based (RBB) model were conducted for nine different hydrocarbons, each consisting of carbon, hydrogen and oxygen, except for graphite (C). The calculations followed the procedure presented in Chapter 5.2.2 in **Eqs. (22)-(32)**. In the calculation the amount of hydrocarbon in the system was derived from the original study. The authors of the original study, Callé et al. (2005), found that in the 20 L vessel, the highest overpressure values for tested cellulose dust were obtained with dust mass of 14.6 g. This amount equals 3.5 times the stoichiometric amount of cellulose dust resulting in concentration amount of 4.5 g/m^3. This value is in good agreement with literature stating that the maximum overpressure is usually reached at three of higher times of the stoichiometric concentration, as stated earlier in Chapter 2.1. The calculations with this model were conducted with the concentration value of 4.5 g/m^3 resulting with conservative values for the explosion severity. The equipment was assumed to be completely occupied by the dust cloud and the ignition point assumed at the center of the vessel.

The chosen hydrocarbons have simple chemical formulas and were chosen from different functional groups. The chemical and thermal properties of the tested hydrocarbons are presented in **Appendix II**. An example of the initial parameter values for cellulose, $C_6H_{10}O_5$, is shown in **Table VIII**.

Table VIII The initial parameter values used in the calculations of explosion severity of cellulose with the RBB model.

m [g]	M [g/mol]	V [m^3]	E_A [J/mol]	A [dm^3/mol s]	ΔH_r [kJ/mol]	T_0 [K]	p_0 [kPa]
14.6	162.14	0.02	9000	12000	1746.46	298	100

The Arrhenius parameters determined for the model are fitted to agree the experimental results obtained by the authors, Callé et al. (2005). The material used in the experiments contained 40 % moisture and thus the fitted parameters also apply for wet materials. For further use of the model, new parameters values should be obtained to apply for other conditions as well. The change in the pre-exponential factor *A* in the RBB model affected the explosion pressure only slightly but it had a stronger effect on the reaction time. When increasing *A* from 12 000 $dm^3/mol \cdot s$ to 1 200 000 $dm^3/mol \cdot s$, the explosion pressure rose from 7.05 bar g to 7.22 bar g but the reaction time changed from 3.0 ms to 0.6 ms.

Due to the uncertainty of the Arrhenius equation parameters, a simplified version of the RBB model was made and tested. In the simplified RBB model, the reaction rate is ignored, and the calculation procedure follows **Eqs. (28)** – **(32)**. The simplified model requires an assumption of the reaction conversion. The calculations were conducted with three different conversion assumptions. First, the reaction overpressure was calculated for stoichiometric combustion reaction with conversion value of 1. This calculation provides the theoretical maximum value of the explosion overpressure. Next, the mass of the hydrocarbon was set to be 3.5 times of the stoichiometric amount and the conversion and overpressure values were solved for the time when all the oxygen in the system had reacted. Finally, the concentration of 4.5 g/m^3 of hydrocarbon was used in the calculations as a comparison for the previous assumption and the conversion and overpressure values were solved similarly.

6.2.2 Calculation of overpressure effects

The calculations of the overpressure effects were conducted following the modelling methods presented in Chapter 5.3. The combustion energy, heat of combustion of TNT and explosion efficiency were chosen as the values recommended in literature. Since dust explosions are usually closer to deflagrations rather than detonations, explosion strength of 7 has been recommended to be used in the case of dust explosion overpressure estimations (CCPS, 2000). The initial parameter values used in the calculations are shown in **Table IX**.

Table IX The initial parameter values used in the calculations of overpressure effects with the TNT, TNO MEM and BST model.

p_0 [kPa]	E_V [MJ/m^3]	E_{TNT} [kJ/kg]	η [-]	Explosion strength [-]
101.325	3.5	4601	0.02	7

6.3 Introducing of accident scenarios

Dust explosion accidents are not comprehensively reported in general compared to gas explosion accidents. In 2003, the U. S. Chemical Safety and Hazard Investigation Board (CSB) launched an investigation solely on dust explosions after three major dust explosion accidents occurred in the U.S. during the same year. Comprehensive reports have been written on several dust explosion accidents since, but the focus of the investigations has been on the causes of the accidents and on the preventative means that could have been taken. Some information of the consequences of the explosions is available, although it is limited. Two dust explosion accidents have been chosen for a closer study to obtain accident data for the comparison and error estimation of the chosen modelling methods.

6.3.1 CTA Acoustics, Inc.

A dust explosion occurred at CTA Acoustics, Inc. (CTA) facility in Kentucky, U.S. in February 2003. The accident caused the death of 7 workers and additional 37 were injured. The facility produced acoustical and thermal insulation and the dust material causing the explosion was identified as phenolic resin that was used as a coating material for the insulation. The ignition point at the facility was determined at a coating oven near the center of production line 405, shown in **Figure 21**. The initial primary dust explosion caused a pressure wave and a fireball that fueled two additional dust explosions in the processing room. (CSB, 2005) The locations of the ignition points of all the explosions as well as the locations of workers at the time of the explosion are shown in **Figure 21**.

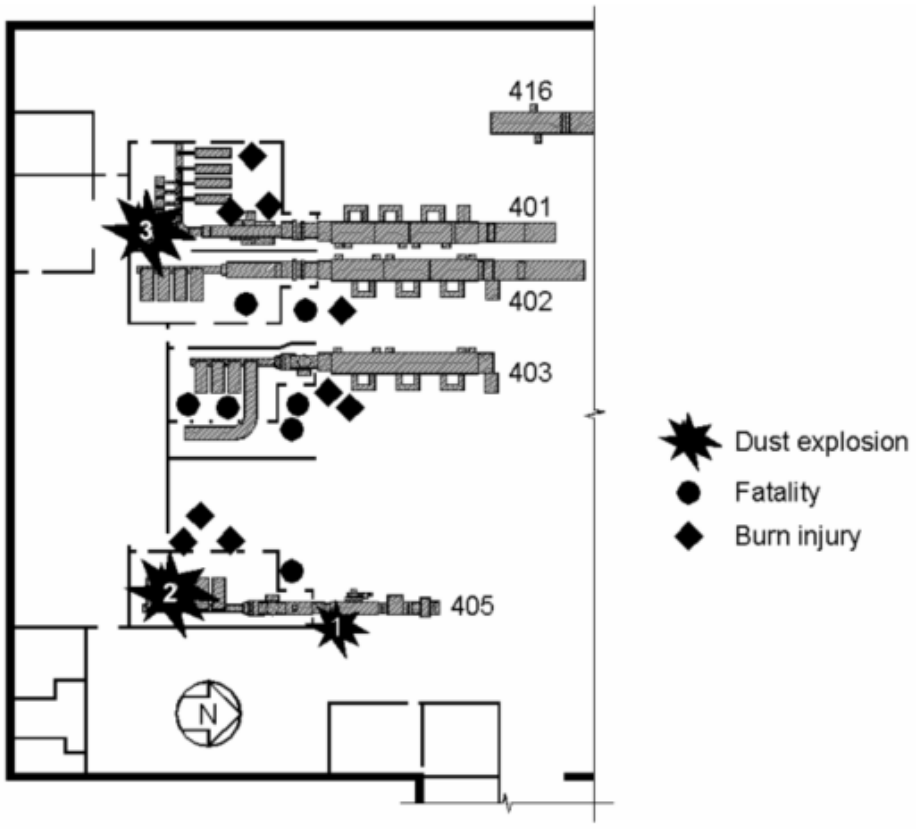

Figure 21 The accident sequence and the workers near the accident locations at CTA Acoustic dust explosion accident. Not all the workers at the time of the accident are shown in the schematic. (CSB, 2005)

The listed damages of the explosions and the resulting fires are presented in **Appendix V**. The overpressure values at different distances were derived from the accident report and are shown in **Figure 22**. The estimations of the overpressure values were derived using estimation table for overpressure effect estimation by Clancey (1972), presented in **Appendix IV**. As can be seen from the dispersion of the estimation points in **Figure 22**, the estimation of the generated overpressures at certain distances is challenging and the estimates contain rather a high level of uncertainty. However, the trend of the data points is logical. **Figure 22** also demonstrates the theoretical fact that the secondary dust explosions are stronger and more severe than the primary dust explosion.

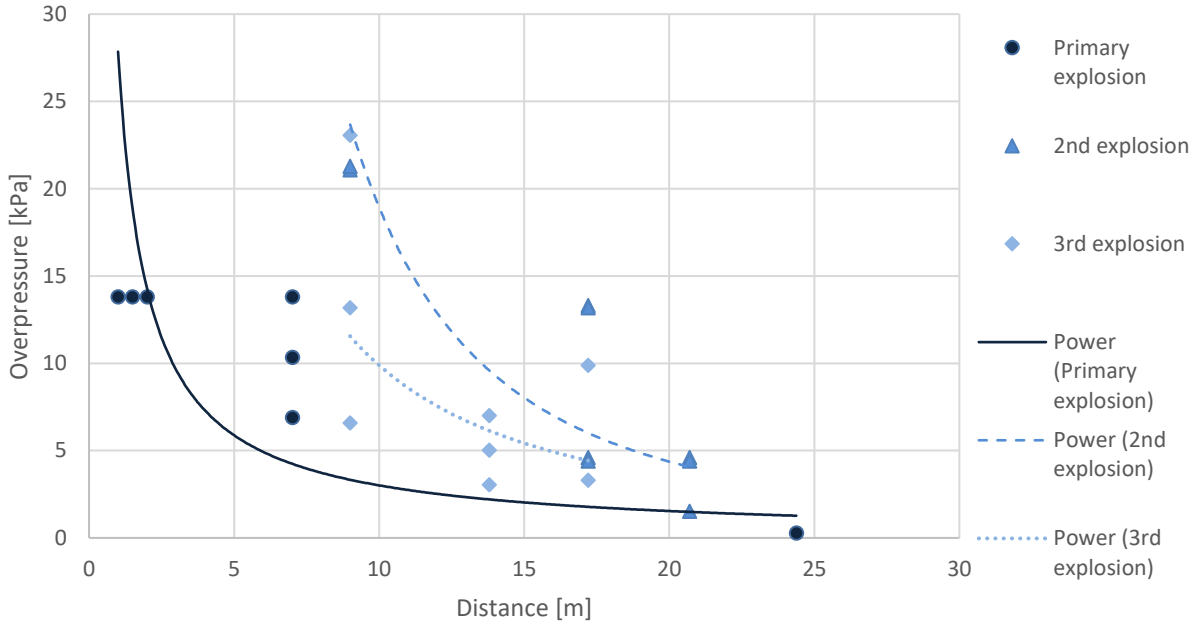

Figure 22 Pressure-distance data extracted from the accident report of CTA Acoustics, Inc. dust explosion.

6.3.2 West Pharmaceutical Services, Inc.

A dust explosion occurred at West Pharmaceutical Services, Inc. facility in North Carolina, U.S. in January 2003. The material identified as the explosion source was polyethylene dust that had accumulated above a suspended ceiling above rubber compounding room in the facility. The thickness of the dust layer was reported to be as high as 0.01 m. The rubber compounding room was the only two-story part of the facility. (CSB, 2004) A schematic of the facility and the location of the likely ignition point in the rubber compounding room are shown in **Figure 23**. The arrows spreading from the ignition point demonstrate the direction of the reported pressure wave and the parts of the surrounding area that received the most severe damages by the explosion.

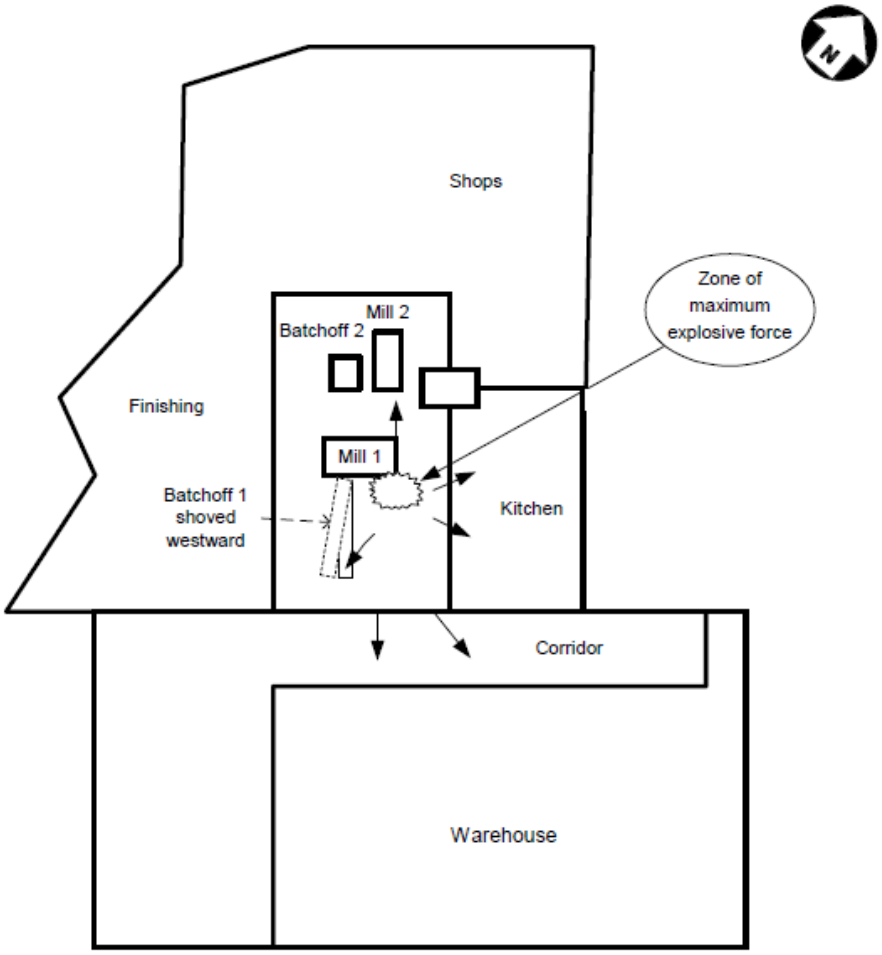

Figure 23 Layout of the West Pharmaceutical Services, Inc. facility and the estimated ignition point of the dust explosion (CSB, 2004).

The listed damages from the explosion are collected in **Appendix VI**. The accident likely caused one main dust explosion in the rubber compounding room while other secondary dust explosions might have occurred elsewhere around the facility. The accident data was mainly reported from the immediate surrounding area of the ignition point so the data points were interpreted as results of the primary dust explosion. The data points derived from the accident report are shown in **Figure 24**. A logical decreasing trend of the data points can be seen from the data set although dispersion is also noticeable.

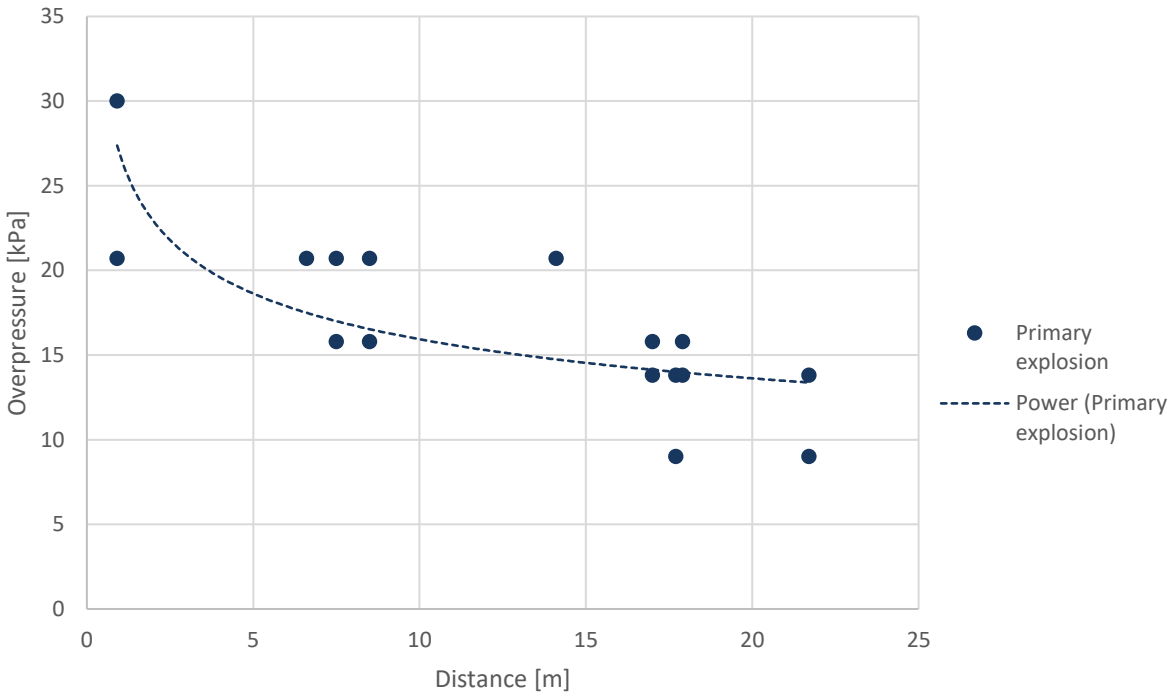

Figure 24 Pressure-distance data extracted from the accident report of West Pharmaceutical Services, Inc dust explosion.

6.4 Overpressure estimations for client cases

Three different scenarios of possible dust explosion hazards were collected from different industries in Finland for testing of the chosen modelling methods for client cases. The TNT model was left out of the calculations due to its predicted poor suitability for dust explosion modelling. A rather simple CFD simulation previously tested for complex explosion risk assessment was conducted for comparison of the other chosen modelling methods, disproportional calculations and TNO MEM and BST models. The scenarios include two different organic dust materials, sugar and peat. The equipment and materials used in the scenarios are presented in more detail below.

Case 1: Peat dust silo

The possible dust explosion consequence analysis of a large silo containing peat dust was estimated with the chosen models. The initial properties and explosibility data of the peat material were derived from the GESTIS-DUST-EX database, presented in **Table X**. The silo is located near ground level.

Table X The material properties of peat dust derived from GESTIS-DUST-EX.

Median particle size [µm]	**Moisture content [% by weight]**	**LEL [g/m^3]**	**p_{max} [bar g]**	**K_{St} [bar m s^{-1}]**	**Explosibility [-]**	**Ignition Temperature [°C]**
38	31	125	8.1	64	St 1	500

Case 2: Sugar dust bucket elevators

Two bucket elevators of different volumes transporting sugar dust were studied. The initial properties as well as the explosibility data of sugar were derived from the GESTIS-DUST-EX database, presented in **Table XI**.

Table XI The material information of sugar dust derived from GESTIS-DUST-EX.

Median particle size [µm]	**Moisture content [% by weight]**	**LEL [g/m^3]**	**p_{max} [bar g]**	**K_{St} [bar m s^{-1}]**	**Explosibility [-]**	**Ignition Temperature [°C]**
25	0.2	60	9.1	140	St 1	350

The two bucket elevators have a high length-to-diameter ratio (L/D). Since the TNO MEM and BST models assume the shape of the cloud to be hemisphere and sphere respectfully, the calculations for the elevators were conducted for one third of the original volume thus resulting in likely more realistic distance estimations. The models are assumed to function well for geometries closer to symmetry.

Case 3: Sugar dust collector

A sugar dust collector used to collect sugar dust from air flow was studied. The sugar dust handled in the collector has the same properties as the sugar dust presented in **Table XI**.

Overview of the used CFD simulation software

A CFD software STAR-CCM+ was used to simulate the overpressure effects for client cases by a CFD simulation experts group to test the usability of simple CFD code for dust explosion consequence analysis. The chosen equipment for the simulation were the sugar dust bucket elevator and the peat dust silo. The STAR-CCM+ is an object-oriented code and it can solve a problem with over one billion cells. The software uses the k-ε and k-ω turbulence models.

A second order implicit coupled flow solver was used in the calculation of the simulation to solve the conservation equations of mass, momentum and energy simultaneously. The simulations used unsteady implicit approach using a pseudo-time-marching approach where a number of inner iterations was involved in the physical time step to converge to the mathematical solution for the given instant of time. The flow was assumed to be inviscid and propagating at the speed of sound and therefore the viscous effects of the flow were ignored. The bottom of the domain was set as a stationary fixed wall whereas the top and the surroundings were set as free stream opening boundary imposing zero-gradient to the flow. This made the calculations simple resulting faster and cheaper calculations while still providing information about the behavior of the pressure wave flow.

7 RESULTS AND ESTIMATION OF ERROR

Calculations were made for the explosion severity estimations according to the reaction-balance-based (RBB) model presented by Callé et al. (2005). A simplified RBB model was also tested. The overpressure effects were calculated with the TNT, TNO multi-energy (TNO MEM) and Baker-Strehlow-Tang (BST) models as well as the disproportion method. The results of the calculations and the estimations of error against chosen validation data are presented in this chapter.

7.1 Results of the reaction-balance-based model

The results obtained from the RBB model for cellulose are presented in **Figure 25**. As can be seen from the figure, the maximum explosion pressure was reached relatively fast with the model. One possible reason for the reaction time can be the fact that in the calculation, all the dust is assumed to heat at the same time. In real life cases, the ignition heats the nearby particles and the combustion of the first dust particles heats the next particles and thus the reacting zone propagates through the dust cloud.

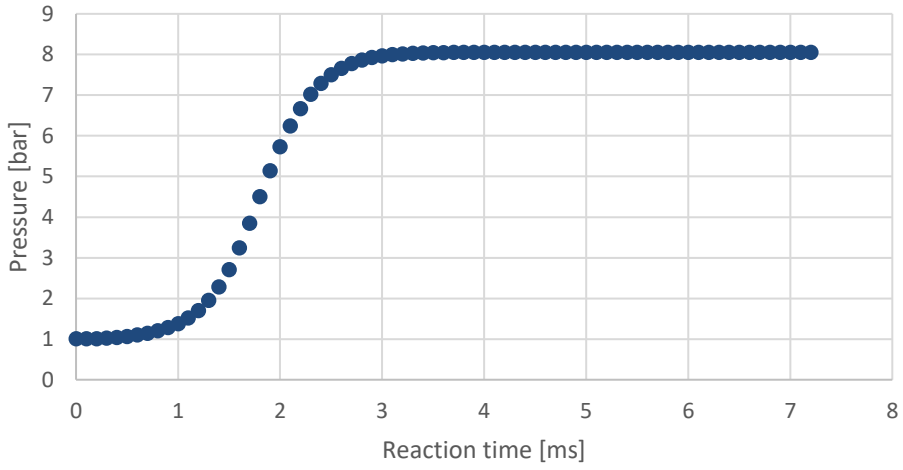

Figure 25 The pressure-time curve of the pressure development of the combustion reaction of cellulose calculated according to the RBB model where V = 20 dm^3, m_{dust} = 14.6 g, A = 12 000 dm^3/mol·s and E_A = 9 000 J.

The calculated overpressure values for the chosen hydrocarbons are presented in **Table XII**. Overpressure values for the same materials were derived from GESTIS-DUST-EX database as a reference. The same reference data was used for the verification of the simplified RBB model.

The obtained results from the calculation are in good agreement with the results obtained by the original authors, Callé et al. (2005). The pressure values of dust explosions are typically in the range of 8 – 12 bar (Dust Explosion Info, 2016; GESTIS-DUST-EX). The pressure values are within the pressure range and they correlate well with the experimental values from GESTIS-DUST-EX. The reaction time however differed from the previous results by Callé et al. (2005) being tenth of that of the original results.

Table XII Comparison of pressure values obtained from the RBB model with values from the GESTIS-DUST-EX database.

Material	**RBB model overpressure [bar g]**	**Dust-Ex overpressure [bar g]**
Cellulose $C_6H_{10}O_5$	7.1	8.6
Glucose $C_6H_{12}O_6$	11.3	9.2
Sucrose $C_{12}H_{22}O_{11}$	11.2	9.0
Lignin $C_{10}H_{12}O_3$	11.1	8.7
Ascorbic acid $C_6H_8O_6$	9.4	9.0
Graphite C	6.8	6.6
Bisphenol A $C_{15}H_{16}O_2$	10.9	9.3
Citric acid $C_6H_8O_7$	8.2	7.4
Fumaric acid $C_4H_4O_4$	8.1	8.5

The calculations with the RBB model only consider the main combustion reaction resulting in CO_2 and H_2O gases as products. In reality the reaction is likely to produce other gases as well, such as carbon monoxide, CO (Stahmer & Gerhold, 2017).

The volume of the dust cloud has very small effect on the reached overpressure when calculated with the simplified RBB model as was expected. The explosion pressures obtained with the model decrease slightly with increasing volume. This also verifies the usability of the standard explosion pressures in GESTIS-DUST-EX database as the pressures are determined in standardized 1 m^3 or 20 L vessels.

A simplified version of the RBB model was tested with three different calculation assumptions of the mass of the hydrocarbon in the system. The results of the calculations are shown in **Tables XIII-XV**. The first calculations were made for stoichiometric assumption setting the conversion at 1. This calculation resulted in the theoretical maximum overpressure values for the explosion reaction of various hydrocarbons. The results of this calculation are presented in **Table XIII**.

Table XIII Calculation results of conversion, mass and overpressure values of the simplified RBB model for the stoichiometric reaction.

Component	**Conversion, *X*** **[-]**	**Mass, *m*** **[g]**	**Overpressure, p_{ex}** **[bar g]**
Cellulose $C_6H_{10}O_5$	1	206.510	10.41
Glucose $C_6H_{12}O_6$	1	229.448	10.51
Sucrose $C_{12}H_{22}O_{11}$	1	217.977	10.45
Lignin $C_{10}H_{12}O_3$	1	119.747	9.86
Ascorbic acid $C_6H_8O_6$	1	269.168	10.70
Graphite C	1	91.792	8.14
Bisphenol A $C_{15}H_{16}O_2$	1	96.920	8.96
Citric acid $C_6H_8O_7$	1	326.234	10.29
Fumaric acid $C_4H_4O_4$	1	295.647	10.29

Next, the model was tested with the mass amount found to result in highest overpressure by Callé et al. (2005). The mass of the dust was set at 3.5 times the stoichiometric amount and the

conversion was solved for when all available oxygen in the system had reacted. The results of this calculation are in **Table XIV**.

Table XIV Calculation results of conversion, mass and overpressure values of the simplified RBB model when the mass of the hydrocarbon was set to 3.5 times the stoichiometric amount.

Component	**Conversion, *X*** **[-]**	**Mass, *m*** **[g]**	**Overpressure, p_{ex}** **[bar g]**
Cellulose $C_6H_{10}O_5$	0.29	722.77	10.63
Glucose $C_6H_{12}O_6$	0.29	803.07	10.73
Sucrose $C_{12}H_{22}O_{11}$	0.29	762.919	10.68
Lignin $C_{10}H_{12}O_3$	0.29	419.113	10.09
Ascorbic acid $C_6H_8O_6$	0.29	942.089	10.93
Graphite C	0.29	321.271	8.35
Bisphenol A $C_{15}H_{16}O_2$	0.29	339.221	9.18
Citric acid $C_6H_8O_7$	0.29	1141.818	10.50
Fumaric acid $C_4H_4O_4$	0.29	1034.767	10.50

The concentration assumption of 4.5 g/m3 resulted in slightly different overpressure values compared to the assumption on 3.5 times of stoichiometric mass. The model was also utilized for this concentration assumption and the conversions were again solved for when all available oxygen had reacted. The results of this calculation are shown in **Table XV**. This version of the simplified model did not provide realistic results for graphite.

Table XV Calculation results of conversion, mass and overpressure values of the simplified RBB model when the concentration of the hydrocarbon was set to 4.5 g/m^3.

Component	**Conversion, *X*** **[-]**	**Mass, *m*** **[g]**	**Overpressure, p_{ex}** **[bar g]**
Cellulose $C_6H_{10}O_5$	0.28	729.63	10.74
Glucose $C_6H_{12}O_6$	0.28	810.702	10.73
Sucrose $C_{12}H_{22}O_{11}$	0.14	1540.322	10.44
Lignin $C_{10}H_{12}O_3$	0.15	810.882	9.86
Ascorbic acid $C_6H_8O_6$	0.34	792.558	11.00
Graphite C	-	-	-
Bisphenol A $C_{15}H_{16}O_2$	0.09	1027.251	8.97
Citric acid $C_6H_8O_7$	0.38	864.558	10.59
Fumaric acid $C_4H_4O_4$	0.57	552.324	10.73

7.2 Error estimation of the RBB model

Error calculations were made for the RBB model against the data obtained from GESTIS-DUST-EX. The calculated errors are shown in **Table XVI** both in bar and in percentage. The RBB model results in good overpressure values for the tested hydrocarbons. Based on the results and the estimated errors the model was most accurate for hydrocarbons that have more closely same molar amount of carbon, hydrogen and oxygen, such as fumaric acid and ascorbic acid, in their chemical formula whereas hydrocarbons with differing amounts of elements, such as lignin and sucrose, resulted in higher error estimates.

The overpressure values in the GESTIS-DUST-EX database are determined with standardized explosion experiments. Thus, the values in the database are likely to also contain a level of error. The explosion reaction of a dust material is not a linear reaction that occurs identically each time. The amount of unreacted dust in the system and level of turbulence effecting the mixing

of the system may vary each time in the reaction resulting in varying results. The values may also vary depending on the conditions and the operator of the experiments and different values for materials can be found in the database. An error estimation of ±0.5 bar would be suggested for the values of the database based on the materials studied in this research.

Table XVI The calculated error of the RBB model for different hydrocarbons compared against the values obtained from GESTIS-DUST-EX database.

Material	**Error**	
	[bar]	**[%]**
Cellulose $C_6H_{10}O_5$	-1.5	17.4
Glucose $C_6H_{12}O_6$	+2.1	22.8
Sucrose $C_{12}H_{22}O_{11}$	+2.2	24.4
Lignin $C_{10}H_{12}O_3$	+2.4	27.6
Ascorbic acid $C_6H_8O_6$	+0.4	4.4
Graphite C	+0.2	3.0
Bisphenol A $C_{15}H_{16}O_2$	+1.6	17.2
Citric acid $C_6H_8O_7$	+0.8	10.8
Fumaric acid $C_4H_4O_4$	-0.4	4.7
Average error	**+0.87**	**14.7**

The simplified RBB model was also validated against the same reference data as the RBB model. Error calculations were made for all three different calculations and are shown in **Table XVII**. From the three calculations, the stoichiometric calculation resulted in closest values compared to the validation data. Higher overpressure values were obtained with the other two calculations, which agrees with literature that the highest overpressure values are reached above the stoichiometric concentration. The calculated error values for the other two calculations are close to the stoichiometric. From the two calculations, the assumption of concentration of 4.5 g/m^3 proved to be insufficient for all the tested hydrocarbons.

Table XVII Error estimation of the simplified RBB model against data from GESTIS-DUST-EX database for three different calculation assumptions of the amount of hydrocarbon in the system.

Component	**Error**					
	Calculation 1		**Calculation 2**		**Calculation 3**	
	[bar]	**[%]**	**[bar]**	**[%]**	**[bar]**	**[%]**
Cellulose $C_6H_{10}O_5$	+1.81	21.05	+2.03	23.60	+2.14	24.88
Glucose $C_6H_{12}O_6$	+1.31	14.24	+1.53	16.63	+1.53	16,63
Sucrose $C_{12}H_{22}O_{11}$	+1.45	16.11	+1.68	18.67	+1.44	16.00
Lignin $C_{10}H_{12}O_3$	+1.16	13.33	+1.39	15.98	+1.16	13.33
Ascorbic acid $C_6H_8O_6$	+1.70	18.89	+1.93	21.44	+2.00	22.22
Graphite C	+1.54	23.33	+1.75	26.52	-	-
Bisphenol A $C_{15}H_{16}O_2$	-0.34	3.66	-0.12	1.29	-0.33	3.55
Citric acid $C_6H_8O_7$	+2.89	39.05	+3.10	41.89	+3.19	43.11
Fumaric acid $C_4H_4O_4$	+1.79	21.06	+2.00	23.53	+2.23	26.24
Average error	**+1.48**	**18.97**	**+1.70**	**21.06**	**+1.67**	**20.76**

7.3 Discussion of the reaction-balance-based model

The RBB model proved to be applicable for the estimation of explosion severity of simple organic hydrocarbons. At the current state, the model is only applicable for hydrocarbons containing only carbon, hydrogen and oxygen. For other materials and hydrocarbons containing other elements as well, some adjustments need to be made for the model. The overpressure values obtained with the model agree rather well with the validation data and literature. As the focus of the modelling was on overpressure effects, the validity of the reached reaction temperatures was not researched. Thus, the use of the model to estimate resulting explosion temperatures is not recommended.

The used parameters of the Arrhenius equation contain some level on uncertainty since they are fitted for experimental data from explosion experiments of cellulose dust. The further use of the model would require validation of these parameters. The simplified RBB model provided a usable tool for overpressure estimations eliminating the uncertainty with the Arrhenius equation parameters. For risk assessment analyses, the model could be calculated with all three calculation assumptions and the highest obtained overpressure value set as the most conservative estimation. This would result in safer risk assessments while remaining near the same error range.

7.4 Overpressure effect calculations

The TNT, TNO multi-energy, Baker-Strehlow-Tang and disproportion models were used to calculate the distance estimations for the two accidents, CTA Acoustics, Inc. and West Pharmaceutical Services, Inc. The obtained values were compared against data derived from the accident reports.

The calculations of the first accident, CTA Acoustics, Inc. facility, were computed for the primary explosion and the second explosion separately to see the possible differences. The calculation results for the primary explosion at CTA Acoustics, Inc. are collected in **Table XVIII** and are also shown graphically in **Figure 26**.

Table XVIII Accident data distance estimations of the first explosion at CTA Acoustics, Inc. computed with TNT, TNO multi-energy, Baker-Strehlow-Tang and disproportional models compared against accident data. For TNO MEM and BST models explosion strength of 7 is used.

Overpressure [kPa]	**Distance from accident data [m]**	**Disproportion [m]**	**TNT [m]**	**TNO MEM [m]**	**BST [m]**
13.8	1.50	3.82	16.51	4.34	6.21
10.35	7.01	4.42	21.02	5.72	7.46
0.28	24.38	26.84	-	181.51	-

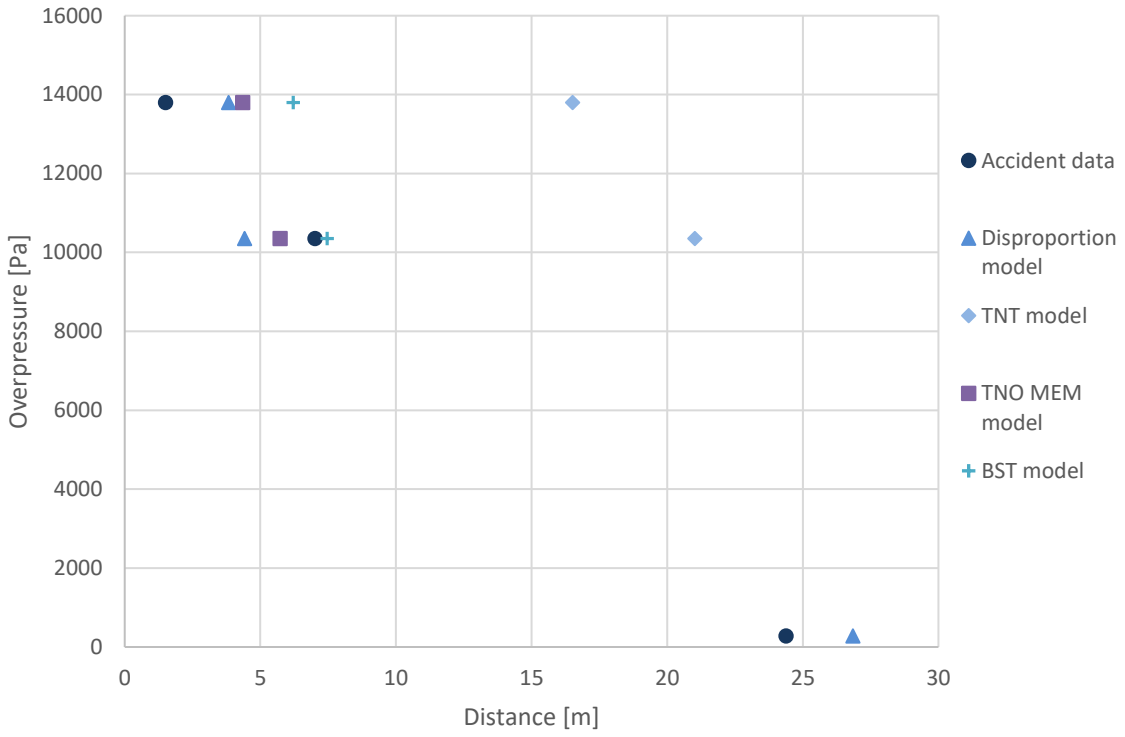

Figure 26 Comparison of estimated distances for overpressure values with TNT, TNO MEM, BST and disproportional models against the data derived from the accident report of the primary dust explosion at the CTA Acoustics, Inc. facility.

The calculated distance estimations with the chosen models for the secondary explosion at CTA Acoustics, Inc. are in **Table XIX** and are also shown graphically in **Figure 27**.

Table XIX Accident data distance estimation of the second explosion at CTA Acoustics, Inc. computed with TNT, TNO MEM, BST and disproportional models compared against accident data. For TNO MEM and BST models explosion strength of 7 is used.

Overpressure [kPa]	**Distance from accident data [m]**	**Disproportion [m]**	**TNT [m]**	**TNO MEM [m]**	**BST [m]**
20.70	1.52	3.12	12.01	3.45	4.35
20.70	4.50	3.12	12.01	3.45	4.35
17.20	4.50	3.43	13.51	3.59	-
17.20	13.24	3.43	13.51	3.95	5.47
9.00	21.19	4.73	22.52	5.92	8.70
0.28	24.38	26.84	-	-	-

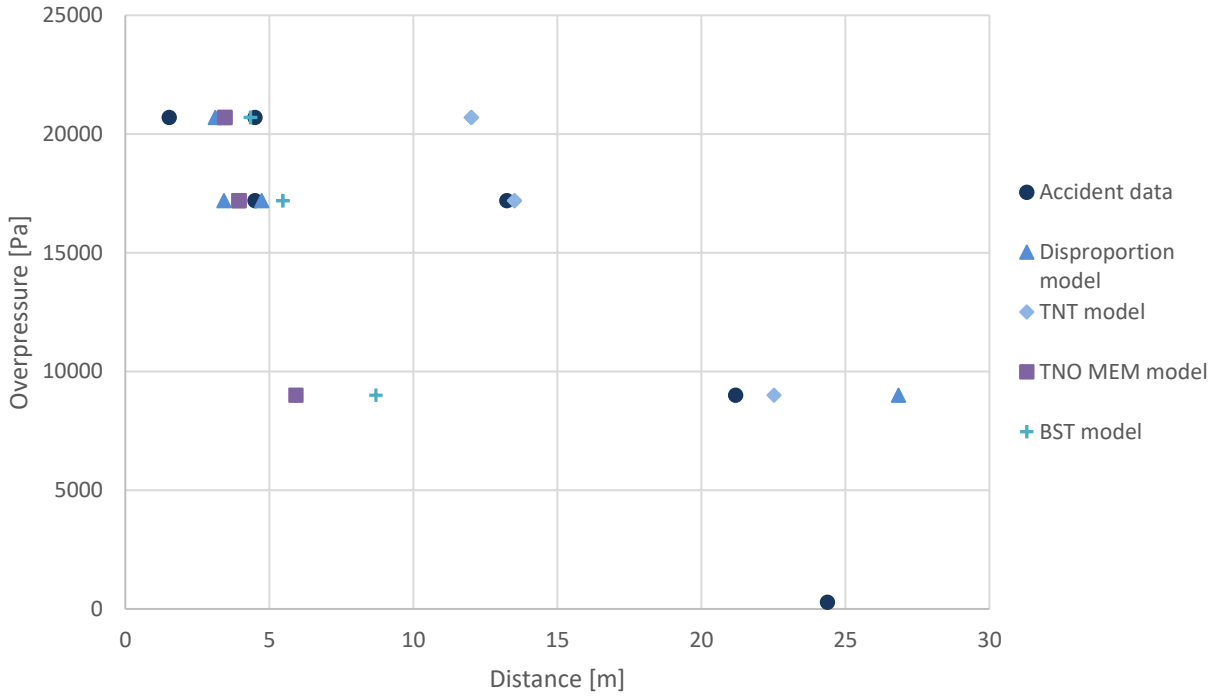

Figure 27 Comparison of estimated distances for overpressure values with TNT, TNO MEM, BST and disproportional models against the data derived from the accident report of the second dust explosion at the CTA Acoustics, Inc. facility.

The calculated distance estimations with the chosen models for the primary explosion at West Pharmaceutical Services, Inc. are in **Table XX** and are also shown graphically in **Figure 28**.

Table XX Accident data distance estimation of the primary explosion at West Pharmaceuticals Services, Inc. computed with TNT, TNO MEM, BST and disproportional models compared against accident data. For TNO MEM and BST models explosion strength of 7 is used.

Overpressure [kPa]	**Distance from accident data [m]**	**Disproportion [m]**	**TNT [m]**	**TNO MEM [m]**	**BST [m]**
30.0	0.91	5.37	6.29	5.96	6.97
20.7	0.91	6.47	7.75	7.45	9.39
20.7	6.6	6.47	7.75	7.45	9.39
20.7	14.1	6.47	7.75	7.45	9.39
15.8	7.5	7.41	9.68	8.52	12.34
15.8	8.5	7.41	9.68	8.52	12.34
20.7	7,5	6.47	7.7	7.45	9.39
20.7	8.5	6.47	7.75	7.45	9.39
13.8	17	7.92	9.88	9.79	13.41
13.8	17.9	7.92	9.88	9.79	13.41
15.8	17	7.41	9.68	8.52	12.34
15.8	17.9	7.41	9.68	8.52	12.34
9.0	17.7	9.81	10.17	13.20	18.78
9.0	21.7	9.81	10.17	13.20	18.78
13.8	17.7	7.92	9.88	9.79	13.41
13.8	21.7	7.92	9.88	9.79	13.41
1.0	1126.54	29.01	-	47.90	-
2.1	1126.54	20.46	-	43.43	-
0.1	40233.6	78.68	-	-	-
0.3	40233.6	55.63	-	298.04	-

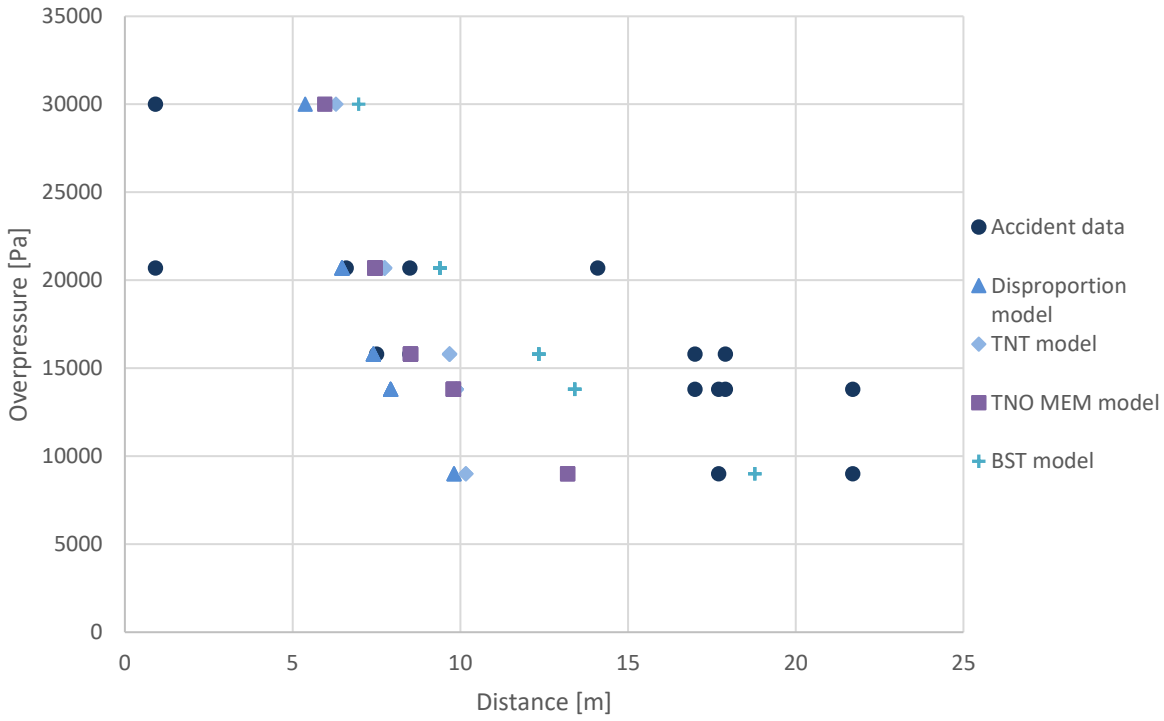

Figure 28 Comparison of estimated distances for overpressure values with TNT, TNO MEM, BST and disproportional models against the data derived from the accident report of the dust explosion at West Pharmaceutical Services, Inc. facility.

7.5 Estimation of error

The distance estimations of the TNT, TNO MEM, BST and disproportion models were compared with the data derived from the accident reports. The data derived from the reports contains an error as well since the estimation method relies on experimentally validated overpressure estimations. The accident reports also contain some uncertainty with the descriptions although they are made as carefully as possible. The calculated error for the TNT, TNO MEM, BST and disproportion models for the case of dust explosion distance estimations are presented in **Tables XXI-XXII** calculated for CTA Acoustics, Inc. accident. The error calculations for the primary explosion are in **Table XXI** and for the second explosion in **Table XXII** for all determined data points. An average error was also calculated for each model.

Table XXI Calculated errors for TNT, TNO MEM, BST and disproportion models against accident data from the primary dust explosion at CTA Acoustics, Inc.

Overpressure [kPa]	Distance from accident data [m]	Disproportion [%]	TNT [%]	TNO MEM [%]	BST [%]
13.8	1.5	154.9	1000.8	189.4	314.3
6.9	7.0	37.0	199.8	18.4	6.38
0.3	24.4	10.1	-	644.5	-
Average error		**67.3**	**600.3**	**284.1**	**160.3**

Table XXII Calculated errors for TNT, TNO MEM, BST and disproportion models against accident data from the second dust explosion at CTA Acoustics, Inc.

Overpressure [kPa]	Distance from accident data [m]	Disproportion [%]	TNT [%]	TNO MEM [%]	BST [%]
20.7	1.5	104.9	688.0	126.6	185.4
20.7	4.5	30.6	166.9	23.3	3.3
17.2	4.5	23.9	200.2	12.3	21.5
17.2	13.2	74.1	2.0	70.2	58.7
9.0	21.2	77.7	6.3	72.1	58.9
0.3	24.4	10.1	-	466.5	
Average error		**53.6**	**212.7**	**128.5**	**65.6**

The estimated error values for the case of West Pharmaceutical Services, Inc. dust explosion with TNT, TNO MEM, BST and disproportion models are presented in **Table XXIII** for all determined data points. An average error was also calculated for each model.

Table XXIII Calculated errors for TNT, TNO MEM, BST and disproportion models against accident data from the primary dust explosion at West Pharmaceutical Services, Inc.

Overpressure [kPa]	Distance from accident data [m]	Disproportion [%]	TNT [%]	TNO MEM [%]	BST [%]
30.0	0.91	490.6	591.6	555.0	666.4
20.7	0.91	611.0	751.2	718.8	931.6
20.7	6.6	2.0	17.4	12.9	42.2
20.7	14.1	54.1	45.1	47.2	33.4
15.8	7.5	1.3	29.1	13.5	64.5
15.8	8.5	12.9	13.9	0.2	45.2
20.7	7.5	13.7	3.3	0.7	25.2
20.7	8.5	23.9	8.9	12.3	10.4
13.8	17.0	53.4	41.9	42.4	21.1
13.8	17.9	55.7	44.8	45.3	25.1
15.8	17.0	56.4	43.0	49.9	27.4
15.8	17.9	58.6	45.9	52.4	31.1
9.0	17.7	44.6	42.6	25.4	6.1
9.0	21.7	54.8	53.1	39.2	13.5
13.8	17.7	55.2	44.2	44.7	24.2
13.8	21.7	63.5	54.5	54.9	38.2
1.0	1126.5	97.4	-	95.7	-
2.1	1126.5	98.2	-	96.1	-
0.1	40233.6	99.8	-	-	-
0.3	40233.6	99.9	-	99.3	-
Average error		**102.3**	**114.4**	**105.6**	**125.3**

7.6 Discussion of the overpressure effect models

The overpressure effect models tested for the use in dust explosion consequence analysis resulted in high levels of error. The estimation of the data from the accident reports was problematic and the obtained data contains uncertainty. The distance estimations obtained with the chosen models did not result in values that would agree with the estimated accident data with required accuracy. This was to be expected with models designed and validated for gas explosions, but the error estimations of the models were higher than anticipated. The Baker-Strehlow-Tang (BST) model would be the recommended choice of these models although it should also be used carefully and acknowledging the error estimations. The choice is reasonable

since the method is based on flame speed rather than congestion of the reacting gas cloud. The disproportion model resulted with good error values compared to the other models, but the model neglects all effects of reflections and allows the pressure wave to diminish linearly which is incorrect based on the theory and literature.

The highest errors with all the models are near the ignition point and far away from the explosion site. In the middle range distances, the models can predict the distances with some level of consistency. The TNT, TNO MEM and BST models were also unable to provide results for all overpressure values. The model curves are determined for higher overpressure values than were the lowest values in the accident data and thus the models could only be used for high enough overpressures. This shows that these models are intended for estimations of severe explosions with high overpressure values. The use of these models in the use of dust explosion risk assessment is left for the decision of the user knowing the limitations of the models.

7.7 Overpressure effects calculations for client cases

The tested models were used to estimate the overpressure effects of possible dust explosions at three different cases from industry in Finland. The TNT model was left out of the comparison since it was predicted to be unsuitable and impractical for explosion consequence analysis in such cases. In addition of the tested models, CFD simulation estimations were received for two of the studied equipment as a reference data as well.

In **Tables XXIV-XXVII** the calculated distances for overpressure values of 30 kPa, 15 kPa and 5 kPa are listed for four different process equipment studied in this report. All the distances are calculated from the center of the explosion. The differences of the calculation methods can be seen from the tables. The CFD simulation results are presented with variance estimations since the pressure wave was not a symmetrical circle.

Table XXIV Distances of different overpressure values for sugar dust elevator 1.

Overpressure [kPa]	Disproportion [m]	BST [m]	MEM [m]	CFD [m]	SFS [m]
30	4.91	12.55	9.07	9 ± 0,5	2.18
15	5.22	20.60	16.41	20 ± 1	3.65
5	5.46	45.19	42.00	54 ± 1	8.24

Table XXV Distances of different overpressure values for sugar dust elevator 2.

Overpressure [kPa]	Disproportion [m]	BST [m]	MEM [m]	SFS [m]
30	4.67	11.95	8.64	2.18
15	4.97	19.62	15.63	3.65
5	5.20	43.04	40.00	8.24

Table XXVI Distances of different overpressure values for sugar dust collector.

Overpressure [kPa]	Disproportion [m]	BST [m]	MEM [m]	SFS [m]
30	6.42	16.41	11.86	2.42
15	6.82	26.95	21.47	4.05
5	7.14	59.12	54.94	9.13

Table XXVII Distances of different overpressure values for peat dust silo from the center of the vessel.

Overpressure [kPa]	Disproportion [m]	BST [m]	MEM [m]	CFD [m]	SFS [m]
30	23.57	63.47	45.88	53 ± 2	12.01
15	25.04	104.19	83.00	80 ± 1	20.08
5	26.19	228.58	212.42	165 ± 5	45.30

The results of overpressure distance estimations for the studied peat dust silo are shown graphically in **Figure 29**.

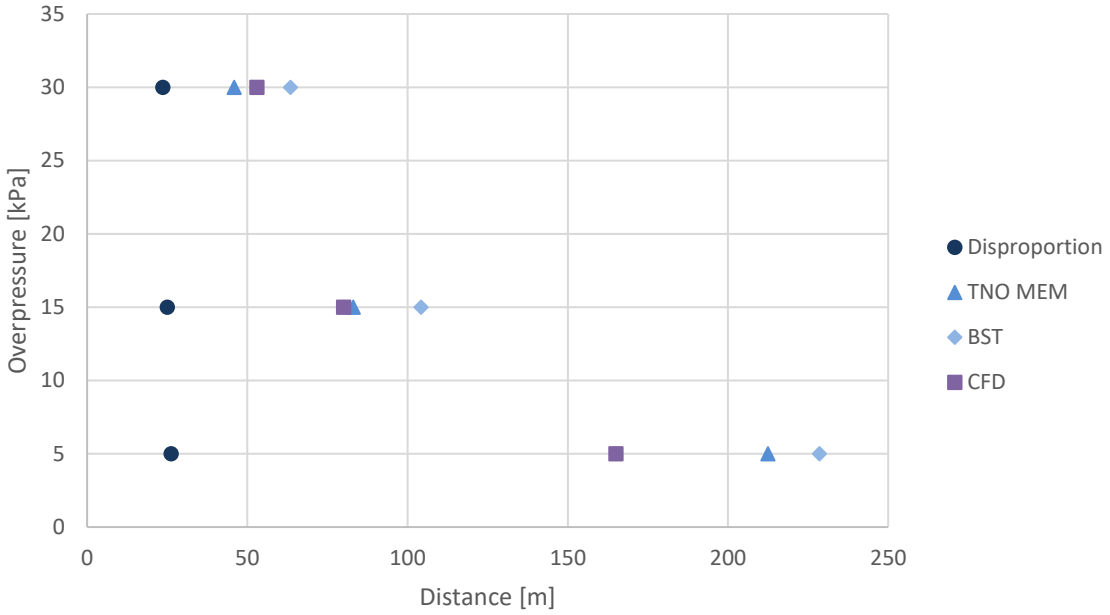

Figure 29 Comparison of the tested modelling methods for explosion overpressure effect for peat dust silo with V = 1500 m^3.

Given the error estimations of the tested models presented before in Chapter 7.5 the distance estimations for the client cases are to be considered with caution. The interpretation of the results is advised to be made knowing the limitations and probable errors of the models and using the values for theoretical maximum values for the given cases.

The CFD results correlate rather well with the other models tested, apart from the disproportional model. The CFD predicts the dissolution of the pressure wave more sharply than the other models, which seems to agree with the theory and accident data presented earlier. This would suggest that the CFD simulation method tested could have the potential to be used for dust explosion risk assessments. Further development and validation with the model would be needed and the results could be very costly.

8 CONCLUSIONS

The aim of this study was to understand the basic mechanisms controlling dust explosions and find modelling methods suitable for dust explosions. The components required for dust explosions were identified and the scope of the research was set to dust explosion occurring inside closed areas. One modelling method for explosion severity estimations was found and tested for various organic materials. Models intended specifically for dust explosion overpressure effects were not found. Three expansion models used for gas explosion modelling were tested for the use in case of dust explosions together with a calculation based on basic physics of pressure.

A model based on reaction balance and thermodynamics of combustion reactions was tested for the estimation of explosion severity of dust explosions. The model was tested with nine different hydrocarbons and good results were obtained with reasonable error estimation. The explosion overpressures of dust materials are usually in the range of 8 to 12 barg and the resulted values with the model were in the range from 7.1 to 11.3 barg. The limitation of the model was the uncertainty of the used Arrhenius equation parameters that could not be validated from literature. For this problem, a simplified model was constructed following the same calculation principle excluding the determination of the reaction rate. The results obtained with the simplified model also resulted with good overpressure estimation for the studied hydrocarbons, the overpressure values ranging from 8.1 to 11.0 barg.

In general, the calculation for explosion severity resulted in overpressure values that were usually higher than the reference values. In process safety risk assessment, this would only result in more conservative estimations which are usually advised. The presented reaction-balance-based (RBB) model and the simplified version could be used for explosion severity estimation together with literature data. For further development of the model and the simplification, parameters such as laminar burning velocity and particle size could be added. In the model calculations, the reaction is assumed to be determined by the combustion of released volatile gases. This agrees with the findings in literature to account for case of very small particles. To obtain more realistic estimation for larger particles as well, the rate determining reaction step should be investigated and the effects of it added to the model.

For the explosion overpressure effect estimation, four different models were tested. The chosen models were TNT equivalence model (TNT), TNO multi-energy model (TNO MEM), Baker-Strehlow-Tang model (BST) and a simple disproportional model. None of the models worked fully well for the studied dust explosion scenarios leading to the conclusion that further development and research with the problem is needed. From the tested methods, BST model would be chosen as the most reliable choice if needed although it also contains a high level of uncertainty. Too precise conclusions and decisions made by the error values estimated for the expansion models is not advised since the absolute certainty of the reference accident data could not be validated. The comparison of the models would be suggested to be made based on the trend of the calculated values by each model and those should be compared with the information provided in literature.

The results derived with the BST model gave very different predictions for the pressure wave expansions compared to the accident data. The model gave much longer distances for the pressure values indicating that the pressure effects would reach further. Usually, gas cloud explosion pressure waves diminish more gradually and since the model is based on vapor cloud explosions, the results can be understood to give over-estimates for the pressure wave of a dust explosion. The values obtained with the BST model can therefore be assumed to give the maximum distance evaluations for the explosion pressure waves.

For further suggestions for the overpressure effect estimations, the reflections of the pressure wave from surroundings should be included as well as the geometry of the vessel where the explosion occurs. A simple CFD software was also tested for client case risk assessments. The used software resulted in promising distance estimations for the studied cases but more development for the modelling is still required. The solid nature of dust was neglected in the simulations and would likely influence the nature of the pressure wave and its propagation behavior.

The research on overpressure effects on dust explosion accidents would require more researching and experimenting. Accident data should be revised more closely from occurred dust explosion accidents specifically concerning the results of the generated pressure waves. Experimental studies on dust explosion pressure waves could also provide a solution for the

problem of understanding the propagation behavior of the pressure waves. This would be costly and time-consuming but might provide useful data for further research.

The research of the modelling methods for dust explosions continues after this study. The experimental studying of dust explosion pressure wave behavior is not in the scope but other methods for model and parameter validations are considered.

REFERENCES

The Government Decree on Safety Requirements for Industrial Handling and Storage of Dangerous Chemicals (856/2012). Suomen säädöskokoelma. Oikeusministeriö. Edita Prima Oy / Edita Publishing Oy. ISSN 1455-8904 / 1237-8904.

Abbasi, T., Abbasi, S. A. (2007). Dust explosions-Cases, causes, consequences, and control. *Journal of Hazardous Materials*, vol. 140, pp. 7-44.

Abuswer, M., Amyotte, P., Khan, F. (2013). A quantative risk management framework for dust and hybrid mixture explosions. *Journal of Loss Prevention in the Process Industries*, vol. 23, pp. 283-289.

Amyotte, P. R., Soundararajan, R., Pegg, M. J. (2003). An investigation of iron sulphide dust minimum ignition temperatures. *Journal of Hazardous Materials*, vol. A97, pp. 1-9.

Amyotte, P. R., Pegg, M. J., Khan, F. I., Nifuku, M., Yingxin, T. (2007). Moderation of dust explosions. *Journal of Loss Prevention in the Process Industries*, vol. 20, pp. 675-687.

Amyotte, P. R., Eckhoff, R. K. (2010). Dust explosion causation, prevention and mitigation: An overview. *Journal of Chemical Health & Safety*, January/February, pp. 15-28.

Amyotte, P. R., Cloney, C. T., Khan, F. I., Ripley, R. C. (2012). Dust explosion risk moderation for flocculent dusts. *Journal of Loss Prevention in the Process Industries*, vol. 25, pp. 862-869.

Amyotte, P. R. (2014). Some myths and realities about dust explosions. *Process Safety and Environmental Protection*, vol. 92, pp. 292-299.

ATEX directive 1999/92/EY on December 16, 1999 of minimum requirements of combustible air mixtures. European parlament and council.

Barton, J. 2002. Dust explosion prevention and protection. Warwickshire, UK: Institution of Chemical Engineers (IChemE). ISBN 0 85295 410 7.

Callé, S., Klaba, L., Thomas, D., Perrin, L., Dufaud, O. (2005). Influence of the size distribution and concentration on wood dust explosion: Experiments and reaction modelling. *Powder Technology*, vol. 157, pp.144-148.

Canadian Centre for Occupational Health and Safety CCOHS. 2018. OSH Answers Fact Sheets: Combustible Dust. [In CCOHS www-pages]. Updated February 19, 2015 [retrieved February 19, 2018].
Available: https://www.ccohs.ca/oshanswers/chemicals/combustible_dust.html.

Cashdollar, K. L. (2000). Overview of dust explosibility characteristics. *Journal of Loss Prevention in the Process Industries*, vol 13, pp. 183-199.

CCPS Center for Chemical Process safety, 2000. Guidelines for Chemical Process Quantitative Risk Analysis, 2nd Edition. American Institute of Chemical Engineers, New York.

Chanley, V. J. (1972). Diagnostic Features of Explosion Damage. 6th International Meeting on Forensic Sciences. Edinburgh, Scotland. Cited in CCPS, 2000.

Chawla, N., Amyotte, P. R., Pegg, M. J. (1996). A comparison of experimental methods to determine the minimum explosible concentration of dusts. *Fuel*, vol. 75, no. 6, pp. 654-658.

Chen, T., Zhang, Q., Wang, J-X., Liu, L., Zhang, S. (2017). Flame propagation and dust transient movement in a dust cloud explosion process. *Journal of Loss Prevention in the Process Industries*, vol. 49, pp. 572-581.

Count Morozzo (1795). Account of a violent Explosion which happened in a Flour Warehouse, at Turin, December the 14th, 1785; to which are added some Observations on spontaneous Inflammations. The Repertory of Arts, Manufactures, and Agriculture. Cited in Eckhoff, 2003.

CRC Handbook of Chemistry and Physics (1986). 66th Edition. Robert C. Weast, CRC Press, Inc.

CRC Handbook of Chemistry and Physics (2018). 98th Edition. Editor: John R. Rumble.

CSB U.S. Chemical Safety and Hazard Investigation Board (2004). Investigation report, Dust Explosion, West Pharmaceutical Services, Inc. Report No. 2003-07-I-NC.

CSB U.S. Chemical Safety and Hazard Investigation Board (2005). Investigation report, Combustible Dust Fire and Explosions, CTA Acoustics, Inc. Report No. 2003-09-I-KY.

Dahoe, A. E., Zevenbergen, J. F., Lemkowitz, S. M., Scarlett, B. (1996). Dust explosions in spherical vessels: The role of flame thickness in the validity of the 'cube-root law'. *Journal of the Loss Prevention in the Process Industries*, vol. 9, issue 1, pp. 33-44.

Dahoe, A. E., Cant, R. S., Pegg, M. J., Scarlett, B. (2001). On the transient flow in the 20-liter explosion sphere. *Journal of Loss Prevention in the Process Industries*, vol. 14, pp. 475-487.

Di Benedetto, A., Russo, P. (2007). Thermo-kinetic modelling of dust explosions. *Journal of Loss Prevention in the Process Industries*, vol. 20, pp. 303-309.

Di Benedetto, A., Russo, P., Amyotte, P., Marchand, N. (2010). Modelling the effect of particle size on dust explosions. *Chemical Engineering Science*, vol. 65, pp. 772-779.

Dobashi, R. (2017). Studies on accidental gas and dust explosions. *Fire Safety Journal*, vol. 91, pp. 21-27.

Dufaud, O., Traoré, M., Perrin, L., Chazelet, S., Thomas, D. (2010). Experimental investigation and modelling of aluminum dusts explosions in the 20 L sphere. *Journal of Loss Prevention in the Process Industries*, vol. 23, pp. 226-236.

Dust Explosion Info, 2016. Dust Explosion Protection. Explosion venting, suppression & containment. [In Dust Explosion Info www-pages]. [Retrieved June 25, 2018].
Available: http://www.dustexplosion.info/dust%20explosion%20protection.htm.

Encyclopædia Britannica, Inc. 2018. Pyrolysis. Chemical reaction. By Sarah E. Boslaugh. [In Encyclopædia Britannica www-pages]. Updated January 31, 2018, [retrieved March 16, 2018].
Available: https://www.britannica.com/science/pyrolysis.

Eckhoff, R. K. (2003). Dust explosions in the process industries. 3rd Edition. Burlington, Vermont, USA: Gulf Professional Publishing.

Eckhoff, R. K. (2005). Explosion Hazards in the Process Industries. 2nd Edition. Houston, Texas, USA: Gulf Publishing Company.

Eckhoff, R. K. (2009). Understanding dust explosions. The role of powder science and technology. *Journal of Loss Prevention in the Process Industries,* vol. 22, pp. 105-116.

Fumagalli, A., Derudi, M., Rota, R., Copelli, S. (2016). Estimation of the deflagration index K_{St} for dust explosions: A review. *Journal of Loss Prevention in the Process Industries*, vol. 44, pp. 311-322.

Fumagalli, A., Derudi, M., Rota, R., Snoeys, J., Copelli, S. (2018). A kinetic free mathematical model for the prediction of the K_{St} reduction with the particle size increase. *Journal of Loss Prevention in the Process Industries*, vol. 52, pp. 93-98.

Harris, R. J. (1983). The investigation and Control of Gas Explosions in Buildings and Heating Plant. British Gas Corporation. Cited in CCPS, 2000.

Haseli, Y., van Oijen, J. A., de Goey, L. P. H. (2011). A detailed one-dimensional model of combustion of a woody biomass particle. *Bioresource Technology*, vol. 102, pp. 9772-9782.

Haseli, Y., van Oijen, J. A., de Goey, L. P. H. (2013). Reduced model for combustion of a small biomass particle at high operating temperatures. *Bioresource Technology*, vol. 131, pp. 397-404.

GESTIS-DUST-EX. IFA Institute for Occupational Safety and Health of the German Social Accident Insurance.
Available: http://staubex.ifa.dguv.de/explosuche.aspx?lang=e.

Kim, Y. S., Lee, M. C., Rie, D. H. (2016). Explosion characteristics of combustible wood dust in confined system: Analysis using oxygen consumption energy. *Journal of Mechanical Science and Technology*, vol. 30, pp. 5771-5779.

Kirkwood Community College, Community Training and Response Center (1997). Combustible Dust: Safety and Injury Prevention. Awareness Training Program. Instructors Manual. SH-17797-08-60-F-9.

Kosinski, P., Hoffmann, A. C. (2005). Dust explosions in connected vessels: Mathematical modelling. *Powder Technology*, vol. 155, pp. 108-116.

Li, G., Yang, H.-X., Yuan, C.-M., Eckhoff, R. K. (2016). A catastrophic aluminium-alloy dust explosion in China. *Journal of Loss Prevention in the Process Industries*, vol. 39, pp. 121-130.

Marmo, L., Cavallero, D. (2008). Minimum ignition energy of nylon fibres. *Journal of Loss Prevention in the Process Industries*, vol. 21, pp. 512-517.

Mining Technology. 2014. The world's worst coal mining disasters. By Akanksha Gupta. Analysis. [In Mining Technology www-pages]. [Retrieved March 7, 2018].
Available: http://www.mining-technology.com/features/feature-world-worst-coal-mining-disasters-china/.

MTV Uutiset. 2017. Vaneritehtaassa tapahtui pölyräjähdys – kaksi loukkaantui, ikkunat lensivät lähes 100 metriltä. [In MTV www-pages]. [Retrieved March 9, 2018].
Available: https://www.mtv.fi/uutiset/kotimaa/artikkeli/jyvaskylassa-keskisuuri-rajahdys-tai-sortuma-paikalla-sijaitsee-upm-n-vaneritehdas/6306920#gs.bbwmjAg.

Nagy, J., Verakis, H. C. (1983). Development and Control of Dust Explosions. New York: Marcel Dekker, Inc. Cited in Eckhoff, 2003.

NFPA 68, 2013. Explosion Protection by Deflagration Venting. Standard. National Fire Protection Association, Quincy, Massachusetts.

Ogle, R. A. (2016). Dust Explosion Dynamics. Warrenville, IL, United States: Exponent, Inc.

Partanen, J. I., Partanen. L. J. (2010). Luentomoniste opintojaksoon Kemiallinen termodynamiikka. Osa 1: kemiallisen termodynamiikan perusteet. Lappeenranta. ISBN 978-952-214-952-7.

Proust, C. (2004). EFFEX: a tool to model the consequences of dust explosions. HAL archieves-ouvertes.fr. HAL Id: ineris-00972453.

PubChem Open Chemistry Database, 2012. Compound Summary for CID 57358748 (Anthracen-1-YL)methanolate. [In PubChem www-pages]. Updated May 19, 2018.[Retrieved May 23, 2018].
Available: https://pubchem.ncbi.nlm.nih.gov/compound/57358748#section=Top.

Rahman, N. A., Takriff, M. S. (2011). Consequence modelling of a dust explosion. Safety and Security Engineering IV, WIT Press, Transactions of the Built Environment, vol. 117, pp. 197-206.

Reaction Design, 2015. CHEMKIN-CFD. [In Reaction Design www-pages]. [Retrieved July 20, 2018].
Available: http://www.reactiondesign.com/products/chemkin-cfd/.

Russo, P., Di Benedetto, A. (2013). Review of a Dust Explosion Modeling. *Chemical Engineering Transactions*, vol. 31, pp. 955-960.

Salamonowicz, Z., Kotowski, M., Pólka, M., Barnat, W. (2015). Numerical simulation of dust explosion in the spherical 20l vessel. *Bulletin of the Polish Academy of Sciences, Technical Sciences*, vol. 63, no. 1, pp. 289-293.

Sari, A. (2010). Comparison of TNO Multienergy and Baker-Strehlow-Tang Models. *American Institute of Chemical Engineers*, vol. 30, no. 1, pp. 23-26.

Sato, M. (1990). Thermochemistry of the formation of fossil fuels. The Geochemical Society, Special Publication No. 2. Editors: Spencer, R. J., Chou, I-M., pp. 271-283.

Savon Sanomat. 2017. Pölyräjähdys pamautti ikkunat karmeineen ulos vaneritehtaalla Jyväskylässä. [In Savon Sanomat www-pages]. [Retrieved March 9, 2018].
Available: https://www.savonsanomat.fi/kotimaa/P%C3%B6lyr%C3%A4j%C3%A4hdys-pamautti-ikkunat-karmeineen-ulos-vaneritehtaalla-Jyv%C3%A4skyl%C3%A4ss%C3%A4/928093.

Seveso III directive 2012/18/EU of the European Parliament and of the Council of 4 July 2012 on the control of major-accident hazards involving dangerous substances. Official Journal of the European Union, L 197/1-197/37.

SFS-EN 1127-1:2011. Räjähdysvaaralliset tilat. Räjähdyksen esto ja suojaus. Osa1: Peruskäsitteet ja menetelmät. Standardi. Suomen Standardisoimisliitto SFS, Helsinki.

SFS-EN 14034-1:2004 + A1:2011. Determination of explosion characteristics of dust could. Part 1: Determination of the maximum explosion pressure p_{max} of dust clouds. Standardi. Suomen Standardisoimisliitto SFS, Helsinki.

SFS-EN 14034-2:2006 + A1:2011. Determination of explosion characteristics of dust could. Part 2: Determination of the maximum rate of explosion pressure rise $(dp/dt)_{max}$ of dust clouds. Standardi. Suomen Standardisoimisliitto SFS, Helsinki.

SFS-EN 14491:2012. Dust explosion venting protective systems. Standard. Suomen Standardisoimisliitto SFS, Helsinki.

SFS-EN 60079-10-2:2015. Räjähdysvaaralliset tilat. Osa 10-2: Tilaluokitus. Pölyräjähdysvaaralliset tilat. Standardi. Suomen Standardisoimisliitto SFS ry, Helsinki.

SFS-IEC 60300-3-9: 1995. Dependability management. Part 3: Application guide. Section 9: Risk analysis of technological systems. Standard. Finnish Electrotechnical Standards Association, Suomen Standardisoimisliitto SFS ry, Helsinki.

Skjold, T., Arntzen, B. J., Hansen, O. R., Taraldset, O. J., Storvik, I. E., Eckhoff, R. K. (2005). Simulating dust explosions with the first version of DESC. *Process Safety and Environmental Protection*, vol. 83, issue B2, pp. 151-160.

Skjold, T., Larsen, Ø., Hansen, O. R. (2006). Possibilities, limitations, and the way ahead for dust explosion modelling. IChemE, symposium series no. 151.

Skjold, T. (2007). Review of the DESC project. *Journal of Loss Prevention in the Process Industries*, vol. 20, pp. 291-302.

Skjold, T. (2014). Flame propagation in dust clouds. Numerical simulation and experimental investigation. Thesis for the degree of philosophiae doctor (PhD), University of Bergen (UiB), Faculty of Mathematics and Natural Sciences, Department of Physics and Technology, Bergen, Norway.

Stahl (2004). The basics of dust-explosion protection. R. STAHL Schaltgeräte GmbH. ID-NR. 00 006 84 77 0.

Stahmer, K-W., Gerhold, M. (2017). Study of the explosion reactions of sucrose, activated charcoal, polyethylene and lignite part 2: Study of the gas phase following the explosion reaction. *Journal of Loss Prevention in the Process Industries*, vol. 48, pp. 216-222.

Tang, M. J., Baker, Q. A. (1999). A new set of blast curves from vapor cloud explosion. *Process Safety Progress*, vol. 18, no. 4, pp. 235-240.

Tenitz, S. (2014). Kaasuräjähdysmallien vertailu ja käyttö suuronnettomuuksien seurausanalyysissä. Master's Thesis. Aalto University, School of Chemical Technology, Department of Biotechnology and Chemical Technology, Espoo, Finland.

Turvallisuus- ja kemikaalivirasto Tukes (2013). Vaurio- ja onnettomuusrekisteri VARO. [In Tukes www-pages]. [Retrieved March 9, 2018].
Available: http://varo.tukes.fi/.

Turvallisuus- ja kemikaalivirasto Tukes (2015[a]). ATEX Räjähdysvaarallisten tilojen turvallisuus. Opas. ISBN 978-952-5649-71-0.

Turvallisuus- ja kemikaalivirasto Tukes (2015[b]). Tuotantolaitosten sijoittaminen. Opas. ISBN 978-952-5649-67-3.

Turvallisuus- ja kemikaalivirasto Tukes (2016). Prosessiturvallisuus ja sen mittaaminen. Opas. ISBN 978-952-5649-79-6.

U.S. Chemical Safety and Hazard Investigation Board (2006). Investigation report. Combustible Dust Hazard Study. Report. No. 2006-H-1.

U.S. Chemical Safety Board CSB. 2009. Imperial Sugar Company Dust Explosion and Fire. [In CSB www-pages]. [Retrieved March 7, 2018].
Available: http://www.csb.gov/imperial-sugar-company-dust-explosion-and-fire/.

Yle Uutiset. 2015. Fortumin uudella Joensuun bioöljylaitoksella pölyräjähdys ja tulipalo – saatiin sammutettua yöllä. [In Yle www-pages]. [Retrieved March 9, 2018].
Available: https://yle.fi/uutiset/3-7861774.

Yle Uutiset. 2017. Pölyräjähdys aiheutti tulipalon Suomen Rehun tehtaalla Turussa. [In Yle Uutiset www-pages]. [Retrieved March 9, 2018].
Available: https://yle.fi/uutiset/3-9695728.

Yuan, Z., Khakzad, N., Khan, F., Amyotte, P. (2015). Dust explosions: A threat to the process industries. *Process Safety and Environmental Protection*, vol. 98, pp. 57-71.

Zhen, G., Leuckel, W. (1997). Effects of ignitors and turbulence on dust explosions. *Journal of Loss Prevention in the Process Industries*, vol. 10, pp. 324-371. Cited in Fumagalli et l., 2018.

APPENDICES

Appendix I	Process chart of the chosen modelling methods for testing
Appendix II	Thermodynamic properties of chosen hydrocarbon materials
Appendix III	Calculation data for the simplified RBB model of chosen hydrocarbon materials
Appendix IV	Damage estimation tables for overpressure estimates
Appendix V	Reported dust explosion accident damages and consequences of CTA Acoustics, Inc. facility
Appendix VI	Reported dust explosion accident damages and consequences of West Pharmaceutical Services, Inc. facility

Appendix I Process chart of the chosen modelling methods for testing.

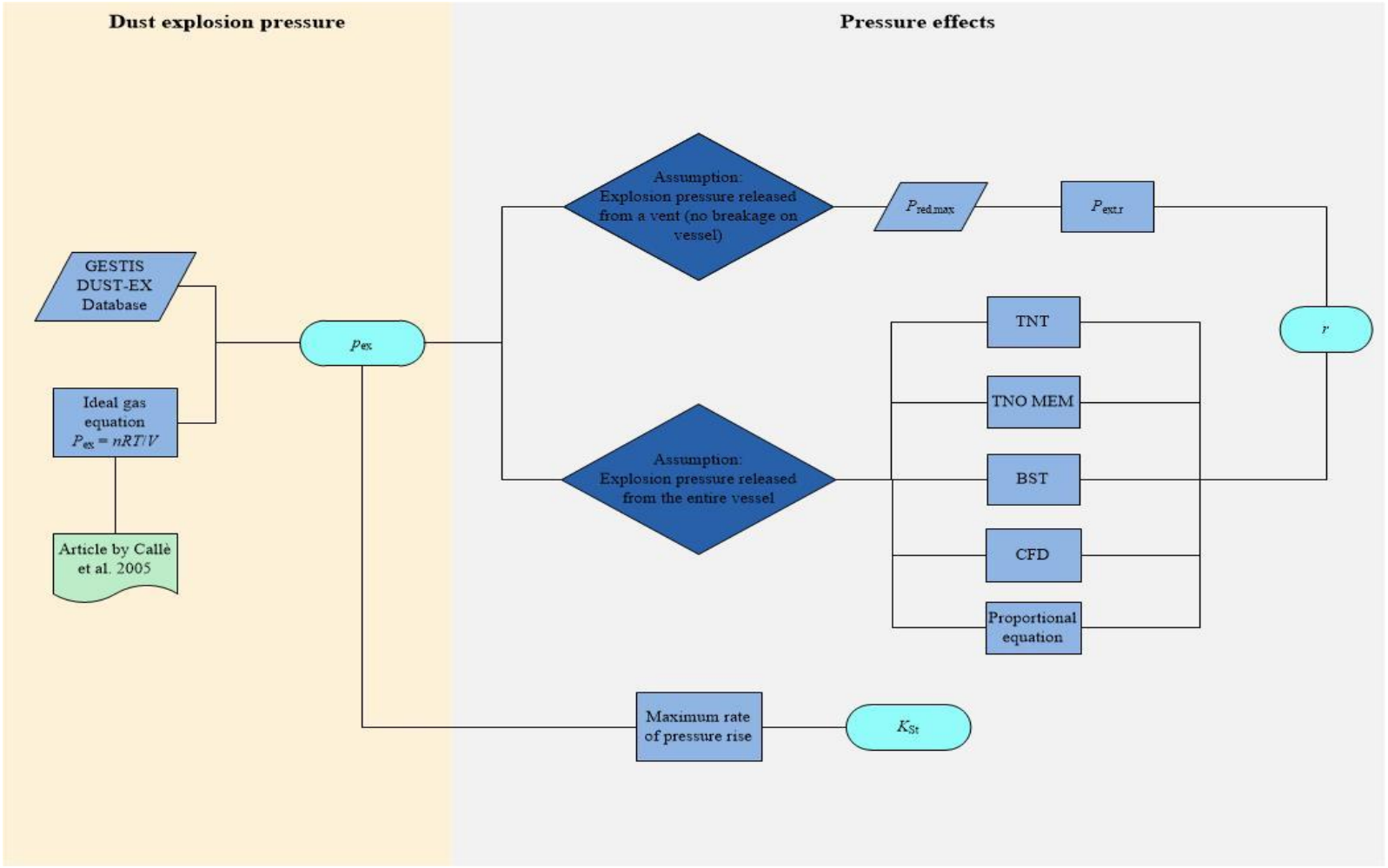

AA 1 Process chart of the chosen modelling methods for the estimation of explosion pressure and the pressure effects.

Appendix II Thermodynamic properties of chosen hydrocarbon materials

A I Material properties of hydrocarbons used in RBB model calculations.

Component	**Chemical formula**	**Molar mass [g/mol]**	**ΔH_c [kJ/mol]**
Cellulose	$C_6H_{10}O_5$	162.140	1746.74 (Callé et al.)
Glucose	$C_6H_{12}O_6$	180.156	2803 (CRC)
Sucrose	$C_{12}H_{22}O_{11}$	342.296	5640 (CRC)
Lignin	$C_{10}H_{12}O_3$	180.196	5170 (Sato, 1990)
Ascorbic acid (Vitamin C)	$C_6H_8O_6$	176.124	2340 (CRC)
Graphite (Carbon)	C	12.011	394 (CRC)
Bisphenol A	$C_{15}H_{16}O_2$	228.278	7821 (CRC)
Citric acid	$C_6H_8O_7$	192.124	1961 (CRC)
Fumaric acid	$C_4H_4O_4$	116.072	1334 (CRC)

Appendix III Calculation data for the simplified RBB model of chosen hydrocarbon materials

A II Overpressures and temperatures of chosen hydrocarbons calculated with three different assumptions. First value (X=1) are calculated for stoichiometric combustion reaction of hydrocarbon. Second set is calculated with the assumption of $m_{hydrocarbon} = 3.5 \cdot m_{hydrocarbon,stoich}$. Third set is calculated with the assumption that the concentration of hydrocarbon in the system is 4.5 g/m^3. For the two latter sets the conversion of hydrocarbon is solved using oxygen as the limiting reactant.

Component	Conversion X [-]	Mass [g]	Overpressure [bar]	Temperature [K]
Cellulose	1	206.51	10.41	2928.271
	0.286	722.77	10.63	2986.52
	0.286	729.63	10.74	3010.764
Glucose	1	229.448	10.51	2877.596
	0.286	803.07	10.73	2933.288
	0.283	810.702	10.73	2932.353
Sucrose	1	217.977	10.45	2901.458
	0.286	762.919	10.68	2958.399
	0.141	1540.322	10.44	2898.424
Lignin	1	119.747	9.86	3004.721
	0.,286	419.113	10.09	3069.699
	0.148	810.882	9.86	3004.25
Ascorbic acid	1	269.168	10.70	2926.189
	0.286	942.089	10.93	2981.944
	0.340	792.558	11.00	2999.387
Graphite	1	93.008	8.14	2679.513
	0.286	325.528	8.35	2741.934
	(1	54.0495	5.05	1775.561)not included
Bisphenol A	1	96.920	8.96	2812.195
	0.286	339.221	9.18	2875.302
	0.094	1027.251	8.97	2813.888
Citric acid	1	326.234	10.29	2726.608
	0.286	1141.818	10.50	2776.406
	0.377	864.558	10.59	2799.653
Fumaric acid	1	295.647	10.29	2822.162
	0.286	1034.767	10.50	2875.857
	0.57	552.324	10.73	2932.641

*Combustion heat 1746,74 kJ/mol from Callé et al., 2005.

Appendix IV Damage estimation tables for overpressure estimates

A III Damage estimates for common structures based on overpressure (Clancey, 1972). These values should only be used for approximate estimates (CCPS, 2000).

Over pressure [kPa]	**Damage**
0.14	Annoying noise (137 dB if of low frequency 10 – 15 Hz)
0.21	Occasional breaking of large glass windows already under strain
0.28	Loud noise (143 dB), sonic boom, glass failure
0.69	Breakage of small windows under strain
1.03	Typical pressure for glass breakage
2.07	"Safe distance" (probability 0.95 of no serious damage below this value); projectile limit; some damage to house ceilings; 10 % window glass broken
2.76	Limited minor structural damage
3.4-6.9	Large and small windows usually shattered; occasional damage to window frames
4.8	Minor damage to house structures
6.9	Partial demolition of houses, made uninhabitable
6.9-13.8	Corrugated asbestos shattering; corrugated steel or aluminum panels, fastenings fail, followed by buckling; wood panels (standard housing) fastenings fail, panels blown in
9.0	Steel frame of clad building slightly distorted
13.8	Partial collapse of walls and roofs of houses
13.8-20.7	Concrete or cinder block walls, not reinforced, shattered
15.8	Lower limit of serious structural damage
17.2	50 % destruction of brickwork of houses
20.7	Heavy machines (3000 lb) in industrial building suffered little damage; steel frame building distorted and pulled away from foundations
20.7-27.6	Frameless, self-framing steel panel building demolished; rupture of oil storage tanks
27.6	Cladding of light industrial buildings ruptured
34.5	Wooden utility poles snapped; tall hydraulic press (40 000 lb) in building slightly damaged
34.5-48.2	Nearly complete destruction of houses
48.2	Loaded train wagons overturned
48.2-55.1	Brick panels, 8 – 12 inches thick, not reinforces, fail by shearing or flexure
62.0	Loaded train boxcars completely demolished
68.9	Probable total destruction of buildings; heavy machine tools (7000 lb) moved and badly damaged; very heavy machine tools (12 000 lb) survive
2068	Limit of crater lip

A IV Key to **Table A VI** (CCPS, 2000).

A. Windows and gauges broken	L. Power lines are severed
B. Louvers fall at 1 – 3 kPa	M. Controls are damaged
C. Switchgear in damaged from roof collapse	N. Block walls fall
D. Roof collapses	O. Frame collapses
E. Instruments are damaged	P. Frame deforms
F. Inner parts are damaged	Q. Case is damaged
G. Brick cracks	R. Frame cracks
H. Debris-missile damage occurs	S. Piping breaks
I. Unit moves and pipes break	T. Unit overturns or is destroyed
J. Bracing falls	U. Unit uplifts (0.9 tilted)
K. Unit uplifts (half tilted)	V. Unit moves on foundation

A V Damage estimates based on overpressure for process equipment (CCPS, 2000).

Equipment	**Overpressure, kPa**																								
	3	7	10	14	17	21	24	28	31	34	38	41	45	48	52	55	59	62	66	69	83	97	110	124	138
Control house steel roof	A	C	D				N																		
Cooling house concrete roof	A	E	P	D			N																		
Cooling tower	B			F			O																		
Tank: cone roof		D				K							U												
Instrument cubicle			A			LM						T													
Fire heater				G	I					T															
Reactor: chemical				A				I					P					T							
Filter				H					F										V		T				
Regenerator						I				IP					T										
Tank: floating roof						K							U												D
Reactor: cracking							I							I							T				
Pine supports							P					SO													
Utilities: gas meter									Q																
Utilities: electronic transformer									H						I					T					
Electric motor										H								I							V
Blower										Q										T					
Fractionation column											R			T											
Pressure vessel: horizontal												PI						T							
Utilities: gas regulator												I								MQ					
Extraction column													I							V	T				
Steam turbine															I						M	S			V
Heat exchanger															I			T							
Tank sphere																I						I	T		
Pressure vessel: vertical																					I	T			
Pump																					I		V		

Appendix V Reported dust explosion accident damages and consequences of CTAAcoustics, Inc. facility

A VI Fire and explosion damage from dust explosion at the CTA facility (CSB, 2003).

Location	Damage	Overpressure [kPa]
Line 405	Concrete block masonry firewall on east side partially collapsed and pushed eastward	13.8
	Metal panels detached at south end of partially enclosed area above blend room deformed in southward direction	10
	Damage to building roof above line	6.9
	Ceiling panels and lights pushed downward	6.9
	Wall and polycarbonate panels of blend room deformed and pushed out in westward direction	6.9
	Combustible material inside curing oven burned away; metal conveyor burned clean and free of debris; no explosion damage observed inside oven	
South of line 405	Concrete block masonry firewalls surrounding room directly south of line and near raw material storage area permanently deformed	13.8
	Fire scorching in area where no masonry walls extend to ceiling; residual burnt resin material attached to open-web steel joists	
Between lines 403 and 405	Concrete block masonry firewall in open bay between lines collapsed	20.7
Line 403	Metal panels above east wall of blend room pushed westward	9.0
	Oven exhaust line and thermal oxidizer inlet line separated	6.9-13.8
Line 402	Metal wall panel separating lines 402 and 403 pushed westward	9.0

Table A VIII cont. Fire and explosion damage from dust explosion at the CTA facility (CSB, 2003).

Location	Damage	Overpressure [kPa]
Line 401	Metal panels of blend room enclosure, particularly in northeast portion, permanently deformed outward	9.0
	Steel columns in blend room permanently bent to west	9.0
	Concrete block masonry firewalls on south end collapsed or severely deformed	15.8
	Building roof above blend room enclosure destroyed	6.9
North wall of plant near west corner	Loading dock door bent	4.8
Production area	Charred combustible material adhered to vertical surfaces; horizontal surfaces, covered by combustible material, primarily charred at exposed exterior surfaces	
Baghouses on lines 403 and 405	Bags burned up	
Dust collectors on lines 401 and 402	Access doors on dust collectors blown off	13.8

Appendix VI Reported dust explosion accident damages and consequences of West Pharmaceutical Services, Inc. facility

A VII Explosion damage from dust explosion at the West Pharmaceutical Services, Inc. (CSB, 2004).

Damage	Overpressure estimate [kPa]	Distance estimate [m]
The force of the blast displaced batchoff #1—a machine that weighs several tons—several feet to the southwest.	20.7 – 68.9	6.6 – 14.1
To the immediate east of this area, the two masonry walls of a hallway used to conduct tours of the facility were blown northeastward into the kitchen. Structural steel in this area was deflected in the same direction.	15.8 – 20.7	7.5 – 8.5
To the southeast, masonry walls for an elevator shaft and stairwell were blown southeastward toward the warehouse. Structural steel and cross bracing were deflected in the same direction (Figure B-1).	13.8 – 20.7	17 – 17.9
The upper-level concrete slab flooring directly over the mill #1 and batchoff #1 areas was heaved upward. The floor to the northwest between the two mixers was also heaved (Figure B-2).	20.7 – 30	0.91
Structural steel for the wall adjacent to batchoff #1 was deflected to the southwest (Figure B-3).	9.0 – 13.8	17.7; 19.8; 21.7